Development of immunoassays for the investigation of peptide antibody interactions in array format

Zur Erlangung des akademischen Grades eines

Doktors der Ingenieurwissenschaften (Dr.-Ing.)

von der KIT-Fakultät für Maschinenbau des
Karlsruher Instituts für Technologie (KIT)

angenommene

Dissertation

von

Dipl.-Ing. Andrea Palermo

Tag der mündlichen Prüfung	03. Dezember 2019
Hauptreferent	Prof. Dr. Alexander Nesterov-Müller
Koreferenten	Prof. Dr. Martin Dienwiebel
	Prof. Dr. Matthias Franzreb

Zusammenfassung

Antikörper erfüllen eine Vielzahl wichtiger Aufgaben im Immunsystem, um uns vor Krankheiten zu schützen. Sie sind darauf konditioniert bestimmte Krankheitserreger spezifisch zu erkennen, darunter zum Beispiel Toxine, Bakterien oder Viren. Sie können uns aber auch schaden, indem sie fälschlicherweise körpereigene (endogene) Strukturen für den Abbau markieren, und somit zu Autoimmunerkrankungen beitragen. Die Erforschung der Immunantwort durch die Bestimmung, welche Antikörper bei einer erfolgreichen Immunreaktion verstärkt produziert werden und an welche Stelle neutralisierende Antikörper auf einem Pathogen binden, würde helfen neue Impfstoffkandidaten zu entwickeln und zum Allgemeinverständnis des zugrunde liegenden Mechanismus beitragen. Neben den Informationen, was Antikörper spezifisch binden, ist es von Interesse, in welcher Konzentration sie im Blut verfügbar sind und mit welcher Affinität sie ihr Ziel binden. Peptid-Arrays bieten eine ideale Plattform für die Untersuchung von Antikörper-Protein-Interaktionen, wobei die Peptide Antikörper-Ziele nachahmen. Mit einem winzigen Probenvolumen können mehrere tausend Peptide gleichzeitig untersucht werden. Um identifizierte Antikörper-Peptid-Interaktionen im Bezug auf Kinetik zu untersuchen, müssen Online-Messungen in mikrofluidischen Kanälen, so genannte *Continuous Flow Assays*, durchgeführt werden. Diese Arbeit gliedert sich in zwei Hauptteile, die das Screening nach Epitopen und die Entwicklung eines experimentellen Aufbaus zur Charakterisierung der Peptid-Epitop-Interaktion umfassen.

Im ersten Teil wurde die Immunantwort gesunder Europäer auf die Tetanus-, Diphtherie- und Keuchhustenimpfung und zwei etablierte Epitope (PALT(A)xET und PEFxGSxP) aus dem Enterovirus und wahrscheinlich *Staphylococcus aureus*, mit Peptidarrays untersucht. Impfstoffspezifische Antikörper wurden durch die Bestimmung ihres linearen Epitops, bis auf die einzelnen Aminosäuren aufgelöst, identifiziert. Dazu wurde die lineare Aminosäuresequenz von Tetanus, Diphtherie und Keuchhustentoxin in Fragmenten (Peptiden) im Array-Format auf einem festen Substrat synthetisiert und mit Serum von 19 gesunden Europäern inkubiert. Für das Tetanustoxin wurde ein Epitop identifiziert ($_{929}$ExxEVIVxK$_{937}$), das von 8 der 19 Individuen gebunden wurde. Die für die Antikörperbindung entscheidenden Aminosäuren (der "Antikörper-Fingerprint") wurden für dieses Epitop durch eine Substitutionsanalyse bestimmt. Bei einer Substitution wird jede Aminosäure durch alle anderen 19 Aminosäuren ersetzt, während der Rest der Sequenz erhalten bleibt. Der Antikörper-Fingerprint kann bestimmt werden, da die Substitution entscheidender Aminosäuren

zum Verlust der Antikörperbindung führt. Die “Antikörper-Fingerabdrücke” zeigten sich bei den drei untersuchten linearen Epitopen ($_{929}$ExxEVIVxK$_{937}$, PALT(A)xET und PEFxGSxP) als stark konserviert. Weiterhin wurde durch Affinitäts-Batch-Chromatographie und ELISA bestätigt, dass Antikörper, die das identifizierte Epitop binden, das aus der Sequenz des Tetanustoxins stammt, auch an das native Tetanustoxin binden. Dies deutet darauf hin, dass das identifizierte Epitop tetanusspezifisch ist.

Im zweiten Teil wurde ein Versuchsaufbau realisiert, um Peptidarrays automatisiert in mikrofluidischen Kanälen zu inkubieren und um auf diese Weise kontinuierliche Durchfluss-Assays durchzuführen. Wechselwirkungen von fluoreszenzmarkierten Antikörpern mit Peptiden können durch den Nachweis von Fluoreszenz mit einem Epi-Fluoreszenz-Aufbau charakterisiert werden. Dazu werden in kurzen Abständen Fluoreszenzbilder aufgenommen und der Anstieg des Fluoreszenzsignals über die Zeit bestimmt. Die Fluoreszenzintensität des Fluorophors DyLight 550 wurde unter Versuchsbedingungen als temperaturabhängig eingestuft. Bei einer konstanten Temperatur (kann die Intensität jedoch für 50min kontinuierlicher Anregung als stabil angenommen werden. Für die schnelle Herstellung von Peptidarrays, die während der Vorversuche benötigt wurden, wurde das Spotten von präsynthetisierten Peptiden (mit einem *C*-Terminal-Cystein) auf 3D-Maleimid-Oberflächen etabliert. Um ein zusätzliches markierungsfreies, bildgebendes Verfahren zur Verfügung zu haben, wurde die Vertikalscan-Interferometrie (engl. *vertical scanning interferometry (VSI)*) für die Qualitätskontrolle von Peptidarrays etabliert.Die durch die Vertikalscan-Interferometrie erhaltenen Höhenprofile wichen nicht signifikant von den Messungen der Rasterkraftmikroskopie (engl. *atomic force microscopy (AFM)*) ab. Spots bis hinunter zu einer Höhe von ca. 1nm können auf einem vergleichsweise großen Sichtfeld von $1.74\,\mathrm{mm} \times 1.31\,\mathrm{mm}$ innerhalb einer Minute abgebildet werden. Zwei verschiedene Ansätze für die Integration von Peptid-Arrays in einen mikrofluidischen Kanal wurden untersucht. Das Abformen von Kanalstrukturen aus Polydimethylsiloxan (PDMS) ist eine schnelle Technik, aber es wurde festgestellt, dass das Kanaldesign auf einen Mindestabstand zwischen den Kanälen beschränkt ist, um Leckagen zu vermeiden. Durch die Zugabe von bis zu $\sim$2 % Graphenpartikeln zum PDMS vor der Polymerisation konnte die Hintergrundfluoreszenz des PDMS um ca. 70% reduziert werden. Der gefertigte Kanal erwies sich bis zu einem Fluss von $3\,\mathrm{ml\,min^{-1}}$ als dicht, wenn er bei einem Drehmoment von $10\,\mathrm{N\,cm}$ festgeschraubt wurde. Das Anpressen führte jedoch zu einer Verformung der PDMS-Kanäle. Dies resultierte in inhomogenen Kanalquerschnitten und ist daher nicht geeignet für eine Konzentrationsanalyse, die eine konstante Kanalhöhe erfordert. Die zweite Art der untersuchten Kanalherstellung ist das *Adhesive Layer Bonding* mit Ordyl SY355. Es ist der erste Ansatz, ein Glassubstrat mit einer funktionalisierten Oberfläche zu verbinden, die für die Herstellung von Mikroarrays verwendet wird. Dieses Verfahren hat das Potenzial, Microarrays für andere Mikrosystemtechnologien verfügbar zu machen. Fluidische Ein- und Ausgänge werden mit einem Laser in ein Glassubstrat gebohrt. Die Wände des Kanals werden aus der *Adhesive Layer*, der Klebeschicht gebildet, die lithografisch aufgebracht und strukturiert wird. Das Parameterfenster für diesen lithografischen Prozess wur-

de mit Belichtungsdosen von $150\,\mathrm{mJ\,cm^{-2}}$ to $220\,\mathrm{mJ\,cm^{-2}}$ und Verbunddrücken von $220\,\mathrm{N\,cm^{-2}}$ to $735\,\mathrm{N\,cm^{-2}}$ bestimmt und ist recht breit. Prozesstemperaturen über $100\,^{\circ}\mathrm{C}$ erwiesen sich als kritisch, da es zu einer Beschädigung der funktionalisierten Oberfläche kam. Die Größe der Bruchfestigkeit der Verbindung wurde durch Zugversuche auf etwa $(305 \pm 50)\,\mathrm{N\,cm^{-2}}$ geschätzt. Daraus ergibt sich eine theoretische Druckfestigkeit von $\sim 4.9\,\mathrm{bar}$ und die Kanäle erwiesen sich bei einer Flussrate von bis zu $750\,\mathrm{\mu l\,min^{-1}}$ als dicht. Der entworfene Versuchsaufbau, einschließlich der Integration von Peptidarrays in mikrofluidische Kanäle, erfüllte nachweislich die Anforderungen für die Durchführung kontinuierlicher Assays an Peptidarrays. Durch die Durchführung einer Kalibrierung der Fluoreszenzsignalintensität auf die Antikörperkonzentration in einem zukünftigen Projekt, wird der Aufbau bereit sein Antikörpertiter zu bestimmen.

Abstract

Antibodies perform a variety of important tasks in the immune system to protect us from diseases. They are trained to specifically target pathogens, which might be toxins, bacteria or viruses. However, they can also harm us by erroneously mark endogenous structures for degradation, which contributes to autoimmune diseases. Studying the immune response by determining, which antibodies are amplified during a successful immune reaction, and which part of the pathogen neutralizing antibodies are binding to, would help to develop new vaccine candidates and contribute to the common knowledge of the underlying mechanism. In addition to the information, what antibodies specifically bind to, it is of interest, in which concentration they are available in the blood and with which affinity they bind their target. Peptide arrays provide an ideal platform for the study of antibody-protein interactions, with the peptides mimicking antibody targets. Using a minute sample volume, several thousand peptides can be examined simultaneously. To study identified antibody-peptide interactions in terms of kinetics, on-line measurements in microfluidic channels, so called continuous flow assays, have to be performed. This work is divided into two main parts, covering the screening for epitopes and the development of an experimental setup to characterize the peptide-epitope interaction.

In the first part, the immune response of healthy European individuals towards the tetanus, diphtheria and pertussis vaccination and two established epitopes (PALT(A)xET and PEFxGSxP) originating from enterovirus and probably *Staphylococcus aureus*, was investigated using peptide arrays. Vaccination specific antibodies were identified by determining their linear epitope in amino acid resolution. Therefore, the linear amino acid sequence of tetanus, diphtheria and pertussis toxin was synthesized in fragments (peptides) in array format onto a solid substrate and incubated with serum of 19 healthy European individuals. For the tetanus toxin, an epitope was identified ($_{929}$ExxEVIVxK$_{937}$), which was targeted by 8 out of 19 individuals. The amino acids crucial for antibody binding (the 'antibody fingerprint'), were determined for this epitope, by substitution analysis. In a substitution, every amino acid is substituted by all of the other 19 amino acids while the rest of the sequence remains conserved. The antibody fingerprint can be determined, since the substitution of crucial amino acids leads to the loss of antibody binding. The 'antibody fingerprints' were found to be strongly conserved among individuals for the three investigated linear epitopes ($_{929}$ExxEVIVxK$_{937}$, PALT(A)xET and PEFxGSxP) . Further, it was further verified by

affinity batch chromatography and ELISA, that antibodies binding the identified epitope originating from the sequence of the tetanus toxin, also bind to the native tetanus toxin. This indicates, that the identified epitope is tetanus specific. For the mapping of the diphtheria toxin linear and cyclic peptides of different length were applied. Five prominent regions were identified in the mapping of cyclic peptides using pooled sera. For the pertussis toxin, three regions of interest could be identified, which also were reported in literature for their ability to induce toxin recognizing antibodies in rodents. However, no distinct antibody fingerprints could be determined for a variety of peptides covering the identified regions. Altogether, the homology in between fingerprints of different individuals targeting the same epitope ($_{929}$ExxEVIVxK$_{937}$, PALT(A)xET and PEFxGSxP) is striking, given the randomness of antibody formation.

In the second part, an experimental setup was realized to incubate peptide arrays in an automated fashion in microfluidic channels to perform continuous flow assays. The interactions of fluorescently labelled antibodies with the peptides can be characterized via the detection of fluorescence using an epi-fluorescence setup design. For this purpose, fluorescence images are taken at short intervals and the increase of the fluorescence signal over time is determined. The fluorescence intensity of the fluorophore DyLight (DL)550 was found to be temperature dependent under assay conditions. However, for a constant temperature ($(24.0 \pm 0.1)\,°C$), the intensity can be approximated as being stable for 50 min of continuous exposure. For the fast production of peptide arrays needed during preliminary experiments, spotting of pre-synthesized peptides (bearing a *C*-terminal cysteine) on 3D-Maleimide surfaces was established. To have an additional label free imaging method at hand, vertical scanning interferometry was established for the quality control of peptide arrays. Height profiles obtained by vertical scanning interferometry did not significantly deviate from atomic force microscopy measurements. Spots down to approximately 1 nm height can be resolved on a comparable large field of view of $1.74\,\text{mm} \times 1.31\,\text{mm}$ within a minute. Two different approaches for the integration of peptide arrays into a microfluidic channel have been investigated. Molding channel structures in polydimethylsiloxane is a fast technique, but the channel design was determined to be restricted to have a minimum distance between channels to prevent leakage. By adding up to $\sim$2 % of graphene particles to the PDMS prior to polymerization, the background fluorescence of polydimethylsiloxane (PDMS) was reduced by approximately 70 %. The fabricated channel proved to be leak-tight up to a flow of $3\,\text{ml}\,\text{min}^{-1}$ when screwed to a torque of 10 N cm. However, the clamping led to a deformation of the PDMS channels. This results in non-homogeneous channel cross sections and is thus not apt for a concentration analysis, which requires a constant channel height. The second type of channel fabrication investigated is adhesive layer bonding using Ordyl SY355. It is the first approach to bond a glass substrate to a functionalized surface, used for micro array fabrication. This method has the potential to make microarrays available to other microsystem technologies. Fluidic in- and outlets are laser drilled into a glass substrate and the adhesive layer is applied and structured lithographically to form the walls of the channel. The parameter window for this lithographic process was determined to be quite broad with exposure

doses ranging from $150\,\mathrm{mJ\,cm^{-2}}$ to $220\,\mathrm{mJ\,cm^{-2}}$ and bonding pressures ranging from $220\,\mathrm{N\,cm^{-2}}$ to $735\,\mathrm{N\,cm^{-2}}$. Process temperatures over $100\,^{\circ}\mathrm{C}$ were found to be critical, since damage of the functionalized surface occurred. The magnitude of fracture strength of the bond was estimated by random pulling tests to be about $(305 \pm 50)\,\mathrm{N\,cm^{-2}}$. This results in a theoretical pressure resistance of $\sim 4.9\,\mathrm{bar}$ and proved to be leak proof for a flow rate of up to $750\,\mathrm{\mu l\,min^{-1}}$. The designed experimental setup, including the integration of peptide arrays into microfluidic channels, was shown to fulfill the requirements for performing continuous flow assays on peptide arrays. By conducting the calibration of fluorescence signal intensity to antibody concentration in a future project, the setup will be ready to further determine antibody titers.

Contents

1 Introduction

Antibodies play a major role in the adaptive immune system of our body, which evolves during our lifetime with every infection, autoimmune disease or vaccination. Antibodies recognize molecular structures (antigens) with high specificity and trigger effector mechanisms, which lead to the elimination of the antigen-carrying pathogen. Antibodies can also target the body's own molecules and, thereby, contribute to autoimmune diseases. Figuring out, which antibodies were amplified in a patient coping especially well with an infection would help to develop new vaccine candidates for example for malaria [91]. Also interesting would be to identify those antibodies, that are specifically amplified in a patient with an autoimmune disease, such a type 1 diabetes [76]. Moreover, if a hitherto enigmatic disease induces the amplification of a special set of antibodies, then the identification of a particular set of antibodies, that correlates with this disease might provide clues to its cause(s). Even without any prior information about the antigen, the appearance of particular antibodies could be correlated to the immune status of a patient and thus, be used as reliable bio markers for until now, hard to diagnose diseases [175]. All of these antibodies are produced in an iterative process by B lymphocytes, that differentiated to plasma cells. A plasma cell is secreting thousands of copies of one type of antibody with an unique specificity towards 'its' antigen into body fluids. The human blood consists of approximately $10\,\mathrm{mg\,ml^{-1}}$ of IgG antibodies, representing mainly the amplified antibody species [53]. It is estimated, that at a given time point, every human has a few thousand carefully chosen antibody species amplified, that are selected from more than 10^6 different 'naïve' B lymphocytes, each displaying a different antibody on its surface [145]. Peptide arrays are a well-established method to investigate which antibodies have been amplified in a patient [73]. They enable multiplexed high-throughput assays and require minimal sample volume. They can even be used to define those amino acids within a peptide, which are mandatory for antibody binding and, thereby, unequivocally discriminate between different antibody species. One such approach would be to display the complete amino acid sequence of an antigen as overlapping peptides, and in array format. When incubated with patient serum, binding peptides can be identified in a single experiment before individual epitopes are characterized in more detail [143]. Next, and by testing more patient sera, experiments of this type should identify those peptides with diagnostic relevance, that could be all assembled on an array in order to diagnose many different diseases in parallel. Another important parameter, however, is the concentration of the different antibody species. A steady concentration would

indicate a chronic disease, while over time increasing or decreasing concentrations would hint to acute or overcome diseases, for example in multiple sclerosis [5], or during acute transplant rejection [169]. This would require to measure the antibody-epitope binding over time in a continuous flow analysis. Although, there are some devices using different measurement principles on the market, they are either limited to one epitope per experiment, or require special sensor surface and are really pricey. Combining high-density peptide arrays with a setup for time resolved detection of antibody binding, could be easily scaled up to determine the concentrations of thousands of different antibody species in parallel and in a single and inexpensive experiment. In the future, such a method could diagnose many diseases in parallel, and, moreover, especially inform the patient about potentially dangerous acute diseases.

1.1 Antibodies

Antibodies are part of the adaptive immune system. They belong to the family of glycoproteins and are collectively summarized under the term 'immunoglobulins' (Ig). The process of their formation and the functions they exert to defend the body are very complex and until now, not fully investigated. More detailed descriptions can be found in textbooks [103, 96].

1.1.1 Structure

The most numerous class of immunoglobulines is the class 'G' (IgG). Antibodies of the IgG type are big Y-shaped axisymmetrical heterotetramerical proteins of 150 kDa. They consist of two identical heavy (H) and two identical light chains (L), which are linked via disulphide bonds as can be seen in figure 1.1.1. The chains can be subdivided into a variable domain (V_L, V_H) and one or three constant domains (C_L, C_H), for the light and the heavy chain respectively. A domain consists of about 110 to 115 amino acids, which are arranged in a loop structure by disulphide bonds. Responsible for antigen binding is the assembly of six regions (hypervariable regions) within the variable domain of both chains (L_1-L_3, H_1-H_3), in which the sequence of amino acids varies widely from antibody to antibody. The conserved regions in between are called frame work regions (FR1-FR4). In the 3D conformation of the antibody, hypervariable regions are located close to each other within the respective variable domain. Further, they are complementary to the epitope (the amino acids on the antigen involved in antibody binding) and are thus also called complementary determining region (CDR). The antigen binding site consists of the assembly of the hypervariable areas of the heavy and the light chain. In humans, there are two types of light chains (κ and λ) and five types of heavy chains (α, γ, δ, ϵ and μ) which are distinct for IgA, IgG, IgD, IgE, and IgM respectively. [96]

1.1.2 Formation

Antibodies are produced by plasma cells, which developed from B cells. To secrete specific IgG antibodies in an immune response, the B cell needs to be activated by a T helper cell.

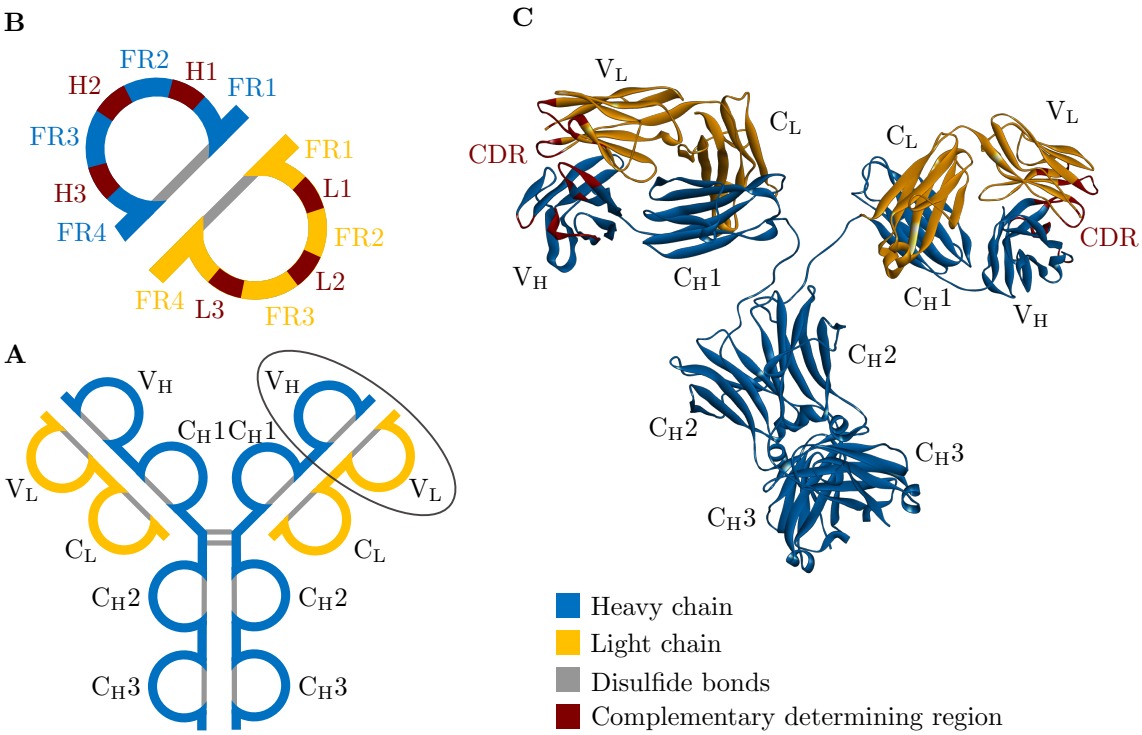

Figure 1.1.1: Structure of a human IgG antibody. A: Schematic structure: heavy chain in blue (constant domains (C_H) and variable domain (V_H)) and light chain in yellow (constant domain (C_L) and variable domain (V_L)). Disulphide bonds are depicted in grey. The region marked with the oval is enlarged in B. B: Detailed scheme of variable domains of heavy and light chain. Red indicates the individual hypervariable regions (L_1-L_3 on the light chain and H_1-H_3 on the heavy chain) flanked by frame work regions (FR1-FR4). C: 3D model of an IgG antibody. The individual hypervariable regions are coloured red and summarized as complementary determining regions (CDR). Depicted using BIOVIA Discovery Studio client [164] based on RCSB PDB (www.rcsb.org) ID 1IGT [59].

B and T cells

B cells (or B lymphocytes) are formed in the bone marrow [145]. Every B cell generates 'its' specific antibody by randomly combining different genetic building blocks. This process is called *somatic recombination* [68]. Every naïve B cell initially presents 'its' unique antibody as the antigen-specific part of the B cell receptor (BCR) on the surface [106, 123]. Those B cells, that survived negative selection (BCR is not functional or is binding endogenous structures) constantly patrol the blood stream and the body until they are activated. This activation process eventually leads to differentiated plasma cells, that secrete large amounts of one specialized antibody into the blood [145].

T cells too, are formed in the bone marrow, but maturate in the thymus [145]. They present degraded antigen fragments by a class of glycoproteins called the major histocompatability complex (MHC) or human leukocyte antigen (HLA) for humans [103]. MHC class I molecules are present in most of the cells in the body and present peptides derived from the proteasome, that digest endogenous proteins, viral or bacterial proteins, which are present in the cytosol of the body cells. Peptides presented from MHC class II proteins usually originate from extracellular fluids or ingested particles, viruses or pathogens. MHC class II proteins are restricted to professional

antigen-presenting cells (B cells, dendritic cells and marcophages).

Activation

The cells of the adaptive immune system sense the presence of pathogens using a wide variety of receptors, which can be summarized under the term pattern recognition receptor (PRR) [74]. Toll-like receptor (TLR), one of the most studied PRR [111, 3], recognize evolutionary conserved molecular structures from pathogens, e.g. peptidoglycans, that are part of a bacterial cell wall, 'wrongly' methylated dsDNA, dsRNA, glycosylation patterns on a surface, or flagellin. This structures are also called pathogen-associated molecular patterns (PAMP) [66] and the binding of a PAMP by an TLR activates the cell, leads to the production of cytokines and the maturation of antigen presenting cells.
For a B cell to differentiate to plasma cells, it needs to be activated by a two step process. First, the BCR needs to bind an antigen, which is processed and then presented by the MHC II on the B cell surface. Further the presence of PAMP needs to be sensed by a PRR. Second, a T-helper cell must specifically recognize the MHC class II presented peptide with its T cell receptor (TCR). This induces the T-helper cell to produce cytokines and other stimulating molecules, that ensure B cell survival and, eventually, B cell proliferation. Plasma cells usually produce large quantities of identical antibodies (*clonal expression*), which have the same antigen specificity as the predecessors IgM antibody and are secreted into bodily fluids [110]. Furthermore, descendants of this B cell subtly modify the surface-presented antibody in a process called *somatic hypermutation* to randomly generate antibody variants, that bind the antigen in higher affinity [103]. This allows the immune system to further increase the antibody affinity towards an antigen and thus specialize the immune response.

1.1.3 Role in the immune response

Secreted antibody species, that recognize a specific antigen, can switch their constant chains to perform different functions in the immune response [86]. For example, an IgM and IgG_1 constant chain can recruit the complement system to eliminate a particular cell, but only when bound to the cell's surface. This initial binding event triggers a cascade of processes that, eventually, result in the elimination of the antibody-targeted cell either by natural killer cells or by macrophages and neutrophil granulocytes (opsonization). Sometimes, however, antibodies can also directly neutralize a pathogenic activity. This type of antibody function is especially important in the neutralization of toxins, e.g. by inhibiting their entry into the cell via a toxin binding cellular receptor. [103]

1.2 Antibody-antigen interaction

The specific interaction of an antibody with its antigen can be attributed to different forces, such as van der Waals forces, electrostatic forces including the hydrophobic effect and hydrogen bonds

[177]. But temperature, pH, ionic strength, presence of detergents, concentration of antibody and other molecules also affect this interaction. Scientists came up with numerous mathematical models for the description of this interaction, which differ in their complexity.

1.2.1 Methods for the characterization of antibody-antigen interaction

There is a large variety of different assay techniques to determine protein affinity and kinetics. They differ in three main characteristics:

- state of the ligand and analyte (dissolved or bound)
- state of measurement (physical principle)
- application of a label

Some assays apply ligand and analyte both dissolved in a liquid phase, whereas others use setups with an immobilized ligand. Which one is better suited probably depends on the character of interaction to be investigated. The state of measurement can either be at equilibrium or before reaching equilibrium. The disadvantage of assays working at equilibrium is the lack of kinetic rate constant determination. There are assays which are label-free and others applying labels (which is mostly a fluorescence dye). A potential disadvantage of labels is their influence to the interaction to be investigated [58]. However labels also enable co-incubation of several different samples on one array, for example reference samples to normalize detected signals [58]. There are various assays in which both ligand and analyte are dissolved in a liquid phase, using different reference methods. For example, isothermal titration calorimentry (ITC) [51], differential scanning calorimetry (DSC) [25], MicroScale thermophoresis (MsT) [67] and Fluorescence-based Thermal Shift Assay [182] apply temperature changes during measurement and $K_{eq} = 1/K_D$ can be derived from $\Delta G = -RTln(K_D)$. Whereas fluorescence polarization (FP) [26] detects the change in linear polarized fluorescence emissions caused by adsorption of analyte to a fluorescent labeled ligand. For different concentrations of analyte K_D can be calculated as $P = P_{min} + \Delta P\,[C/(K_D + C)]$ where P, ΔP and C are the measured polarization, total change in polarization and the total concentration of analyte [26].

A variety of methods use immobilized ligands and microfluidics to generate a continuous flow of sample over a sensing surface. This allows for the determination of kinetic rate constants and analyte concentration. For example, quartz cristal microbalance (QCM) [55] and surface acoustic wave (SAW) [82] use acoustic waves to detect an increase in mass to the sensor surface. surface plasmon resonance (SPR) [129] and reflectometric interference spectroscopy (RIfS) [36] use optical principles for detection. In SPR the change in refractive index of the solvent close to the surface is measured. Therefore transverse magnetic (TM)-polarized light is directed onto a prism in different angles of incidence and a spectrum is detected for the total reflected light from the sensor surface. These angle dependent spectra show a surface specific minimum which shifts through adsorption

of analyte to the sensor surface. A special sensor surface made of gold is needed. In RIfS the interference of reflected light at thin layers is measured. By adsorption of analyte to the sensor surface, a change in physical thickness of sensor surface occurs which results in a change of reflected light intensity [36]. Due to the sensitivity of refractive index for this measurement, device compatible sensor surfaces having a customized refractive index are needed. All these methods are restricted to one ligand per assay, since they lack the possibility to measure signals on defined areas of the sensor surface. This flaw is addressed in the next generation of SPR and RIfS setups, which introduced *imaging* to the methods. For the localized detection of the reflected light a charge coupled device (CCD) camera, in the case of surface plasmon resonance imaging (SPRi), or a diode array spectrometer in the case of reflectometric interference spectroscopy imaging (iRIfS), is used. However, these systems are extremely pricey and also need special expensive substrates, onto which pre-synthesized ligands need to be spotted.

There are approaches overcoming the need for special sensor surfaces, which apply fluorescence for the detection of protein binding. The fluorescence is excited by coupling a laser into a planar waveguide and thus produce an evanescence field. Duveneck *et al.* [34] and Plowman *et al.* [124] use gratings to couple the light in the waveguide. This gratings have to be structured onto the substrate prior to the array production, which makes the method unsuitable for standard combinatorial peptide arrays. The Naval Research Laboratory around Frances S. Ligler couples a laser into a planar waveguide, which may be a glass substrate, via its precise ground side surface [52]. Apart from the mere detection of a variety of analytes (toxins [134, 133], bacteria [135, 133], allergens [32], and small molecules like trinitrotoluene (TNT) [88]), their system has been demonstrated to be able to determine the concentration of fluorescently labelled analytes [52]. However, the size of the spots they use for these assays is with approximately $1\,\mathrm{mm}^2 \times 1\,\mathrm{mm}^2$ quite large [39]. Applying smaller spots would increase the throughput of screenable interactions, but would also decrease the sensitivity, if the detection area is kept constant in size.

1.2.2 Interaction models

To depict protein binding in terms of adsorption and desorption processes, protein affinity and kinetic rate constants are used. The expression 'affinity' refers to the strength of interaction between two proteins as the sum of attractive and repulsive forces [161]. The affinity or equilibrium constant K_{eq} is defined as the ratio of association rate constant k_a ($\mathrm{M}^{-1}\,\mathrm{s}^{-1}$) to dissociation rate constant k_d (s^{-1}) and has dimensions of M^{-1}. It represents the ratio of concentration of bound to unbound antibody at equilibrium. With the following assumptions,

- antibody is monovalent
- only one epitope is recognized
- both reactants must be homogeneous regarding to binding sites

- reaction takes place in solution and in equilibrium

all models can be derived from the Law of Mass Action (formula 1.2.1).

$$Ab + X \underset{k_d}{\overset{k_a}{\rightleftharpoons}} AbX \tag{1.2.1}$$

$$K_{eq} = \frac{k_a}{k_d} = \frac{[AbX]}{[Ab][X]} \tag{1.2.2}$$

Where [Ab] is the molar antibody concentration, [X] the molar antigen concentration, k_a the association rate constant and k_d the dissociation rate constant. Further, the relation of unbound species as difference of total concentration (index $_t$) and concentration of bound species, can be derived from the law of mass action [177].

$$[Ab] = [Ab_t] - [AbX] \tag{1.2.3}$$

$$[X] = [X_t] - [AbX] \tag{1.2.4}$$

Determining K_{eq}

By inserting 1.2.4 into formula 1.2.1, different models for the determination of K_{eq} can be obtained. To gain experimental data, different defined concentrations of analyte have to be incubated with a constant amount of ligand, and either the amount of bound or free analyte has to be determined at equilibrium state. The probably most common model is the Scatchard-Plot [139], where the ratio of concentrations of bound to free analyte is plotted versus the concentration of bound analyte.

$$([Ab_t] - [AbX])K_{eq} = \frac{[AbX]}{[X]} \tag{1.2.5}$$

However, as the information of binding at equilibrium does not reflect *in vivo* conditions properly, the rate constants (k_a, k_d) have to be determined for a more accurate interpretation of binding events [30].

Determining k_a and k_d

To draw more information about the interaction under study, the adsorption process needs to be monitored, before equilibrium is reached and the ligands are saturated. This can be achieved by continuous flow assays. They consist of a continuous sample stream guided over a sensor surface, which detects the increasing complexation of antibody and ligand. Most setups for this kind of assays, SPR, RIfS, SAW and QCM are discussed in section 1.2.1 (5). Is the antibody present in excess and the reaction is governed by reaction kinetics (mass transport can be neglected) $[Ab]_t$, the antibody concentration at time t, can be approximated with its initial value [112]. the differential

form of this first order reaction is:

$$\frac{d[AbX]}{dt} = k_a[Ab]_t[X]_t - k_d[AbX]_t \tag{1.2.6}$$

$$\frac{d[AbX]}{dt} = k_a[Ab]_t([X]_0 - [AbX]_t) - k_d[AbX]_t \tag{1.2.7}$$

Where $[Ab]_t$ is the molar concentration of unbound antibody at time t and $[X]_0$ is the the total concentration of antigen. In excess the antibody concentration can be approximated with its inicial value [112].

$$\frac{d[AbX]}{dt} = k_a[Ab]_0([X]_0 - [AbX]_t) - k_d[AbX]_t \tag{1.2.8}$$

Assumed, that the increase of signal intensity is directly proportional to $[AbX]_t$ equation 1.2.8 may be rewritten as

$$\frac{dI}{dt} = k_a[Ab]_0(I_{max} - I_t) - k_d I_t \tag{1.2.9}$$

Where I_t denotes the signal at time t and I_{max} the maximal signal intensity, that would be obtained if all antigens were bound. O'Shannessy and Winzor present an integrated form for this equation, which contains the pseudo-first-order rate constant k_{obs} and I_{eq}, the signal at equilibrium.

$$I_t = I_{eq}[1 - exp(-k_{obs}t)] \tag{1.2.10}$$

$$k_{obs} = k_a[Ab]_0 + k_d \tag{1.2.11}$$

By repeating the experiment with several different initial concentrations of antibody at a constant flow rate the corresponding k_{obs} can be calculated. By plotting k_{obs} versus $[Ab]$ the rate constants k_a and k_d can be obtained. Another way to obtain k_d is through an desorption experiment, where antibody solution is substituted by buffer [113].

$$I_t = I_0 exp(-k_d t) \tag{1.2.12}$$

Determining [*Ab*]

In the early nineties, Robert Karlson published the calibration free concentration analysis for the label free detection method using surface plasmon resonance. To perform this analysis, a continuous, laminar sample flow over a sensing surface is needed. The flow of sample with the concentration $[Ab]_0$ of analyte creates a concentration gradient to the sensor surface, where analyte $[Ab]_S$ interacts with immobilized ligands. This binding or complex formation can be monitored for example by optical methods to obtain a signal over time. To estimate the concentration of sample $[Ab]_0$ binding to the ligand, Robert Karlsson proposed a two compartment model [71, 72]. The analyte has to be transported from the bulk phase close to the sensor surface, to be able to interact with the ligand. The model defines the sensor surface as an infinite sink ($[Ab]_S = 0$) for a fully mass transport limited reaction rate. The transport of analyte from bulk phase to the sensor

surface due to convection and diffusion can be estimated by mass transfer k_M.

$$k_M = 0.98 \left(\frac{D}{h}\right)^{\frac{2}{3}} \left(\frac{f}{bx}\right)^{\frac{1}{3}} \tag{1.2.13}$$

Which depends on the diffusion coefficient of the analyte D, the geometry of the microfluidic channel h height and b width, volumetric flow rate f and the distance from the flow entrance x (see [152] for more information). The mass transport limited case is at hand when $k_M \ll k_a[B]$. In this case, the equation can be simplified to

$$\frac{[AbX]}{dt} = k_M([Ab]_0 - K_D/(1/q - 1)) \tag{1.2.14}$$

where q is $\frac{[AbX]}{[AbX]_{max}}$ the degree of saturation [72]. As long as the response level is lower than the response level at equilibrium or saturation, the equation can be further simplified to

$$\frac{[AbX]}{dt} = k_M[Ab]_0 \tag{1.2.15}$$

Since $\frac{d[AbX]}{dt}$ is the detected signal and k_M can be estimated by the diffusion coefficient of the analyte, geometry parameters and flow rate, the initial sample concentration $[Ab]_0$ can be determined. To ensure the mass transport limited case, the experiment has to be repeated at different flow rates. If the slope of the signal is proportional to the increase in flow rate, the mass transport limitation is at hand.

1.3 Peptide arrays

For the investigation of antibody-binding, the use of peptide arrays is a well-established method [73]. They enable multiplexed high-throughput assays while requiring minimal sample volume. A peptide array consists of a substrate which might be a membrane [45], gold [163] or glass [14] onto which functional groups are generated or a polymer film containing functional groups is crafted [159]. Amino acid monomers or whole peptides are coupled to the substrate within distinct areas called spots. Advances in synthesis methods lead to an increasing number of peptide spots per surface area [90, 18]. Also, synthesis strategies for cyclic peptides [81], which mimic simple conformational epitopes, are being adapted for arrays [24].

Amino acids

The genetic code contains twenty natural amino acids (proteinogenic amino acids) from which proteins are produced by translation [77]. All proteinogenic amino acids have an amino group (-NH_2) at the α-carbon atom (the carbon atom closest to the carboxyl group), as well as a characteristic residue (-R) and a carboxyl group (-COOH) [83]. The chemical properties of an amino acid are determined by the characteristic residue consisting of a branched or unbranched carbon chain, which may have functional groups [70]. Amino acids are classified by their characteristic residue

(R) into polar, which can be subdivided into neutral, acidic and basic, and non polar, which can be subdivided into alkyl chains, branched chains and aromatics [115].

Peptides

In nature, the coupling of two amino acids to form a di-peptide is effected by a condensation reaction in which a carboxyl group reacts with an amino group, whereby a water molecule is released [115]. While the neighboring -C-C and -N-C bonds can freely rotate, the peptide bond is rigidly fixed in one plane, which leads to a limited flexibility of the peptide chain [9]. In the standard nomenclature the amino acid sequence of peptides is noted from the amino group (N-terminus) to the carboxyl group (C-terminus) as from left to right [77]. For the chemical peptide synthesis, amino acids monomers have to be activated and, in order to couple amino acids in a particular sequence, the use of protective groups is required [83]. Following the 9-fluorenylmethoxycarbonyl (Fmoc) strategy [101], orthogonal protection groups are used. The amino group is protected by a base-labile Fmoc-protection group [21] while the functional groups of the characteristic residues are protected using different acid-labile groups. The C-terminus can be activated by a pentafluorophenyl ester (OPfp), resulting in a direct coupling. More details on protective strategies used in chemical peptide synthesis can be found in textbooks [149].

1.3.1 Synthesis

Robert Merrifield introduced a novel method for the technical peptide synthesis, called solid phase peptide synthesis (SPPS), back in 1963 [98]. He fixed the growing peptides to a solid phase, which made the process automatable for the first time. Based on this, the first automated combinatorial fabrication method for peptide arrays, the SPOT synthesis, was introduced by Ronald Frank [44] in 1992. Densities of up to 25 spots per cm^2 can be achieved with this technique [19]. Nowadays, peptide arrays are produced commercially by different combinatorial synthesis methods: SC2 [12], a progression of the SPOT method by Intavis [65], a lithographic process involving microfluidics [119] by LC Science [85] and a particle-based method [158] by Pepperprint [120].

Particle-based synthesis

The particle-based peptide array synthesis method utilizes pre-activated and Fmoc-protected amino acid monomers mixed into a polymer serving as solid solvent and matrix material. The micro meter sized particles formed from this mixture, are deposited onto functional surfaces using an adapted laser printer with 20 toner cartridges, one for each proteinogenic amino acid monomer. By introducing heat, the particle matrix becomes viscous and the amino acid monomers can diffuse to the surface of the synthesis carrier and couple to the amino groups. In the following steps, unbound amino acids and the residual particle matrix and the Fmoc protection group of the freshly coupled amino acids are removed. The deposition of the particles, melting of the particle matrix and coupling of the amino acid monomers with subsequent washing and deprotection is repeated until the synthesized peptide has reached the desired length. With this technique a

peptide density of 800 spots per cm^2 ($200\,\mu m^2 \times 400\,\mu m^2$) can be realized. Since all 20 possible monomers can be deposited in one synthesis cycle, followed by the coupling, the total number of cycles is equal to the peptide length in amino acids. Significantly fewer cycles are required compared to the lithographic method, where the number of cycles is calculated as the sum of the number of different amino acid monomers per layer (n_L) for a given peptide length (n) ($\sum_{i=1}^{n} n_{Li}$).

The advancing development of new synthetic methods will allow for even higher spot densities, which will make the study more informative and affordable. The recently developed laser based synthesis method realizes already spot densities of 17 000 spots per cm^2 [90]. Other promising methods may even increase the before mentioned density by a factor of ten [18].

Spotting pre-synthesized peptides

In cases, where no high-throughput or flexible peptide content is required, pre-synthesized peptides can be used to couple to a functional surface. Of cause, this limits the number of different peptides available, but for assay development or control experiments, which get along with a small number of different peptides, this decreases expenses and time exposure. A typical method to array pre-synthesized peptides onto a functional surface is the deposition with a liquid handling system [165]. Peptides are therefore dissolved in solvent or buffer. They need to contain a functional group or ligand, which allows the peptide to react and bind to the functional surface. Spot sizes are determined by the minimal volume to be deposited, as well as the interplay of substrate hydrophobicity and buffer, which influence the spreading of the deposited drop. The reaction yield of peptide binding to the functional groups of the substrate depends among others on the reaction time, which is determined by the time it takes for the deposited drop to evaporate. This is affected by ambient temperature and humidity. Another factor is the density of functional groups on the substrate, which can not be influenced for commercially purchased surfaces. As described in section 1.3.1 (p. 10 ff) there are different common synthesis strategies. The maleimide-click reaction [125] allows the peptide to be completely deprotected and thus dissolved in aqueous solution at neutral pH, which spares the seals and tubes of the spotting robot and reduces the produced organic solvent waste. For this reaction, peptides need to contain a C-terminal cysteine to bind covalently to the maleimide immobilized on the surface. However, no cystein should be present in the actual peptide sequence itself.

Functionalized surfaces

Different functionalized surfaces are commonly applied for the synthesis of peptide arrays, which differ in thickness, composition and in the type of functional groups. For the binding of antibodies to a surface-bound peptide, the role of the surface hydrophobicity should also not be underestimated. Even though most of the hydrophobic moieties of a protein are put over to the protein inside, some parts on the protein surface may also be hydrophobic. This depends strongly on the protein. For proteins with significant surface hydrophobicity, hydrophobic surfaces act repellent

and may bedevil a potential interaction. A rather hydrophilic surface however, might lead to an increase in unspecific interaction of proteins with the surface. The property of the functionalized surface also affects the contact angle of aqueous drops and plays therefore a role in the deposition procedure of spotting.

1.3.2 Quality control of produced peptide arrays

To determine the quality of peptide synthesis on a planar, functionalized surface is quite difficult. Classical methods for the determination of concentration suffer from the minute amount of peptide, which must be cleaved from the surface, being mostly below the limit of detection (LOD). Techniques used in material science can be applied to some extend, for example, the molecular and atomic composition of the top monolayer of a functionalized surface can be investigated using time of flight secondary ion mass spectrometry (ToF-SIMS) [11] or X-ray photoelectron spectroscopy (XPS) [173], the latter which also produces quantitative information on oxidation states of the topmost surface and chemical composition. Also atomic force microscopy (AFM) was already deployed to characterize the surface topography of protein micro arrays [31]. However, these methods are time consuming and are restricted to a micro meter sized area for detection. Peptide spots therefore, are normally visualized indirectly, either by incubation with a fluorophore or fluorescently labelled antibodies. There are optical techniques, which allow for a destruction- and label-free imaging of protein layers like ellipsometry [128, 69] or reflectometry interference spectroscopy (RIfS) methods [92, 16] and among them the SARFUS technique [155]. This technique has been shown to be able to measure heights of peptide-antibody layers with a lateral resolution of $0.45\,\mu m\,pixel^{-1}$ and a field of view (FOV) of $365\,\mu m \times 284\,\mu m$. Some studies report the use of vertical scanning interferometry (VSI) to characterize surface roughness of membranes [78] and engineering surfaces [156] as well as topographic and geometric investigations of cells [146]. However, the vertical feature size investigated in these studies is in the micro meter range. The same applies to the lateral dimensions of the field of view. Further, these techniques all require either custom glass substrates with special anti-reflective layers, silicon substrates or are rather complex to set up [49].

Indirect spot visualization using fluorophores

The detection of protein binding to peptides is commonly realized by the use of fluorescence markers, which are highly sensitive, but prone to photo bleaching at long or intense exposure [138] and quenching effects at higher concentrations of fluorophore. The fluorophore dye can be designed to bind directly to spectific functional groups of the peptide. In this way, fluorescence signals indicate indirectly the accumulated presence of peptides bearing functional amino groups on the array surface. Another option is to conjugate the fluorophore dye to an antibody. Fluorescent labelled antibodies bind specifically and exclusively to correct synthesized corresponding peptides.

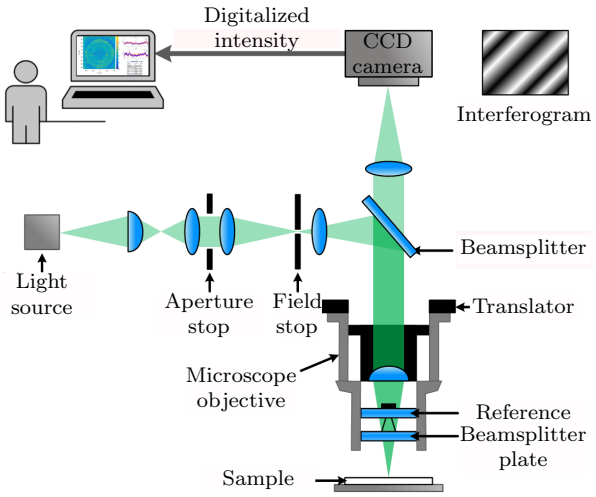

Figure 1.3.1: Sketch of a Vertical Scanning Interferometer with Mirau lens system and a detector array/CCD camera connected to a computer where the obtained interferograms are analyzed by a software and topographic 3D models are calculated. Reprinted with permission [116].

The resulting fluorescence signals therefore indicate the presence and the location of correct synthesized peptides. Overall, fluorescence can not be quantified using these methods and the density or purity of synthesized peptides can not be determined. A statement about density and purity is, to the best of our knowledge, not possible.

Label free spot visualization using VSI

Vertical scanning interferometry (VSI) is an optical technique, which is independent of special substrate coatings and is suitable for glass substrates, which are common for micro arrays. A scheme of the setup can be seen in 1.3.1. VSI uses the interference of two coherent beams of light to determine differences in their optical path length. Therefore, a beam of light is emitted by a light source and separated by a beam splitter, located in the Mirau lens system, into a sample and a reference beam. The sample beam is passing the splitter and is reflected off the sample surface and directed back to the objective, whereas the reference beam is reflected off the splitter. The beams are directed back together and form an interference pattern of dark and light fringes, which are sampled by a CCD camera. The distance between objective and sample and thus the path difference of the respective beams are changed continuously in a scanning motion. The obtained interferograms are analyzed by a software to calculate the surface height pixel by pixel, and topographic 3D models are generated. A z-resolution of down to the subnanometer range can be achieved, while imaging a FOV in the millimeter range.

1.3.3 Application

Peptide arrays are used in a large variety of protein binding studies. They are usually applied for binding studies for either screening for linear epitopes [126, 48, 117, 175], which may qualify as diagnostic markers [23, 104, 100], cell adhesion assays [38], kinase activity assays [4, 63], protease

substrate specifity assays [136], or for the diagnosis of diseases [87]. Also in the identification of food allergens [79] or the study of antigens causing autoimmunity [130, 102]. In recent years, peptide arrays have evolved from mimicking linear epitopes towards simple conformational ones by combinatorial synthesis of circular peptides in array format [24]. This extends the field of application, as has been shown recently for rituximab, a therapeutic antibody for breast cancer treatment [122]. Although, peptide arrays contribute to the investigation of immune responses on a large scale, in the following the focus will be on the investigation of which part of a protein is exactly targeted by an antibody (epitope mapping) down to amino acid resolution (substitution analysis).

Epitope mapping

Epitopes can be classified into two categories [50]: (1) linear epitopes, which might be sequential or continuous, and (2) conformational epitopes, where the amino acids of the epitope are distantly allocated on the sequence, but are close in the 3D native form of the protein. The procedure of screening for antigen specific epitopes is also called epitope mapping and is illustrated in figure 1.3.2. Usually the peptides are synthesized as 15meres to cover all linear epitopes if possible, which are reported to be mainly up to 12 amino acids long [20], with at least three consecutive peptides.

Starting from the linear amino acid sequence of a protein of interest, a peptide array, which displays this sequence as overlapping fragments, is synthesized. The resulting array is then incubated with human serum to allow antibodies to get into contact with the peptides, and bind to them if the amino acid sequence is targeted by the antibody. For peptide spots which have been recognized by human antibodies, the fluorescently labelled secondary antibody can be excited in a fluorescence scanner and emit a fluorescence signal. Bands of consecutive peptide spots exhibiting high fluorescence intensities are a strong indicator for an epitope. The shift in the amino acid sequence in between peptides should be as small as possible, preferably one amino acid, to increase the chance of detecting linear epitopes by facilitating the differentiation between real epitopes and unspecific interactions.

Substitution analysis

The goal of the substitution (or replacement) analysis is to determine those amino acids within an epitope, which are crucial for antibody binding, the so called antibody fingerprint [176]. The analysis was first established in 1987 by Geysen *et al.* [50]. Back then, amino acids were exchanged only against alanine, but nowadays combinatorial synthesis of peptide arrays allows for a complete substitution using all other 19 amino acids. Amino acids, which were found to be crucial for antibody binding, are also named the antibody fingerprint or binding motif. In recent studies, these fingerprints were used to determine the specificity of antibodies towards the viral capsid protein (VP1) of enteroviruses (EVs) [93] and tetanus toxin [117], the read-out of the human antibody

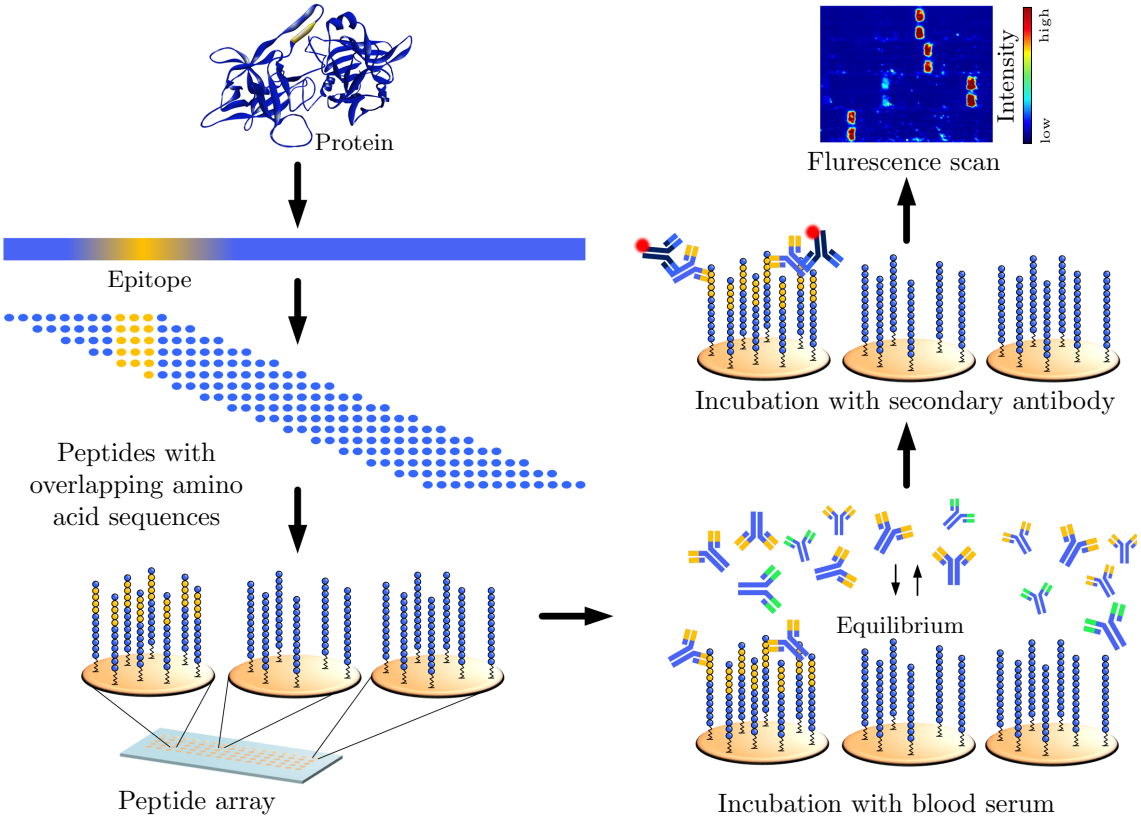

Figure 1.3.2: Work flow of epitope mapping. From the linear amino acid sequence of a protein of interest overlapping fragments are generated, which are synthesized in array format. Every spot contains various copies of one peptide. The peptide array is then incubated with human blood serum. Unbound antibodies are washed away and bound antibody species are detected by incubation with fluorescently labelled secondary antibody, which allow for detection of fluorescence signals. Parts of the figure are based on [174], reprinted with permission.

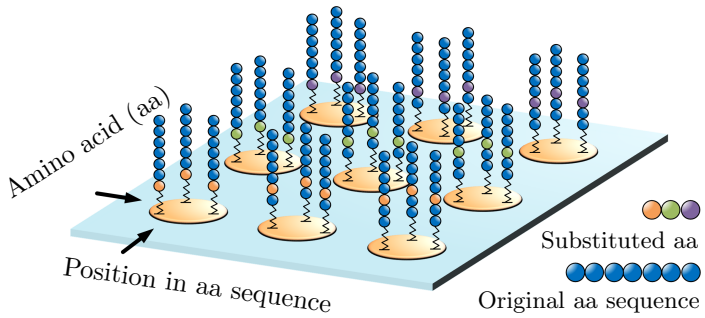

Figure 1.3.3: Scheme of the substitution analysis. Amino acids of the original sequence are depicted as blue spheres, amino acids to be substituted as orange, green and purple spheres. One position of the amino acid sequence is substituted by all other amino acids, while the rest of the sequence remains conserved. Black arrows indicate the column in which the position of the substituted amino acid remains constant, and the row in which the type of the amino acid to be substituted remains constant.

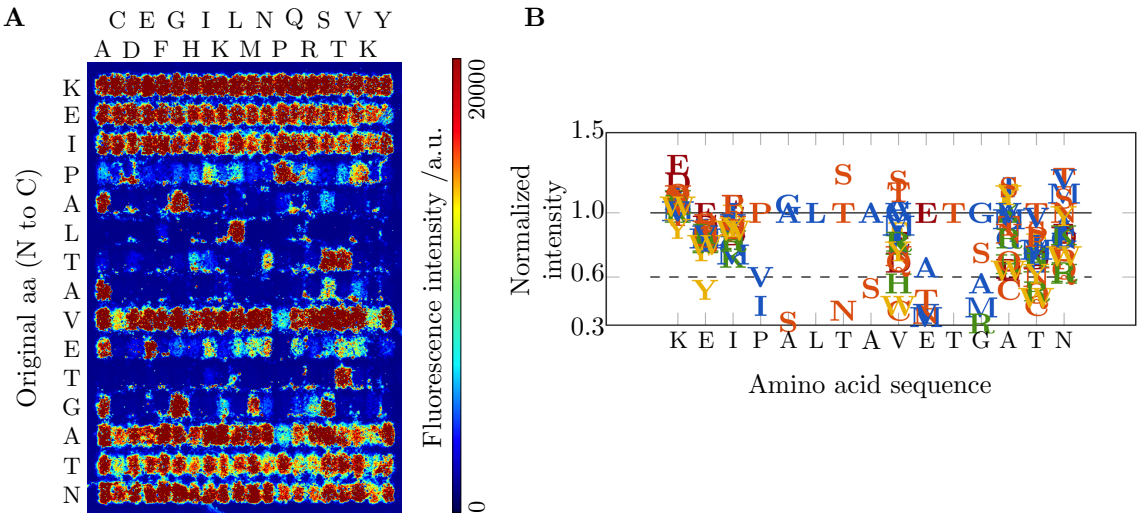

Figure 1.3.4: Example of a substitution analysis. A: Fluorescence scan of a substitution analysis for the antigenic EV peptide KEIPALTAVETGATN. The amino acid position in which the substitution takes place is noted on the left side of the scan (bottom to top is *N*- to *C*-terminal). Amino acids, which were substituted, are noted on top of the scan from left to right. The contrast of the image was adjusted. The scale bar equals 1 mm. B: Normalized fluorescence intensities for every substituted amino acid in regard to the original amino acid for all positions of the motif sequence. From experience, normalized intensities below 0.6 are regarded as negligible. The obtained motif is PALTAxETG.

repertoire [176] and for diagnostic purposes in Lyme disease [175]. They have shown to be helpful to identify potential cross-reactivity of these antibodies, e.g. with human proteins.

For a substitution, every amino acid in a peptide representing a potential epitope, is substituted by all of the other 19 amino acids while the rest of the sequence remains conserved (see figure 1.3.3). For 15mere peptides, this results in 300 peptides (15 x 20 amino acids), which are synthesized in duplicates or triplicates on an array and are incubated with serum. The amino acids, that are crucial for the binding of the specific antibody, can be located since their substitution leads to the loss of antibody binding and thus to the loss of the fluorescence signal. Besides the sequence variants generated in this way, each row also contains the peptide with the original sequence of amino acids. As an example, figure 1.3.4 A shows the fluorescence scan of a substitution analysis of an EV antigenic peptide. In the sixth row from the top (original amino acid is lysin (L)), no fluorescence signals can be observed except for the sequence variant containing the original amino acid. This position is thereby defined as crucial for antibody binding since substitution of the original amino acid leads to the loss of the fluorescence signal. The normalized fluorescence intensity for all duplicates or triplicates of each peptide variant to the original peptide in each row is plotted in figure 1.3.4 B. From experience, normalized intensities smaller than 0.6 are regarded as negligible. The thus obtained antibody fingerprint can be employed to query protein databases for the identification of potential cross-targeted antigens.

1.4 Motivation

Since decades antibodies are used to diagnose diseases. Usually the amount of found pathogen-specific antibodies is therefore quantitated. The measured 'titer' is defined as the highest dilution factor, that still yields a positive reading [166]. Obviously, it is highly relevant for a physician to ascertain, which antibodies were developed by a patient, in order to approach the appropriate therapy. The specificity of diagnosed antibodies provide information on the pathogens, that invaded the patient, whereas the disease status can be derived from the titer: A rising titer hints to an ongoing and acute infection. An unchanged titer indicates a chronic infection, while a falling titer signals, that the patient's immune system managed to successfully tackle the infection. However, when double-checking these widely accepted and very obvious facts, a crucial question arises: How come, that we can diagnose specific infections by using only very few selected antigens? Textbook knowledge teaches, that millions of different antibodies are randomly generated in every human, but obviously the vast majority of different individuals – at least for all of the diagnosable diseases – somehow agree to always target the same or a few selected antigens, although e.g. bacterial pathogens code for thousands of different proteins. One way to refine this – very crucial – question is to investigate exactly, what is targeted by the antibodies of different patients. Nearly all Europeans are vaccinated against tetanus, diphtheria, and pertussis and it is obviously the antibodies of these vaccinated patients, that reduced the once terrifying death toll of these toxins to nearly zero.

This thesis is divided into two main parts. The first part is devoted to the high-throughput screening of disease-specific epitopes and the comparison of antibody fingerprints of different individuals using peptide arrays. Therefore, the peptides as sub-parts of the proteins used to vaccinate patients, were investigated whether they are interacting with patient sera. The amino acid positions within the found peptide-epitopes, mandatory for antibody binding, were then determined. Of special interest are patient sera, that interact with the same pathogen derived peptide (the 'epitope'), but, moreover, even rely on the same amino acids within the peptide's sequence for specific binding (the 'antibody fingerprint'). These different patients would have generated the same or very similar antibody species, whatever the underlying mechanism. The relevance of such a finding is less obvious, but it is certainly reasonable to assume, that an antibody, that is found in different patients and still binds the exactly same antigen, plays an important role in the immune defense.

While the first part deals with the processes to detect peptide-antibody interactions, the second part of this PhD thesis is devoted to the engineering of those interactions in a high-throughput format. Obviously, a peptide array can be equipped with many different diagnostic peptides, which holds the promise to facilitate many different diagnostic tests at the same time and at unrivalled cost. In order to compete with standard testing, however, such an array-based diagnosis should also

quantitate the different antibody species, i.e. it should be possible to identify the pathogen-specific antibodies which are amplified over time, or to the contrary, indicate a victorious immune response. Therefore, an experimental setup is designed to automate the peptide array based immuno assays by using a continous sample flow across the peptide array. This requires the integration of peptide arrays into a microfluidic system and a system to detect antibody-peptide binding. Preliminary studies are performed to establish an automated analysis of antibody concentration on peptide arrays using the designed setup.

One day such an approach might yield a cheap point of care system, that could use a single blood droplet to detect, e.g. all the relevant diseases, and, moreover, inform the nurse or physician about dangerous acute infections.

2 Screening for disease specific peptide-antibody interactions on peptide arrays

Screening for epitopes is of great interest in identifying potential bio markers, therapeutics and in the development of vaccinations. In this chapter the work flow of epitope screening, as applied recently [175, 176], was extended by two validation steps. In the first step, the specificity of the observed interaction and in the second step the specificity of the peptide binding antibody towards the native toxin is examined. As a model system the human immune response of different individuals towards tetanus, diphtheria and pertussis was investigated. For the epitope mapping also cyclic peptides, enabled by recent development in peptide array synthesis, were used for screening. The applied method (section 2.2.4 and 2.2.3 on page 25f) and the results concerning the tetanus toxin were recently published by Palermo and Weber *et al.* [117].
Additionally, the antibody fingerprints of ten individuals towards two motives, which were selected from recent publications, were compared for further immunological insights into antibody specificity among different individuals.

2.1 Model systems

2.1.1 Tetanus, diphtheria and pertussis

All three diseases are caused by bacterial A-B-class exotoxins. The exact epitopes of neutralizing antibodies originating from a tetanus, diphtheria and pertussis (TDP) vaccination are still unknown. For the immunization against tetanus and diphtheria, the toxins are partly denaturized by heat or chemically treatment to produce the antigenic but inactivated form of the toxin, called toxoid. For the immunization against pertussis, two different vaccine types are available. The whole cell vaccine, using killed bacteria cells, and acellular vaccines containing one or more purified pertussis antigens (PT, FHA, PRN and FIM types 2 and 3) [179]. The world health organization (WHO) recommends to start the immunization 6 to 8 weeks after birth by giving three doses of a tetanus, diphtheria and whole cell or acellular pertussis combination vaccine (TDwP or

TDaP) in 4 to 8 weeks intervals followed by a booster $\leq$ six months later [179]. The respective combination vaccines available differ in the bacterial clone used in production, the concentration of antigen components, the purification method and inactivation treatment as well as adjuvants and preservatives [180]. A 84 % global vaccination coverage for TDP was reached in 2011, however the coverage in low- and middle-income countries was reported to be nonetheless poor [94]. The identification of peptides raising neutralizing antibodies against this toxins, could not only contribute to our understanding of the processes involved in the immune response, but in the long term it could also contribute to the development of peptide-based vaccines that have the advantage of being more stable and affordable than protein based ones.

The results of this study are presented in the sections 2.2 Tetanus toxin, 2.3 Diphtheria toxin and 2.4 Pertussis toxin. The tetanus, diphtheria and pertussis toxins were displayed in overlapping amino acid sequences on peptide arrays and incubated with human blood serum. Peptides were synthesized as spot duplicates to account for artifacts. To enable interaction with the *N*- and *C*-terminal parts of the toxin, spacer of alternating glycine and serine (GSGSGSG) were added respectively. To simplify the data analysis, a frame of hemagglutinin (HA) (YPYDVPDYAG [178]) and FLAG (DYKDDDKGG [62]) or enterovirus (KEVPALTAVETGAT [114]) peptides was synthesized as a frame around the array.

2.1.2 LxAxET and PEFxGS motifs

The two epitopes were selected from recent publications due to their strong antibody interaction. The LxAxET motif [93, 176] is an epitope originating from the capsid of the EV genus [131] and the PEFxGS motif originates probably from *Staphylococcus aureus* [176]. These motifs, published by Weber *et al.* [176], were detected by next generation sequencing of a phage display library and possible epitopes were subsequently validated by incubating peptide arrays with the serum of one single individual. To investigate, whether the reported fingerprints are specific for the individual under study or occur in several individuals, substitution analysis was conducted using a larger study population (section 2.5 LxAxET motif and section 2.6 PEFxGSxP motif).

2.2 Tetanus toxin

The tetanus toxin is an exotoxin of the A-B-class, secreted by *Clostridium tetani*, a Gram-positive bacillus found in soil [29]. It blocks inhibitory transmission in the central nervous system [151]. The toxin is produced as an inactive, single chain polypeptide [151] consisting of 1315 amino acids [37], that is transformed to an active di-chain molecule. It is structured in a light chain (Mw: 50kDa), the A-moiety, and a heavy chain (Mw: 100kDa), the B-moiety, which are joined by a disulphide bond [140]. The *C*-terminal part of the heavy chain (H_C) consists of two sub domains (H_C-C and H_C-N). The amino terminal half of the H chain (H_C-N) is responsible for membrane translocation and the carboxyl terminal half of the heavy chain (H_C-C) carries the receptor binding

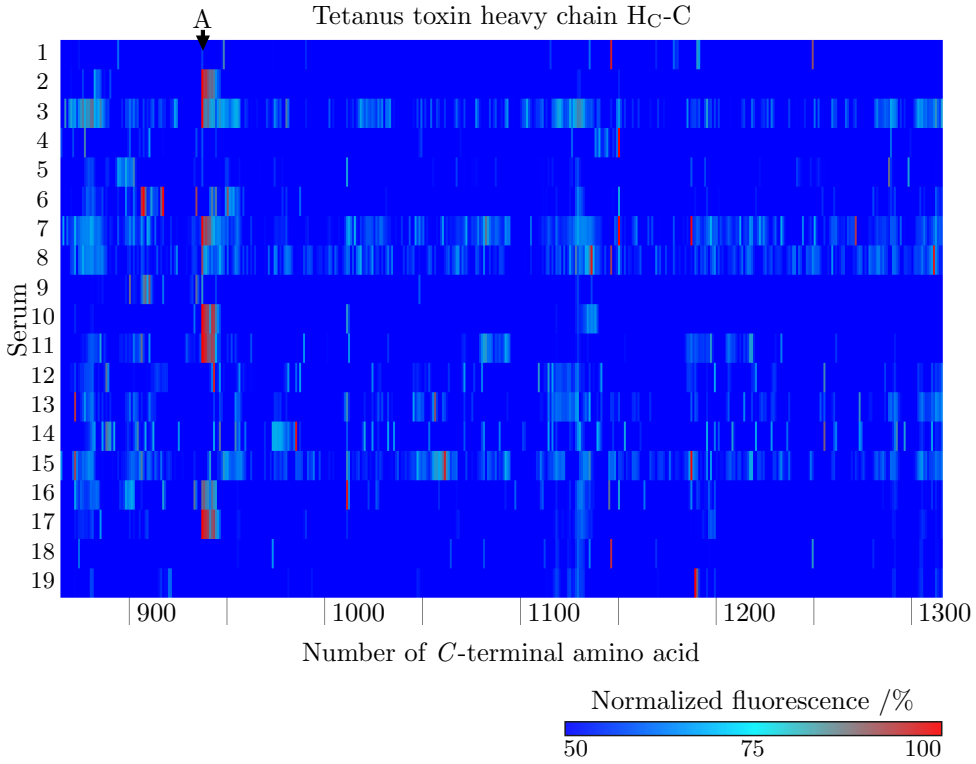

Figure 2.2.1: Heat map of the linear epitope mapping for the tetanus toxin heavy chain amino acids 865 to 1316 for nineteen sera of vaccinated Europeans using 15mere peptides with an overlap of fourteen amino acids. Peptides are numbered according to the number of the peptides C-terminal amino acid in the toxin sequence. Fluorescence intensities were normalized to the respective maximum intensity of each serum. Each row represents the fluorescence intensities of one serum. A prominent band of consecutive peptide spots is marked with the letter 'A'. Heat map on the basis of [117]. Reprinted with permission.

domain [141]. It is not jet fully understood how antibodies are able to neutralize the tetanus toxin, but early studies of monoclonal antibodies from mice suggest that different epitopes are targeted and also synergistic effects of different antibodies lead to its neutralization [170].

2.2.1 Epitope Mapping

In this study, the antibody response of nineteen vaccinated Europeans towards the tetanus toxin, displayed as peptides with overlapping amino acid sequences (15mers with a lateral shift of one amino acid) was investigated. The sera were tested for their IgG tetanus titer by ELISA (see table A.3.1 on page 88 for individual titers). All individuals possessed full protection according to WHO standard [2]. The fluorescence intensity was normalized to the maximum fluorescence intensity of each array respectively. Figure 2.2.1 shows the heat map of the C-terminal half of the heavy chain (amino acids 865 to 1316). The complete heat map is given in figure A.3.1 on page 89 for the light chain and figure A.3.2 on page 90 for the complete heavy chain.

Aside from a broad distribution of interaction between the different sera and peptides, a band of successive peptide spots is targeted by the serum of eight different individuals. One serum, number

9, showed only weak interaction with just the first peptide spots of the before mentioned band. The region containing the identified potential epitope ($_{923}$IHLVNNESSEVIVHK$_{937}$) is located on the *C*-terminal domain of the heavy chain (H_C-C), which was reported to be very likely immunogenic [42]. This region (H_C-C) was also found to be targeted by neutralizing monoclonal antibodies in mice [57, 181]. Lavinder *et al.* simulated the binding of antibodies to H_C-C, and found it is masking the ganglioside binding site, which is responsible for the cell entry of the toxin [84]. The linear epitope identified by them in two vaccinated individuals by epitope mapping with a lateral shift of three amino acids is located on the *C*-terminus of the H_C-C domain ($_{1225}$LRVGYNAPGIPLYKK$_{1239}$) [84]. This sequence did not show any reactivity with any of the nineteen sera tested.

2.2.2 Substitution analysis

The peptide $_{923}$IHLVNNESSEVIVHK$_{937}$ showed interaction with nine out of nineteen investigated sera in the epitope mapping. The individual fingerprints, resulting from the substitution analysis conducted for these nine sera, are depicted in figure 2.2.2. For eight of the nine sera (serum: 1, 2, 4, 5, 7, 10, 15, 16), the fingerprints were highly conserved and resulted in $_{929}$ExxEVIVxK$_{937}$, where 'x' represents an amino acid that is not crucial for antibody binding. Among the sera tested, the interaction with the amino acid H_{936} is less stringent than other positions of the identified fingerprint. As can be seen in figure A.4.1 on page 91 in the appendix. For serum 16 the position H_{936} is not part of the antibody fingerprint since substitution does not result in the loss of fluorescence intensity. Regarding the other sera, it was not possible to correlate amino acid characteristics like hydrophobicity, charge and size with the observed binding behaviour of individual sera for this position (see figure A.4.2 on page 91).
Serum 9 showed a different fingerprint ($_{923}$IxxVN$_{927}$), consisting of only three amino acids (see figure 2.2.2). This could be explained by unspecific interaction or a different HLA type of this patient. In future studies, the HLA type of each serum should be determined and a larger pool of sera should be screened to investigate if a correlation between HLA type and targeted epitopes can be observed.

A query of the "UniProtKb/Swiss-Prot" protein database (release 2016/11 of 30-Nov-16: 553231 entries) with the "ScanProsite tool" [22] for the motif [DE]-x-x-E-[IV]-I-[IV]-[CDEHIMNSTV]-K resulted in 47 hits. The query included splice variants (Swiss-Prot) and excluded fragments. A list of all hits of the query can be found in the appendix table A.4.2 page 92. To screen for potential antigens, proteins originating from *homo sapiens* were excluded, since endogeneous antigens would probably cause a noticeable autoimmune reaction. Apart from *Colstridium tetani*, the human rhinovirus strain 3 and 14 also share the identified motif on the *N*-terminal part of the capsid protein VP1 [132]. The *N*-terminal part was reported to be immunogenic in strain 89 but does not contain the identified motif. The rhino virus strain 14 is less immunogenic [108] and in addition, the motif is located on the inside of the virus, which is not part of the proposed receptor binding or neutralization site [154]. Therefore, due to the great rhinovirus diversity of over 100 strains [118] and the low protection against reinfection, it seems unlikely that eight of nineteen individuals

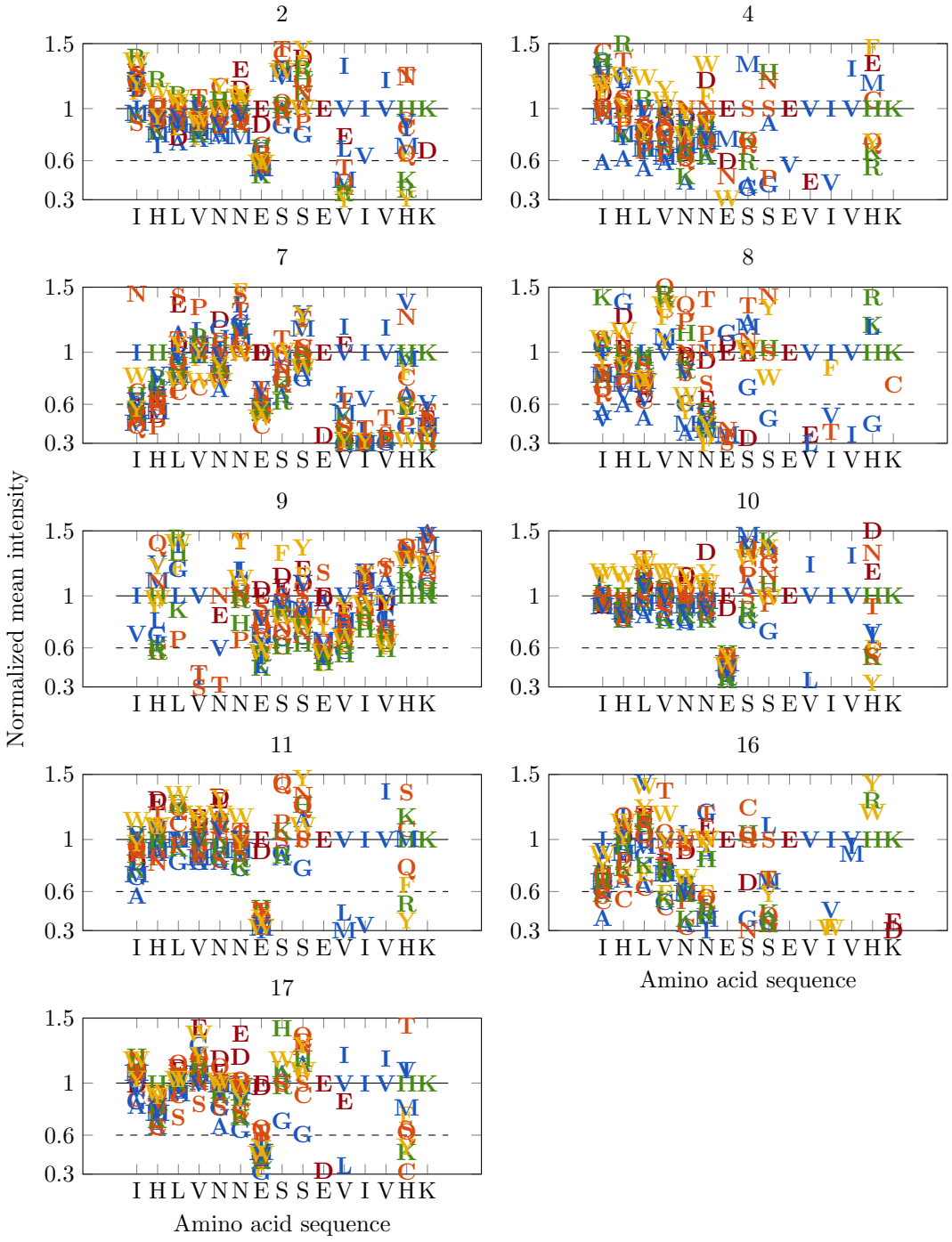

Figure 2.2.2: Fingerprints for $_{923}$IHLVNNESSEVIVHK$_{937}$ of 8 out of 19 sera tested. The relative mean fluorescence intensities are plotted in reference to the original amino acid in the substituted peptide sequence (one letter code). Mean fluorescence intensities were calculated from triplicate spots. The original sequence is depicted on the x-axis. Intensities of peptide variants were correlated to the intensity of the original peptide in each row respectively. Each peptide variant is represented by the letter of the amino acid that was substituted at the respective position. Amino acids are colored according to their chemical properties. Red: negatively charged; green: positively charged; orange: polar, uncharged; yellow: nonpolar, aromatic; blue: nonpolar, alipathic.

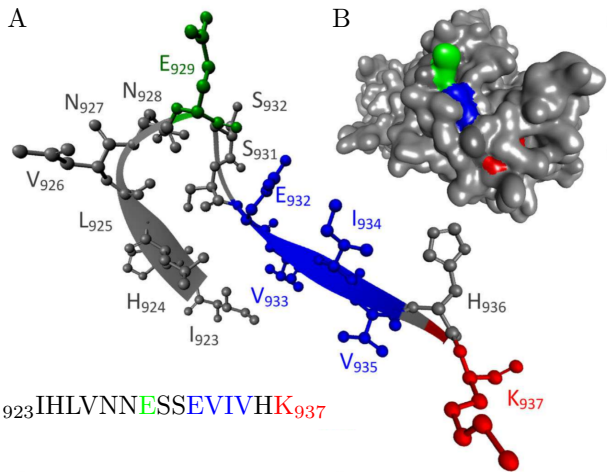

Figure 2.2.3: *Three-dimensional structure of the heavy chain of the tetanus toxin. Conformation of the investigated epitope A) and molecular surface B) are depicted using BIOVIA Discovery Studio client [164] based on RCSB PDB (www.rcsb.org) ID 1A8D [75]. Fingerprint regions identified in the substitution analysis are highlighted in color.* Reprinted with permission.

share the exact same antibody specificity toward only two rhinovirus strains.

In figure 2.2.3, the fingerprint is mapped onto the three-dimensional structure of the tetanus toxin. The conformation of the amino acid sequence in the native toxin is in part a beta strand ($_{923}$IHLV$_{926}$ and $_{933}$VIVH$_{936}$) and in part coil ($_{927}$ENNESSE$_{932}$ and K$_{936}$). The relevant part of the identified antigenic peptide $_{929}$ESSEVIVHK$_{937}$ is located on the protein surface and the amino acids S$_{930}$, E$_{932}$, I$_{934}$ and H$_{936}$ protrude from it. This might indicate that the antigen binding site on the antibody could be an extended or protruding surface.

2.2.3 Validation of antibody-peptide interaction on different surfaces

Based on the data presented in the previous section it remains unclear, whether the observed interaction of serum nine with the identified epitope was specific. In the epitope mapping serum 9 was just interacting with the first peptide of the consecutive band recognized by the other eight sera (see figure 2.2.4 C for comparison). Also the identified potential fingerprint of serum 9 towards $_{923}$IHLVNNESSEVIVHK$_{937}$ consisted of just three amino acids covering a length of just 4 amino acids (figure 2.2.2). Therefore, the interaction was tested on a second peptide array platform using pre-synthesized and purified peptides to exclude unspecific interaction with not completely synthesized amino acid sequences and the array polymer surface. The sequence IHLVNNESSEVIVHK-βA-D-βA-polyethylene glycol-C$_{COOH}$ was spotted onto 3D-Maleimide functionalized surfaces. Further information on the spotting procedure can be found in section 4.1.2 on page 75. As positive control the previously identified sequence MVPEFSGSFPMR [176], containing the PEFxGSxP motif (see section 2.6), was used. Two negative controls were derived from the substitution analysis: IHLVNESSEVIVHR and IHLVNNESSEVIAHK were identified to prevent

the binding of the corresponding antibody species. Each array contained 36 copies of each of the

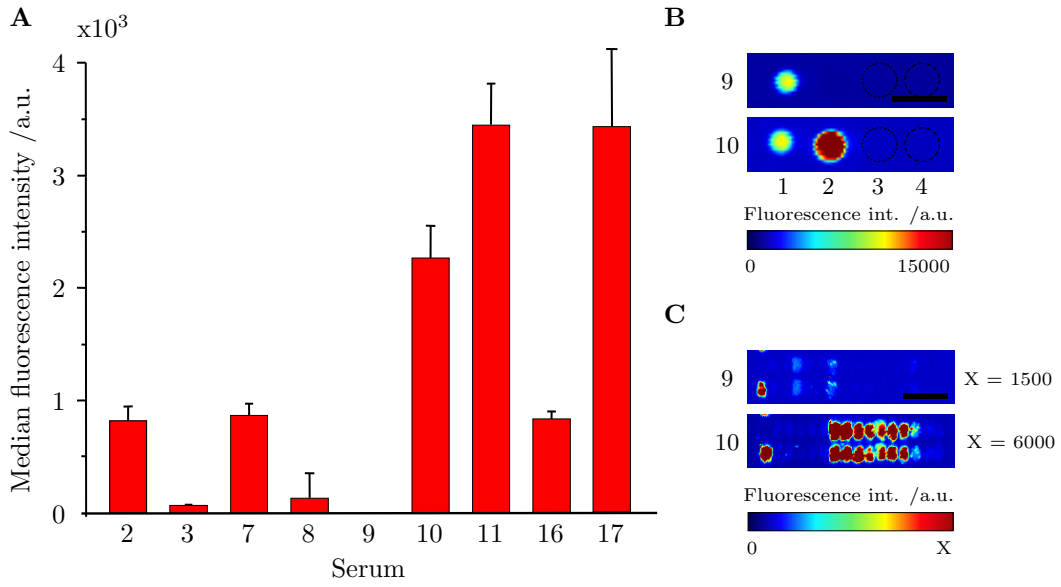

Figure 2.2.4: Validation of the serum interaction towards the identified epitope on a spotted peptide array. Four different pre-syntheized and purified peptides have been spotted onto 3D-Maleimide surfaces: 1: MVPEFSGSFPMR positive control [176]. 2: $_{923}$IHLVNNESSEVIVHK$_{937}$, antigenic peptide used for the isolation of antibody species and representing the identified epitope. 3: IHLVNNESSEVIVH**R**: first negative control. 4: IHLVNNESSEVI**A**HK, second negative control. Amino acids differing from the sequence of the antigenic peptide (2) are highlighted through bold letters. Arrays consisted of 36 spots per peptide. A: Median fluorescence intensity of peptide 2 for the nine sera that showed interaction with the identified epitope in the epitope mapping. No fluorescence was detected for serum 9. B: Detail of the fluorescence scan of the peptide array showing the four spotted peptides incubated with serum 9 and 10 respectively. Scale bar represents 0.5 mm. C: Detail of the fluorescence scan of the epitope mapping showing the band of consecutive peptide spots incubated with serum 10 and the equivalent spots incubated with serum 9. First single spot in the section belongs to the control frame. Contrast was adjusted for each detail individually and maximal intensity in a.u. is 1500 and 6000 for serum 9 and 10 respectively. Scale bar represents 1 mm. Based on [117] and reprinted with permission.

four before mentioned peptides. Figure 2.2.4 shows the background corrected median fluorescence intensities for the respective sera. Except for serum 9, the other eight sera exhibited interaction with the peptide representing the identified epitope. Regarding the negative controls, very weak to no interaction was detected. Therefore, it can be concluded that the interaction of serum 9 and the identified epitope is not specific.

2.2.4 Verification of antibody specificity towards native toxin via alternative arrays

To determine, whether the interaction of antibody species with the identified epitope was induced by the tetanus vaccination, the antibody species was isolated from serum using batch chromatography and their specificity towards the native tetanus toxin was validated by enzyme-linked immunosorbend assay (ELISA). The purification and isolation of antibody species included two chromatography steps. In the first step, protein G was used to purify the IgG and remove all the other serum components. In the second step, the amino acid sequence IHLVNNESSEVIVHK

was pre-synthesized and immobilized on the chromatography resin to isolate specifically antibodies binding to this epitope. Details on the process can be found in section 4.4 on page 78. The donor of serum 11 received a tetanus vaccination prior to the next serum donation. Anti tetanus IgG titer raised from $1.0\,\mathrm{IU\,ml^{-1}}$ before vaccination to $4.7\,\mathrm{IU\,ml^{-1}}$ six month after vaccination. The post-vaccination serum was purified and the concentration of isolated antibody species was calculated from OD_{280} to be $0.053\,\mathrm{mg\,ml^{-1}}$. The efficiency of the isolation was controlled by incubating the isolated antibody species on a peptide array containing the peptides of the epitope mapping. The fluorescence scan can be seen in figure A.5.1 on page 104. Fluorescence signals were observed solely for peptides containing the identified ExxEVIVxK motif.

In the tetanus ELISA experiment, the isolated antibody species resulted in an OD_{450} of 0.85 at a dilution of 1:2, which is comparable to the OD_{450} of 0.74 for the respective serum prior to purification at a dilution of 1:1000. This verifies their ability to bind to the native tetanus toxin and thus suggests that the identified motif does originate from vaccination with the tetanus toxoid.

More information about the tested individuals would be desirable to correlate for example HLA sero type, vaccine type used for vaccination and a history of other infections to the fact that an individual targets the identified epitope.

2.3 Diphtheria toxin

The diphtheria toxin is produced by a phage, which is infecting *Corynebacterium diphtheriae* as a single polypeptide chain of about 62 kDa [1] and with a total length of 567 amino acids [54] (including the 32 amino acid long leader peptide which is not part of the native diphtheria toxin). Like the tetanus toxin, the diphtheria toxin is an A-B class toxin, that catalyzes the covalent attachment of the adenosin diphosphate (ADP) ribose moiety of nicotinamide adenine dinucleotide (NAD) to eucariotic elongation factor 2 (eEf-2) after activation. The A-moiety contains the *N*-terminal catalytic domain C, and the B-moiety the *C*-terminal receptor-binding domain R and a central translocation domain T [10]. It was shown earlier, that the A-moiety contains an immunodominant epitope for B cells [167], and the B-moiety contains a T-cell epitope [15] as well as fragments which, when expressed as synthetic peptides, showed reactivity in proliferation assays on unselected $CD4^+$ cells [127]. However it is still unclear which epitopes are targeted by antibodies that neutralize the diphtheria toxin. Also there is only little correlation between ELISA data detecting IgG and toxin neutralization assays [147].

2.3.1 Epitope mapping

Therefore, the antibody response of nineteen vaccinated Europeans towards the diphtheria toxin was investigated using peptide arrays. Anti-diphtheria IgG titer was determined by ELISA for

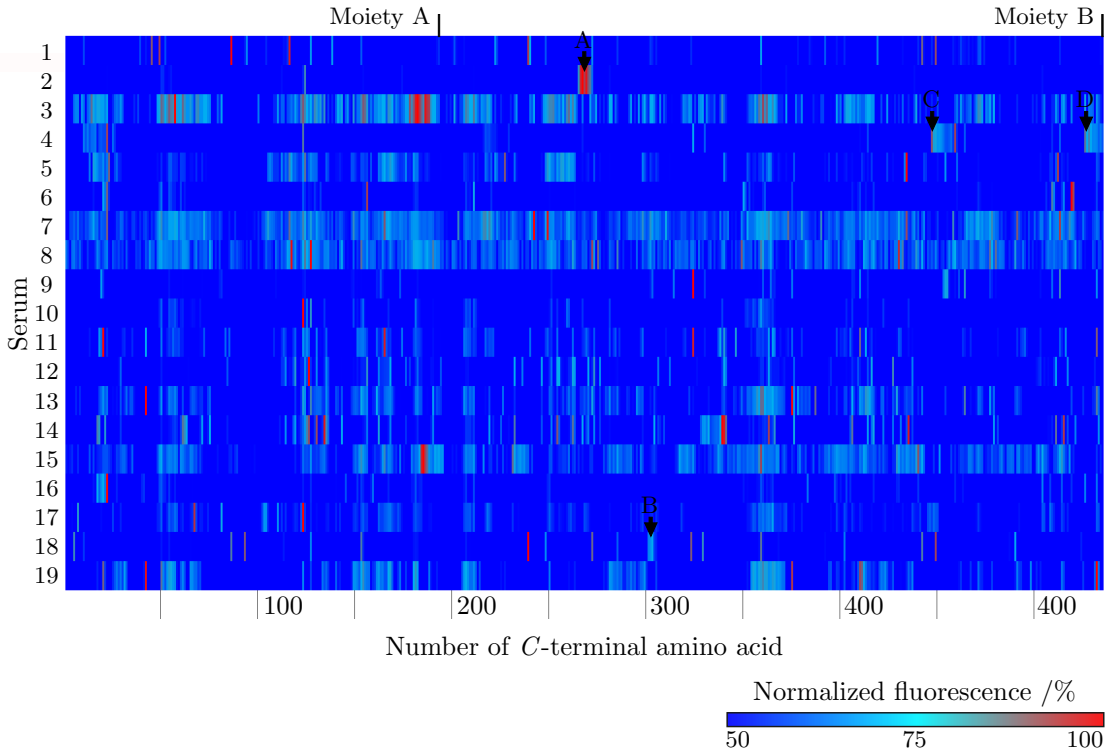

Figure 2.3.1: Heat map of the linear epitope mapping of diphtheria toxin for sera of nineteen vaccinated Europeans using 15mere peptides. From left to right, the peptides represent the linear sequence of amino acids of the toxin as overlapping fragments with a lateral shift of one amino acid (excluding the leader peptide). Fluorescence intensities were normalized to the respective maximum intensity of each serum. Arrows indicate distinct fluorescent bands of consecutive peptides for individual sera.

all sera. Except for serum 12, the titers of all sera indicate full protection against diphtheria. Individual titers are listed in the appendix table A.3.1 on page 88. For the epitope mapping, the complete amino acid sequence (567 amino acids [54]) was designed as linear 15 and 20mere peptides as well as cyclic 7, 10 and 13mere peptides with a lateral shift of one amino acid.

Linear 15mere peptides

Normalized fluorescence intensities are presented in figure 2.3.1. Normalized intensities appear to be quite high, but this results from the narrow distribution of absolute intensities and the normalization to the highest signal for each serum respectively. For some sera, a band of consecutive fluorescent peptide spots was observed and marked with arrows in figure 2.3.1. A band of approximately five consecutive peptide spots (residues 252 to 270) interacting with serum 2 and 17, is flagged by 'A'. The range (residues 287 to 302) is flagged by 'B' and interacting with serum 18. For serum 4, two bands of consecutive peptide spots have been identified. The first band 'C', ranges from residue 433 to 451 and the second 'D', from 512 to 532. Range C is overlapping with the sequence $_{431}$GVLLPTIPGKLDYNKSKTHI$_{450}$, which was reported to be a CD4$^+$ cell epitope recognized by 63 % to 71 % of the 99 individuals tested [33]. For C and D, the band of consecutive peptides shows a decrease of fluorescence intensity from left to right, as expected. However,

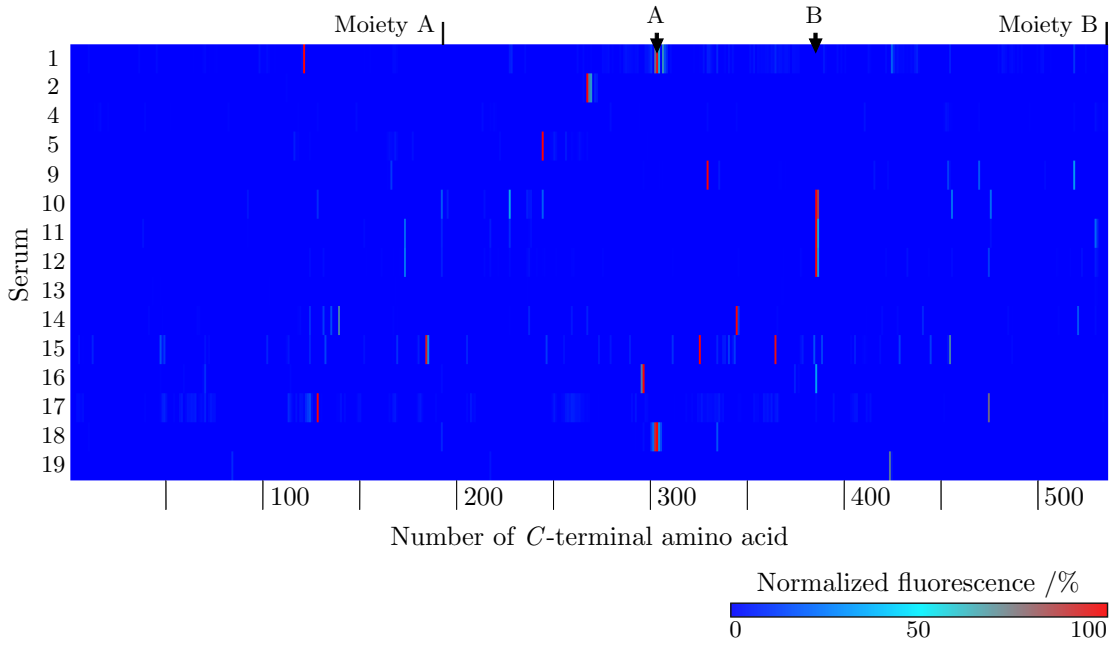

Figure 2.3.2: Heat map of the linear epitope mapping of toxin for sera of 15 vaccinated Europeans using 20mere peptides. From left to right, the peptides represent the linear sequence of amino acids of the diphtheria toxin as overlapping fragments with a lateral shift of one amino acid. Fluorescence intensities were normalized to the respective maximum intensity of each array. Arrows indicate fluorescent peptide spots coinciding in two (A) or three (B) sera.

the single peptide, flanking the bandes on the right side and exhibiting a fluorescence intensity comparable to the maximal intensity of the band, is unusual.

Summarizing, only little match between different individuals could be observed (A) and no distinct epitope, recognized by multiple sera, was identified.

Linear 20mere peptides

Perera and Corbel [121] reported the reaction of human serum to a 17mere peptide (residues 141 to 157) of the A-moiety in immunoblotting experiments. To exclude the peptide length as cause for the lack of detected significant interaction, the mapping was repeated for fifteen of the before tested nineteen sera using linear 20mere peptides. The pre-staining showed strong interaction of the secondary antibody with peptides containing *C*-terminal lysines. This might be caused by unspecific interaction between the negatively charged fluorophore and the amino acid lysine, which is positively charged at neutral pH. To account for this, fluorescence signals resulting from the pre-staining were subtracted from those of the main staining. Peptides, which showed fluorescence intensities twice the average signal intensity in the pre-staining, were excluded from further evaluation. The corresponding normalized fluorescence intensities are depicted in figure 2.3.2. After excluding signals resulting from the pre-staining, only few peptide-serum interactions remained. Also the absolute fluorescence intensities are weak compared to the controls. The arrow marked with 'A' in figure 2.3.2 is flagging a band of ≈ seven consecutive fluorescent peptide spots ($_{283}$VNVAQVIDSETADNLEKTTA$_{302}$) appearing for serum 1 and 18. This sequence was

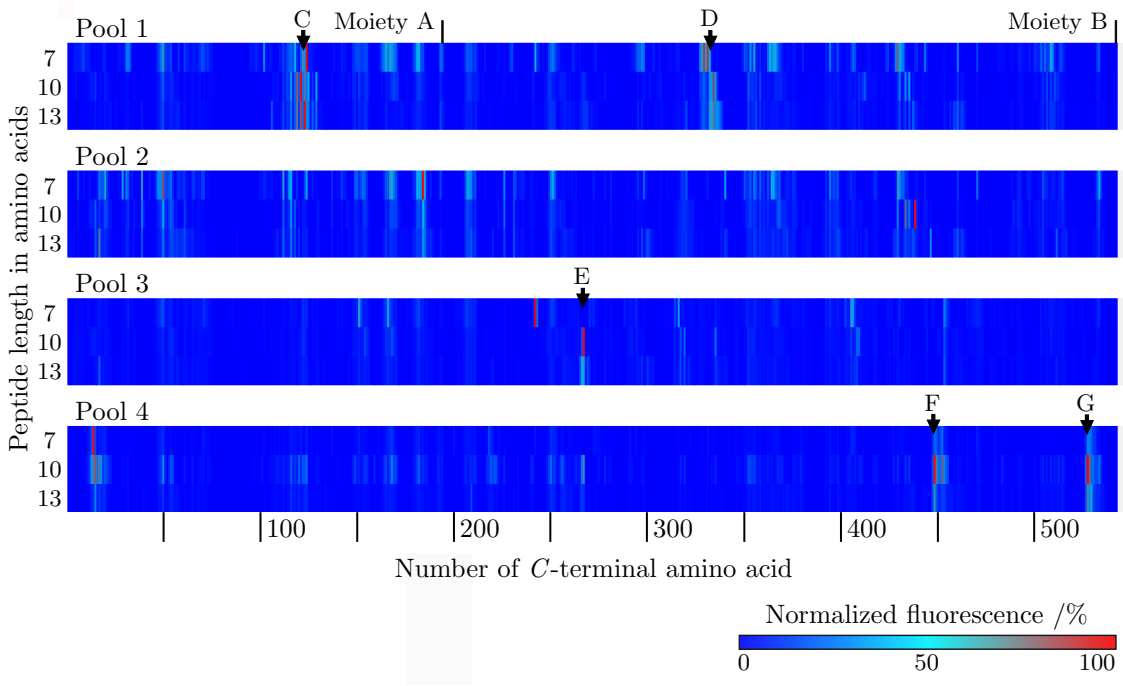

Figure 2.3.3: Heat map of the cyclic epitope mapping of diphtheria toxin. Sera of 19 vaccinated Europeans were pooled and incubated on peptide arrays containing cyclic 7mere, 10mere and 13mere peptides. From left to right, the peptides represent the linear sequence of amino acids of the diphtheria toxin as overlapping fragments with a lateral shift of one amino acid. Fluorescence intensities were normalized to the respective maximum intensity of each array. Arrows indicate distinct fluorescent bands of consecutive peptides. Pool 1: serum 1, 2, 3, 19, 11. Pool 2: serum 14, 4, 5, 12, 13. Pool 3: serum 17, 6, 7, 16. Pool 4: serum 8, 9, 18, 10, 15.

previously detected for serum 18 in the epitope mapping using 15mere peptides (b). Fluorescence signals for the sequence $_{366}$NLFQVVHNSYNRPAYSPGHK$_{385}$ marked with 'B' in figure 2.3.2, can be observed for the sera 10 to 12. This sequence was introduced by Pillai *et al.* [15] as T-cell epitope. However, the absolute fluorescence intensities for the respective peptide spots are low compared to controls and no distinct band of consecutive spots was observed. It has to be further investigated whether this interaction is specific. Since no promising potential epitope, recognized by several sera, was identified using linear peptides, the epitope mapping was extended to cyclic peptides. Triebel *et al.* hypothesize, that diphtheria epitopes are mainly conformational [8].

Cyclic peptides

To investigate the interaction of serum antibodies with simple conformational fragments of the diphtheria toxin, cyclic 7mere, 10mere and 13mere peptides with a lateral shift in the sequence of one amino acid were applied for epitope mapping. The results are presented in figure 2.3.3. Since the array content is increasing threefold due to different peptide lengths (7mere, 10mere and 13mere), the human sera were pooled in four groups. Again a significant interaction of the secondary antibody was observed for the pre-staining, and these regions were treated as described before. The average fluorescence intensity for pool 2 and 3 was low compared to the

Table 2.3.1: Prominent regions of the epitope mapping of the diphtheria toxin using linear and cyclic peptides of different lengths. Amino acids being part of coil structures are printed in bold.

Region	Type	Pool	Length	Amino acid sequence
A	linear		20	$_{283}$VNVAQV**ID**SETA**DN**LEKTTA$_{302}$
C	cyclic	1	7, 10, 13	$_{113}$**GLSLTEP**LMEQ**VGT**EEF$_{123}$
D	cyclic	1	7, 10, 13	$_{329}$AV**HHNT**EEIVAQSIALS$_{336}$
E	cyclic	3	10, 13	$_{255}$**LEH**PELSELKTVT$_{267}$
F	cyclic	4	7, 10, 13	$_{436}$**TIPGK**LDV**NKSKT**HISV$_{452}$
G	cyclic	4	7, 10, 13	$_{515}$QKTV**DH**TKVNSKLSL$_{529}$

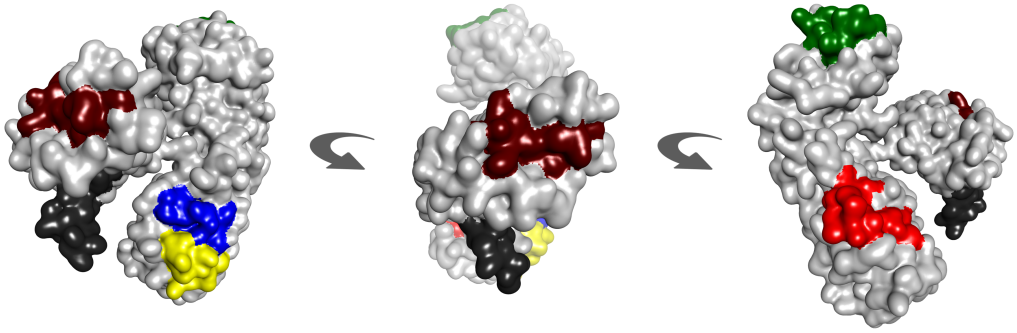

Figure 2.3.4: Mapping of the prominent regions onto the molecular surface of the diphtheria toxin. The toxin is displayed in different angles. Regions are coloured as follows: A red, C green, D blue, E yellow, F ruby and G black. Depicted using BIOVIA Discovery Studio client [164] based on RCSB PDB (www.rcsb.org) ID 1SGK.A [10].

controls. Five regions consisting of consecutive peptides were observed for individual serum pools and varying peptide length (see table 2.3.1). Region F is partly overlapping the amino acid sequence ($_{431}$GVLLPTIPGKLDYNKSKTHI$_{450}$), which was found to be reacting with CD4$^+$ cells of all human individuals tested by Raju *et al.* [127]. For region D an overlap of the six *C*-terminal amino acids to another CD4$^+$ epitope was noted [127]. To better estimate, whether these regions are specific for individual sera or can be correlated to the reported epitopes, the epitope mapping using cyclic peptides should be repeated for each serum respectively.

In figure 2.3.4 the identified regions are mapped onto the 3D structure of the diphtheria toxin. The regions are flanked by sequence loops and are exposed to the protein surface.

Within the scope of this study, no prominent potential linear epitopes across samples have been found for the diphtheria toxin by using up to 20mere peptides on peptide arrays. However the mapping of cyclic peptides, mimicking coils as simple conformational structures, resulted in five regions, which might be worth of further investigations.

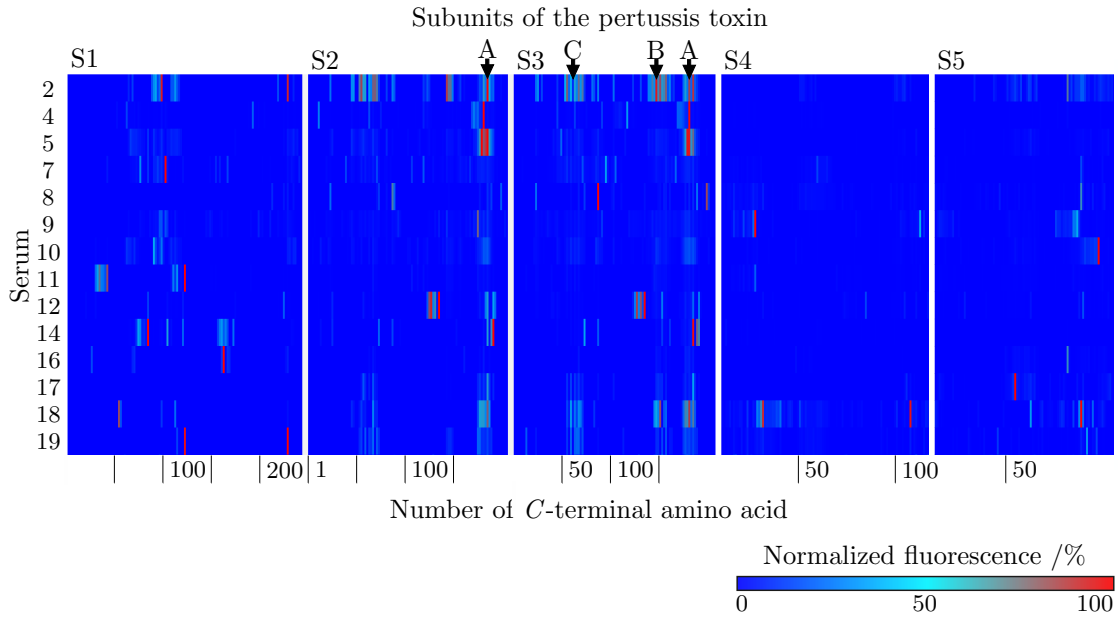

Figure 2.4.1: Heat map of the linear epitope mapping of the pertussis toxin for fifteen sera of vaccinated Europeans using 15mere peptides. From left to right, the peptides represent the linear sequence of amino acids of the toxin as overlapping fragments with a lateral shift of three amino acid. Fluorescence intensities were normalized to the respective maximum intensity of each serum. Each row represents the fluorescence intensities of one serum. Prominent bands of consecutive peptide spots were marked with letters according to their sequence similarities.

2.4 Pertussis toxin

The pertussis toxin is produced by *Bordetella pertussis*, and plays a major role in the pathogenesis of the whooping cough [89]. It belongs to the A-B-class of toxins and is structured as hexamer, consisting of five individual sub units (S1 - S5) and two copies of S4 (total MW 150 kDa [107]. S1 represents the A-moiety which expresses a ADP-ribosyltransferase activity using NAD as the ADP-ribose donor [89]. The B-moiety is comprised of the S2 and S4 units which are connected by S5 to S3 and S4 [28]. The amino acid sequence of S3 and S3 are up to 70 % identical [107]. It was suggested that S2 and S3 are likely to be involved in the receptor binding sites [89]. In mice, the regions of amino acids 1 to 17 and 169 to 186 of S1 have shown to be neutralizing epitopes [7].

2.4.1 Epitope mapping

In this study, the antibody response of fourteen vaccinated Europeans towards the pertussis toxin was investigated. An anti-pertussis antibody titer was determined for all individuals involved in this study (see table A.3.1 page 88 in the appendix) by ELISA. According to WHO standards the titers of all tested individuals correlate with long term protection [2]. The sequence of all five sub units (865 amino acids [160]) was divided into two parts. The first part contained the sub units 1 to 3, and the amino acid sequence was synthesized as overlapping 15mere peptides with a lateral shift of three amino acids. In the second part, sub unit 4 and 5 were also synthesized as 15mere

Table 2.4.1: Prominent regions of the epitope mapping of the pertussis toxin. Amino acids being part of coil structures are printed in bold.

Region	**Subunit**	**Amino acid sequence**
A	2	$_{164}$RVHVSKEEQY**YDYEDATFE**TYALTGISICN$_{193}$
	3	$_{164}$RVHVSKEEQY**YDYEDATFQ**TYALTGISLCN$_{193}$
B	3	$_{129}$SVIGAC**ASPYEGRYRDM**YDALRRLLYMIYMS$_{159}$
C	3	$_{41}$LQTYLRQI**TPGWS**IYG**LYDG**TYL**GQAYGG**II$_{71}$

peptides, but due to fewer total number of amino acids the lateral shift was reduced to one amino acid. The results are presented in figure 2.4.1.

The overall fluorescence intensity for all arrays within this experiment was rather low. A broad distribution of interaction between antibodies of different samples and peptides was observed for S1. On S2 and S3, four regions can be identified consisting of bands of consecutive fluorescent spots. This regions can be reduced, according to the similarity of their amino acid sequences, to three prominent regions (A, B, C in figure 2.4.1). Table 2.4.1 lists the amino acid sequences of the identified regions. The most noticeable region A, identified in six sera, differs in just one amino acid on the respective sub unit (S2: E_{182}; S3: Q_{182}). Region B and C were identified in three sera respectively. They also have an equivalent on S2, which differ in four of eleven amino acids being part of a coil structure for region B and and twelve of fifteen amino acids being part of coil structures for region C. However, the obtained absolute fluorescence intensities of the regions B and C on S2 are notably weaker than on S3 and were therefore neglected.

The identified regions were mapped onto the surface of the pertussis toxin to check their surface accessibility. All amino acids located on coils show a surface accessibility for all regions on S2 and S3 (see figure 2.4.2). The *N*-terminal part of the identified region A on S3 was found to induce pertussis toxin recognizing antibodies in mice and rabbits, when vaccinated with a synthetic peptide (164 to 174 [27] and residues 164 to 178 [144] respectively). The so induced antibodies were also found to be neutralizing in mice (residues 149 to 174) [27]. For region B, some parts are reported to be targeted by anti-pertussis sera in ELISA and immunoblot experiments (residues 134 to 149 [144]) but antibodies induced by a synthetic peptide failed to bind the native toxin in an ELISA experiment (S3 residues 123 to 154 [27]). Antibodies raised against the synthetic peptide S3.41-64 (S3 residues 37 to 64 corresponding to the identified region C) in mice also were able to bind the native toxin in ELISA [27], and the residues 35 to 50 elicited pertussis toxin recognizing antibodies in rabbits [144].

To further investigate, whether the identified regions contain potential human epitopes, a substitution analysis of the respective sequences was performed (see section 2.4.2).

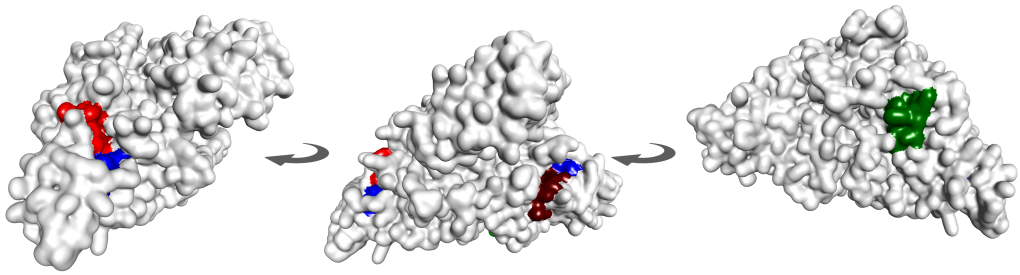

Figure 2.4.2: Mapping of the prominent regions A, B, C onto the molecular surface of the pertussis toxin. The toxin is displayed in different angles. Region A is coloured in bright (S2) and in dark red (S3), region B in green and C in blue. Depicted using BIOVIA Discovery Studio client [164] based on RCSB PDB (www.rcsb.org) ID 1PRT [75].

2.4.2 Substitution analysis

The previously identified regions A, B and C (section 2.4, page 31) were split in overlapping fragments, as can be seen in table 2.4.2, and investigated in a substitution analysis. The sera 8, 16 and 17 were excluded, since they did not show any significant interaction with the regions A - C in the epitope mapping. A table, summarizing which peptide was substituted for which serum, can be found in the appendix table A.4.1 on page 92. For the 44 conducted substitution analysis, only five resulted in detectable fluorescence signals. Serum 4 was interacting with P2, P4 and P6 and serum 18 with P2 and P6. Except for serum 4 on P2 the overall fluorescence intensity of the other four substitution analysis was very weak compared to the controls. The resulting normalized mean intensities are depicted in figure 2.4.3. For serum 4 on P4 and serum 18 on P2 no distinct fingerprint can be obtained.

The other substitutions resulted in short fingerprints, consisting in two to five amino acids spread across a length of two to six amino acids. Serum 4 is interacting with $_{168}$SK$_{169}$ on P2, but not with its equivalents on P3 and P4, which are shifted six and twelve amino acids in the direc-

Table 2.4.2: Sequences of the peptides P1-P8 which were tested in the substitution analysis for the pertussis toxin. Peptides were derived from the previously identified regions A, B and C covering the respective regions of highest overall fluorescence intensity.

Name	Sequence
Region A	$_{164}$RVHVSKEEQYYDYEDATFETYALTGISICN$_{193}$
P1	$_{173}$YYDYEDATFETYALT$_{187}$
P2	$_{167}$VSKEEQYYDYEDATF$_{181}$
P3	$_{161}$ISVRVHVSKEEQYYD$_{175}$
P4	$_{155}$LIYVAGISVRVHVSK$_{169}$
Region B	$_{129}$SVIGACASPYEGRYRDMYDALRRLLYMIYMS$_{159}$
P5	$_{136}$PYEGRYRDMYDALRR$_{150}$
Region C	$_{41}$LQTYLRYITPGWSIYGLYDGTYLGYAYGGII$_{71}$
P6	$_{49}$TPGWSIYGLYDGTYL$_{63}$
P7	$_{53}$SIYGLYDGTYLGQAY$_{67}$
P8	$_{57}$LYDGTYLGQAYGGII$_{71}$

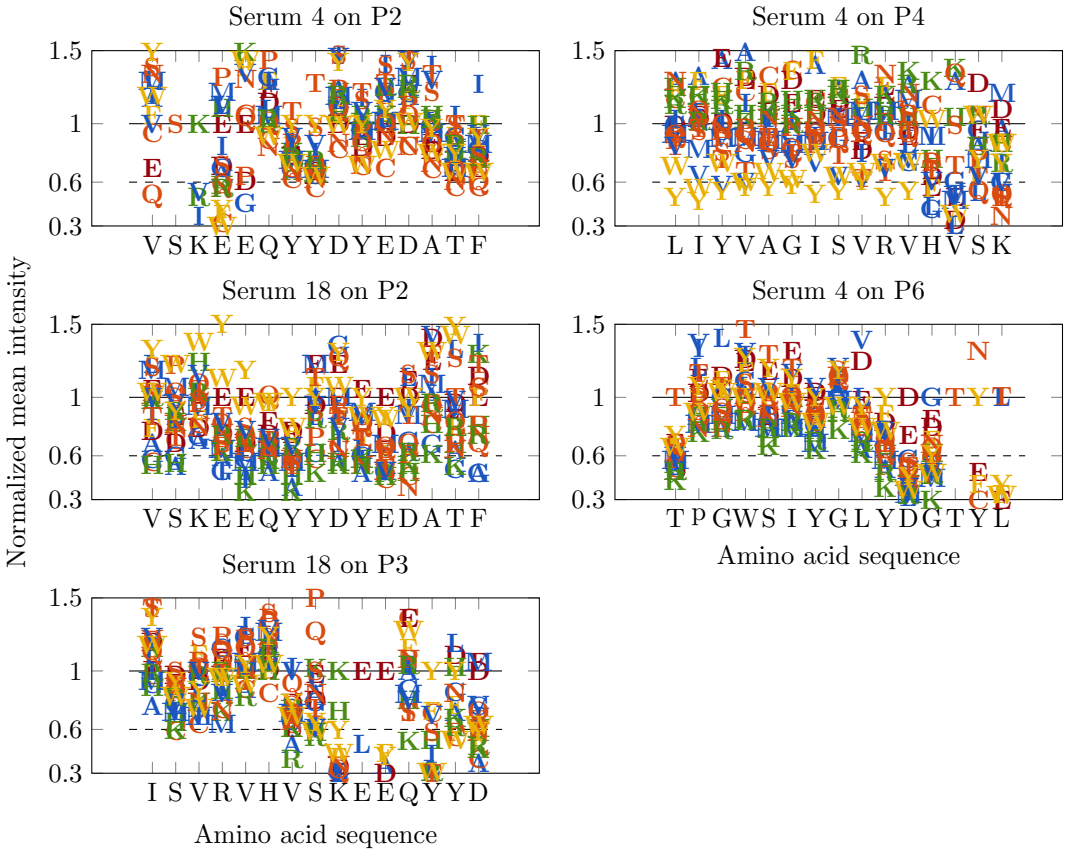

Figure 2.4.3: Results of the substitution analysis of the regions A, B, C (section 2.4) of the pertussis toxin. The relative mean fluorescence intensities are plotted in reference to the original amino acid in the substituted peptide sequence (one letter code). Mean fluorescence intensities were calculated from two copies of the substitution analysis located on two different slides of the same batch, for each serum respectively. The original sequence is depicted on the x-axis. Intensities of peptide variants were correlated to the intensity of the original peptide in each row respectively. Each peptide variant is represented by the letter of the amino acid that was substituted at the respective position. Amino acids are colored according to their chemical properties. Red: negatively charged; green: positively charged; orange: polar, uncharged; yellow: nonpolar, aromatic; blue: nonpolar, alipathic.

tion of the N-terminus respectively. In addition, the number of amino acids crucial for antibody binding is only two, which suggests that the observed interaction is unspecific. This also applies to serum 18, which is interacting with P2 and P3 (but not P4) where the substitution of P2 does not reveal any fingerprint while P2 does contain the amino acids identified as crucial on P3. No conclusion can be drawn, whether the interaction could be specific or not.

Quality issues of the peptide arrays can be ruled out, since the experiment was repeated on two batches of arrays and the fluorescence intensity of the HA control was sufficiently high. Also the serum was freshly defrosted for the experiment. In further studies, the specificity of serum-peptide interaction for the peptides P1-P8 derived from the identified regions A, B and C in the epitope mapping should be verified on a different functionalized surface with pre-synthesized and purified peptides (as described for tetanus in section 2.2.3 on page 24). Also the sequence overlap of peptides covering the regions could be increased and a lower dilution of serum could be tested.

2.5 LxAxET motif

The LxAxET motif originates from the capsid of the EV genus [131]. EVs are a genus of small, positive-sense single-stranded RNA viruses in the *picornavididae* family. The large number of antigenic distinguishable members of the EV genus have been categorized as EV serotypes [40]. The most popular groups of serotypes are the polioviruses, Coxsackie viruses, rhinovirus and echovrius. The virus capsid is non-enveloped, about 300 Å in diameter [60] and consists of four virus structural proteins VP1, VP2, VP3 and VP4 [61] whose 60 copies are arranged to form the virus icosahedral capsid [95]. The capsid protein VP4 is located on the inner surface of the capsid and is essential for virion stability [93], whereas VP1 interacts with host cell receptors to provide virion attachment to target host cells. VP1, VP2, and VP3 differ mainly in the amino acid sequence of the loops, which connect the beta-strands with the *N*- and *C*-terminal sequences extruding from the beta-barrel domain and give the enterovirus its distinct antigenicity [93].

2.5.1 Substitution analysis

In this study, the LxAxET motif containing EV antigenic peptide $_{615}$KEIPA**L**T**A**V**ET**GATN$_{629}$ (VP1) [114, 99] was chosen for substitution analysis. The amino acid sequence originates of the capsid protein VP1 of the polio virus (Sabine strain 3) and substitution was conducted for sera of ten individuals. The obtained fingerprints are depicted in figure 2.5.1 page 36. Their homology in between different individuals is striking. A comparison of the most conserved amino acids among the fingerprints of all individuals, resulted in the fingerprint PALT(A)xET, in which x stands for a position not crucial for the antibody recognition and amino acids in brackets are considered to be part of the fingerprint for half of the investigated individuals. This fingerprint differs from the one reported by Weber *et al.* (LxAxET). The increased number of investigated samples and the amino acid sequence tested could be a reason for this. Weber *et al.* used thirteen different 12mer peptides in the substitution analysis, which resulted from a phage display screening and tested one patient serum. A query of the "UniProtKb/Swiss-Prot" protein database (release 2016/11 of 30-Nov-16: 553231 entries) with the "ScanProsite tool" [22] for the motif [PV]-[ASG]-[LAM]-[TS]-[ASGDEF]-[AGSVIL]-E-[TVI]-[GS] resulted in 48 hits. The query included splice variants (Swiss-Prot) and excluded fragments. A list of all hits of the query can be found in the appendix table A.4.3 page 95. To screen for potential antigens, proteins originating from *homo sapiens* were excluded, since endogenous antigens would probably cause a noticeable autoimmune reaction. Also proteins originating from exotic microorganisms and mammals and plants were excluded, since intra cellular enzymes or other proteins of mammals or plants enter the human body via the digestive system and are thus denatured during digestion. After applying these restrictions, capsid proteins of the Coxsackievirus, Echovirus and Poliovirus remained. Figure 2.5.2 shows the mapping of the fingerprint onto the three-dimensional structure of the assembly of VP1-VP4. It reveals that the amino acids of the identified fingerprint are either part of beta strands ($_{624}$ETG$_{626}$) or coils ($_{615}$KEIPALTAV$_{623}$ and $_{627}$ATN$_{629}$). The conformation of the sequence is a U-turn, as

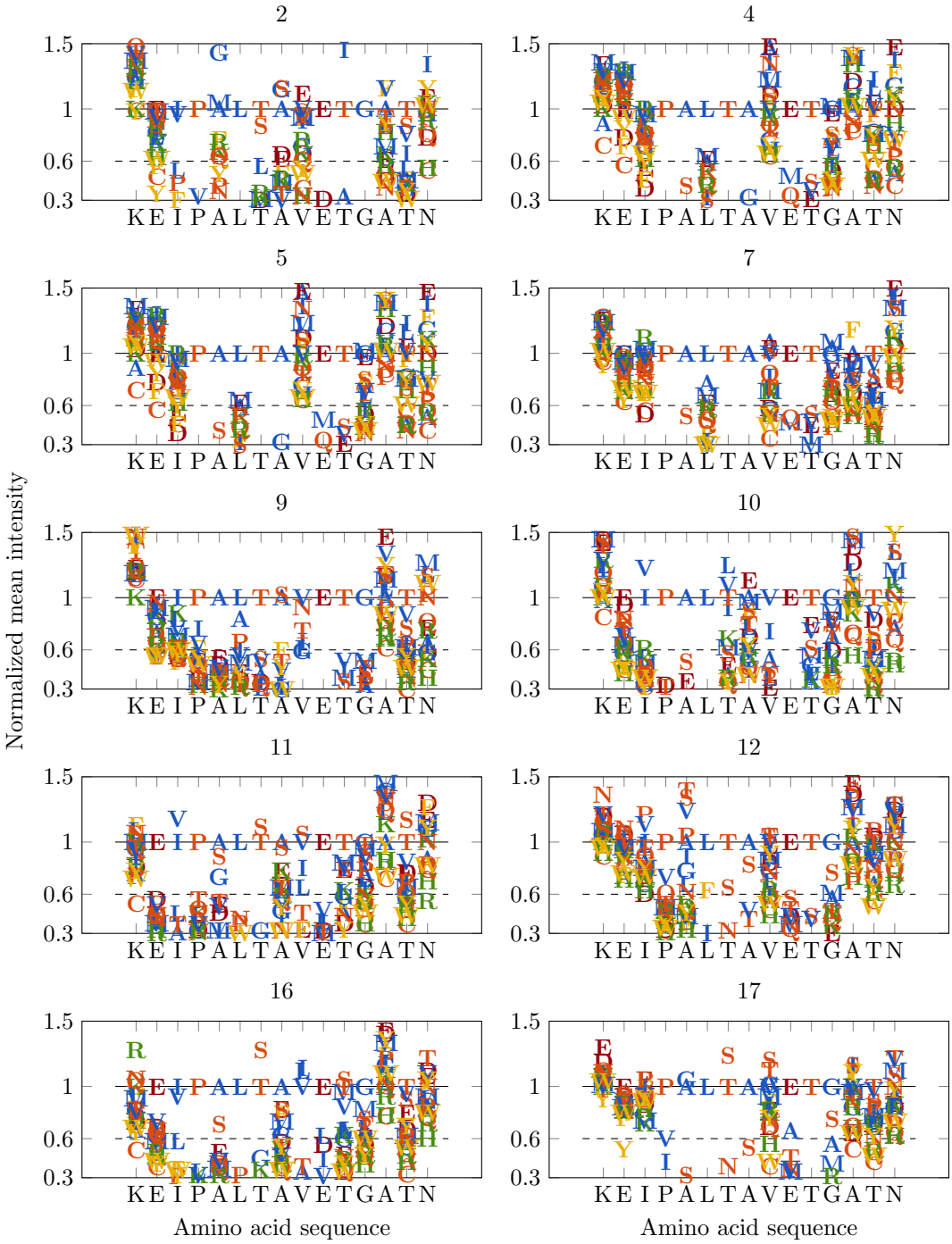

Figure 2.5.1: Fingerprints of $_{615}$KEIPALTAVETGATN$_{629}$ of 10 individuals. The relative mean fluorescence intensities are plotted in reference to the original amino acid in the substituted peptide sequence (one letter code). Mean fluorescence intensities were calculated from triplicate spots. The original sequence is depicted on the x-axis. Intensities of peptide variants were correlated to the intensity of the original peptide in each row respectively. Each peptide variant is represented by the letter of the amino acid that was substituted at the respective position. Amino acids are colored according to their chemical properties. Red: negatively charged; green: positively charged; orange: polar, uncharged; yellow: nonpolar, aromatic; blue: nonpolar, alipathic.

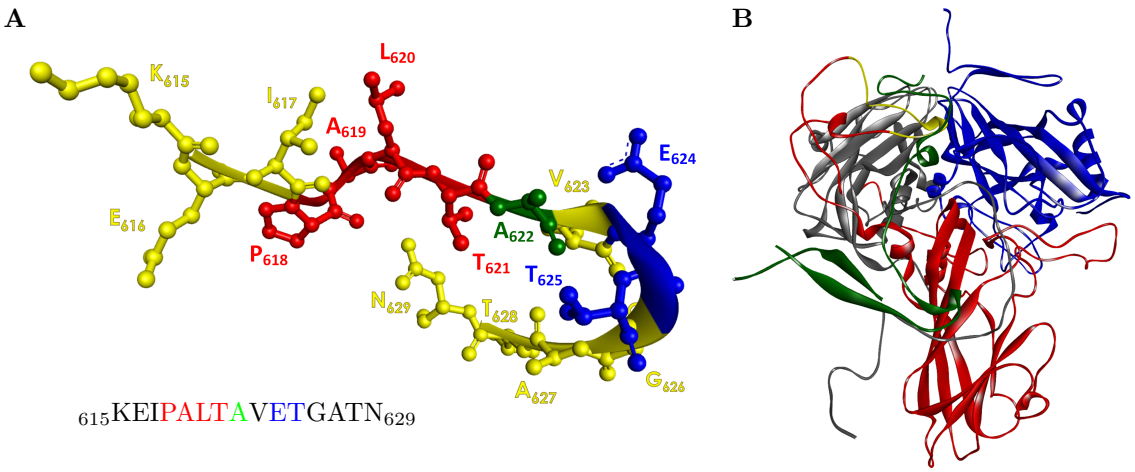

Figure 2.5.2: Enterovirus capsid epitope. A: EV capsid epitope with colour coded fingerprint. B: Capsid building block assembled from VP1 (red), VP2 (blue), VP3 (gray) and VP4 (green). The epitope on VP1 is highlighted in yellow.

can also be seen in figure 2.5.2 (left side). The amino acids K_{615}, I_{617}, L_{620}, A_{622}, E_{624}, T_{625} and G_{626} are protruding from the protein. Although $_{615}$KEIPALTAVETGATN$_{629}$ is located inside the virus capsid according to x-ray structure models, Roivainen *et al.* propose that the virus capsid is changing its confirmation in solution [131] and the epitope containing region of VP1 is externalized and thus can be targeted by antibodies nonetheless. This reversible alteration of confirmation suggests that this region may play a specific role in the early virus host cell interactions [131] and it was proposed to be important in the virus's penetration of the host cell plasma membrane [46].

2.6 PEFxGSxP motif

The prior published PEFxGS motif originates probably from an extracellular binding protein of *Staphylococcus aureus* [176]. *S. aureus* is the the major cause of hospital-acquired bacteremia in humans and can infect virutally every organ system of the body [148]. The growing resistance of methicillin and vancomycin [109] in *S. aureus* have promoted new interest in a novel treatments and the identification of protein antigens as candidate vaccine components could be beneficial [150]. Therefore the peptide $_{227}$HYVPEFKGSLPAPRV$_{340}$, originating from an protein of the extracellular matrix of *Staphylococcus aureus*, was substituted and incubated with serum of ten individuals.

2.6.1 Substitution analysis

The obtained fingerprints are depicted in figure 2.6.1 page 38. As observed for the PALT(A)xET motif, the homology of fingerprints among different individuals is astonishing. A comparison of the individual sera for the amino acids, which are most conserved among all individuals resulted in the fingerprints PEFxGSxP, where x stands for a position not crucial for the antibody recognition. The obtained fingerprint is one amino acid position longer than the one reported by Weber *et al.*. This

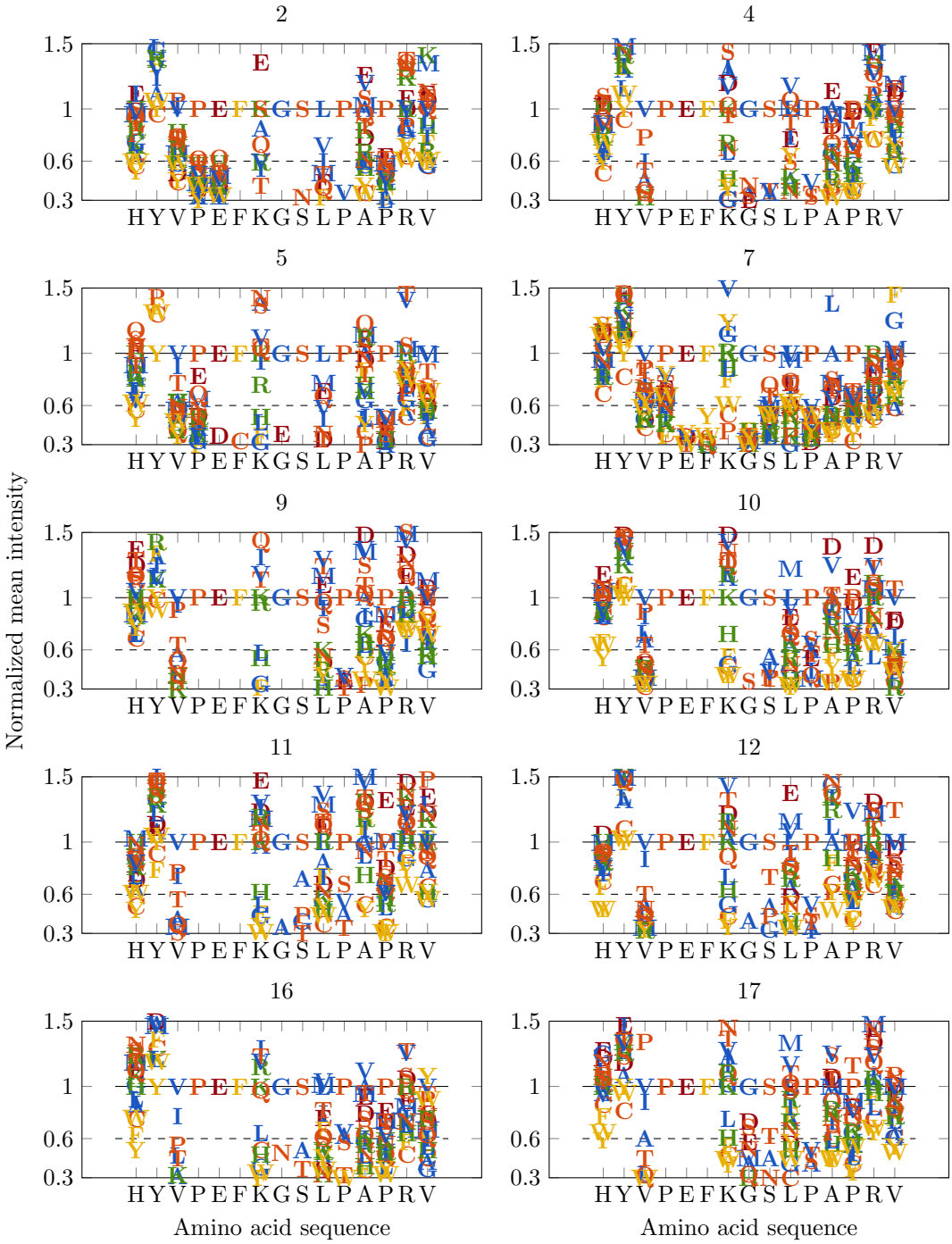

Figure 2.6.1: Fingerprints of $_{227}$HYVPEFKGSLPAPRV$_{340}$ of 10 individuals. The relative mean fluorescence intensities are plotted in reference to the original amino acid in the substituted peptide sequence (one letter code). Mean fluorescence intensities were calculated from triplicate spots. The original sequence is depicted on the x-axis. Intensities of peptide variants were correlated to the intensity of the original peptide in each row respectively. Each peptide variant is represented by the letter of the amino acid that was substituted at the respective position. Amino acids are colored according to their chemical properties. Red: negatively charged; green: positively charged; orange: polar, uncharged; yellow: nonpolar, aromatic; blue: nonpolar, alipathic.

may result from the increased number of investigated samples and also from the sequence of amino acids tested. Weber *et al.* used eight different 12mer peptides in the substitution analysis, which resulted from a phage display screening. A query of the "UniProtKb/Swiss-Prot" protein database (release 2016/11 of 30-Nov-16: 553231 entries) with the "ScanProsite tool" [22] for the motif [VPI]-P-E-F-x-[GDS]-[STA]-x-[PVAS] resulted in 37 hits respectively. The query included splice variants (Swiss-Prot) and excluded fragments. All hits of the query can be found in the appendix table A.4.4 page 99. After applying the same restrictions as described for the PALT(A)xET motif (section 2.5) to exclude the very unlikely origins, two potential causative agents remain: an extracellular matrix protein-binding-protein originating from *Staphylococcus aureus* and the non characterized protein YMR317W originating from *Saccharomyces cerevisiae*. The part of the protein structure of the extracellular matrix protein of *S. aureus*, onto which the identified motif is located, has not yet been resolved by crystallography and can thereby not be visualized in a 3D model.

2.7 Conclusion

With the presented method, epitopes can be screened and the toxin specificity of the epitope-binding serum antibody can be tested. This was demonstrated for the first time on the tetanus toxin. The epitope $_{929}$ExxEVIVxK$_{937}$, identified in eight out of nineteen individuals, is strongly conserved in between individuals. Further, neutralization studies should be conducted to investigate the role of the identified epitope.

For the diphtheria toxin, the whole range of peptides were applied in the epitope mapping: linear peptides with a length of fifteen and twenty amino acids and cyclic peptides with a length of seven, ten and thirteen amino acids. No prominent potential epitope across samples have been identified using linear peptides. However, five prominent regions could be identified in the mapping of cyclic peptides using pooled sera. To determine, whether these interactions are specific for individual sera, or can be found in multiples, the mapping should be repeated for every individual serum. For future screenings, also protein like structures should be applied to mimic more complex conformational epitopes. Synthesis strategies therefore are currently investigated [97].

In the epitope mapping of the pertussis toxin, three regions could be identified, which were also reported in the literature for their ability to induce toxin recognizing antibodies in mice or rabbits and some parts within this regions even raised neutralizing antibodies in mice. However, no distinct antibody fingerprints could be determined for a variety of peptides covering the three identified regions. For one individual a fingerprint was obtained for one peptide, but since the motif is not discernible for the substitution analysis of an overlapping peptide, the specificity of the observed interaction remains to be further investigated.

The data presented clarify the importance of verifying the specificity of observed peptide-antibody interaction in cases of doubt. Spotting pre-synthesized peptides onto a chemically different functionalized surface is a fast and easy but costly way in doing so. After identifying epitopes, it has to

be tested, whether the antibodies interacting with the peptide are also targeting the corresponding protein. This can be realized by isolating the antibodies using affinity batch chromatography and ELISA experiments. For most diseases that are subject to vaccination, ready to use ELISAs are purchasable. However, to test the ability of antibodies to target other native proteins, the development of ELISA experiment is required. This applies for example to the PEFxGSxP motif, where it remains to be determined, whether antibodies interacting with the peptide also target the native protein.

For both motifs, selected from literature, fingerprints of all tested individuals are highly conserved. Altogether, the homology in between fingerprints of different individuals targeting the same epitope (ExxEVIVxK, PALT(A)xET and PEFxGSxP) is astonishing, given the randomness of antibody maturation. It would be very interesting to test further individuals to obtain statistical representative data in the future.

and 13mere peptides have been applied.

2.8 Outlook

The strong conservation among the individual antibody fingerprints of the epitopes $_{929}$ExxEVIVxK$_{937}$, PALT(A)xET and PEFxGSxP, identified in healthy European individuals, is astonishing. However, for representative data more individuals have to be analyzed. Also the HLA type of each serum should be determined in future studies, to investigate if a correlation can be observed to the ability to target an epitope. The epitope $_{929}$ExxEVIVxK$_{937}$, which showed to be targeted by tetanus specific antibodies, should be subject to neutralization studies in mice, to investigate the role of the antibody species in the immune response. The mapping of the diphtheria and pertussis toxins did not result, like for the tetanus toxin, in potential epitopes identified across serum samples. However, the five regions revealed by epitope mapping using cyclic peptides might be worth further investigations. Also the substitution analysis of the prominent regions obtained for the linear epitope mapping of the pertussis toxin should be repeated using a different set of peptides. Further, the development of an ELISA for *S. aureus* is of great interest, since the multidrug-resistant strains of *S. aureus* cause severe implications or even death in immune suppressed patients. Finding neutralizing antibodies would be the first step towards the development of an vaccination.

3 Preliminary studies for peptide array based continuous flow assays

After the identification of an specific epitope, the concentration of antibody binding this epitope (antibody titer) is of great interest. The course of antibody titer over time can elucidate which antibodies are amplified over time for example during a victorious immune response, a chronic inflammation or an autoimmune reaction. The information content acquired by immunoassays using peptide arrays can be extended from the screening for binding sites, as described in the previous chapter, to further characterize the antibody-peptide interaction in terms of their thermodynamic and kinetic rate constants, from which antibody concentration can be derived. This measurement requires a time resolved detection of antibody-peptide interactions, which can be realized by a continuous sample flow over the peptide array and a detection system for the visualization of binding events.

To implement a continuous flow using low sample volumes, the peptide array has to be enclosed into a microfluidic channel. Connecting the channel to a microfluidic network allows to automate the incubation of the array and thereby to reduce the hands-on time. Using fluorescence for the detection of interaction is a well established method for peptide arrays. Continuous flow experiments require a time-resolved fluorescence detection over a longer period of time, which could result in bleaching or quenching of the fluorophore. Therefore, the stability of the fluorophore under experimental conditions has to be tested. In order to meet the increased consumption of peptide arrays during the development of the experimental setup of the continuous flow assay, low priced, rapid to produce peptide arrays are needed. Peptide spots need to be homogeneous in shape and density and the spot size has to be matched to the resolution and sensitivity of the detection system. During the establishment of this array production method, the need came up to visualize the peptide array unbiased by a fluorophore dye.

3.1 Requirement specification

In the following, the particular requirements of all components of the experimental setup are further specified.

3.1.1 Peptide arrays

Although high quality peptide arrays are commercially available, the price of $> 600\,€$ per slide and delivery periods of up to six [120] weeks are not suited for a rapid and versatile method development. For this reason, a simpler method for array production has to be established. During the development of a continuous flow assay these arrays do not need to be synthesized in a combinatorial manner since a limited number of peptides will be used for test purposes. The quality of a thus produced peptide array is defined as the homogeneity of the shape, size and position of all spots on the respective array. However, the most important factors defining array quality are the peptide density per spot and the chemical surface properties of the array. They are difficult to determine, since the total amounts are extremely low and surface bound and can therefore just be qualitatively compared. To allow the spot to be detected by a camera, the spot area should not decline 100 pixel. Also the spots should be constant in shape and size to facilitate image processing. Further, the array surface should be comparable to the PEPperCHIP®in surface hydrophobicity to be able to reproduce conditions for assays at equilibrium state since from experience the surface shows good compatibility with antibodies [159].

3.1.2 Label free visualization of peptide spots in the context of peptide array production

As mentioned in section 1.3.2, quality control of peptide array production is realized by fluorescence dependent surface visualization. However, fluorescence dyes are prone to quenching effects and the labeling performance may be compromised by surface interactions. In addition to these visualization techniques, a label free method would be advantageous. The accuracy of the label free surface measurement should be determined by comparison with an other established method, such as AFM. The time consumption of the imaging procedure is supposed to be comparable to a high resolution fluorescence scan, which is about 10 h for a whole surface at a resolution of $1\,\mu m\,pixel^{-1}$. This requires the scanning of a FOV as large as possible and allows for stitching of the single measurements. Also the limit of spot detection should be determined.

3.1.3 Detection system for the visualization and determination of antibody-peptide interaction using fluorescence

An experimental setup has to be constructed to excite and detect fluorescence in a microfluidic channel. Within the FOV the illumination needs to be homogeneous to guarantee a reproducible excitation independent of the location. A compromise of large FOV and high resolution has to be

found. The FOV should ideally be $1\,\mathrm{cm}^2$, to be comparable to other devices. And spots should be resolved with a minimum of ≈ 100 pixel per spot area, while maintaining a FOV as large as possible.
Time intervals between single images have to be minimized to at least one per minute and the sensitivity of the detection system has to be determined. Also, the stability of fluorescence intensity under assay conditions has to be examined.

3.1.4 Microfluidic system

To establish a continuous flow of sample over the peptide array, the array needs to be integrated into a microfluidic channel, which can be connected to a fluidic network including a pump, valves and buffer reservoirs. Channels geometry should not exceed 5 % deviation due to production to guarantee reproducible flow profiles. The liquid needs to be free of bubbles, which will compromise the flow profile and might even settle in the channel. For the determination of kinetic rate constants the assay has to be repeated several times, varying either the sample concentration or the flow rate [71]. Placing several channels onto one peptide array will increase the accuracy of the experiment, due to variations in the ligand density, which is to be expected among different batches. An increase in the number of assays performed on one array also increases the reproducibility and accuracy of the measurement. Further, the whole incubation process should be automated.

3.2 Peptide array production by spotting

A protocol for the spotting of pre-synthesized peptides was established. Peptides are covalently bound by a thiol-maleimide click reaction [125]. The use of protection groups can therefore be reduced to cysteines within the amino acid sequence of a peptide and peptides can thus be dissolved and handled in aqueous solution instead of dimethyl sulfoxide (DMSO) or *N,N*-dimethylformamide (DMF). The aqueous solution containing pre-synthesized peptides can be deposited onto the functionalized surface by a spotting robot. The deposition of peptides and the following passivation of the array surface can be accomplished in several hours for about 12 € per slide plus the pro rata costs of the peptides (approx. 2 € per 15-17mere peptide per array, costs for functionalized surface not included).

Four different functional surfaces (100 %-poly(ethylene glycol)methacrylate (PEGMA), PEPperCHIP®, 3D-Amino and 3D-Maleimide) have been compared in regard of their ligand density and surface hydrophobicity. In order to adjust the spot size as desired, the relationship of spot diameter and number of drops per spot was determined. Further, the accuracy of drop positioning on the surface by the spotting robot was determined and resulting spot shapes were investigated.

3.2.1 Comparison of ligand density of different functional surfaces

The 100 %-PEGMA-surface, the PEPperCHIP®and the 3D-Amino surface have been functionalized with maleimidobutyryloxysuccinimide ester according to the protocol described in section 4.1.2 Peptide array synthesis by spotting (p. 75). The 3D-Amino surface did not require a removal of the Fmoc-protection groups prior to functionalizing with maleimidobutyryloxysuccinimide ester and the 3D-Maleimide surface was ready to use without any further treatment. Since there are no analyses available capable to quantify substances in the subnanomolar range on surfaces, the ligand density, or grade of derivatization of the four surfaces was compared indirectly by coupling Fmoc-protected D-cysteine (Fmoc-D-Cys-OH) in excess from solution to the surfaces (4.1.2 Maleimide-click-reaction of Fmoc-D-Cys-OH from solution, p. 76). In a second step the Fmoc-protection group was removed and the forming piperidine dibenzofulvene adduct (PDFA) was quantified by

Table 3.2.1: Indirect comparison of the maleimide load on four different functional surfaces by quantifying the piperidine dibenzofulvene adduct of Fmoc-D-Cys-OH which was coupled from solution to the prior applied maleimide. As a reference, the mean grade of derivatization was quantified on 100 %-PEGMA surfaces ($n = 10$) and PEPperCHIPs®($n = 13$) before any further functionalization was conducted.

Surface	**Grade of derivatization in nmol cm^{-2} post maleimide**	**Reference**
100 %-PEGMA	8.1	8.2 ± 6.3
PEPperCHIP®	0.7	0.8 ± 0.4
3D-Amino	0.4	
3D-Maleimide	0.6	

measuring the adsorption at 301 nm (4.1.1 Synthesis of 100% PEGMA surfaces, p. 75). As references the PDFA was quantified for 100 %-PEGMA surfaces and PEPperCHIPs®before any further functionalization was conducted. The results are summarized in table 3.2.1. The grade of derivatization of maleimide is comparable to the one of the references for the 100 %-PEGMA surface and the PEPperCHIP®. From our experience, the observed large deviations of $< 50\,\%$ are common for micro arrays due to synthesis related variances in between surfaces and the low amounts of PDFA which are in the range of the lower detection limit of UV/Vis photospectrometry or even below. As to be expected, the 100 %-PEGMA surface showed the highest concentration of PDFA and thus indirect, of maleimide per square centimetre. The extinction measured for the PEPperCHIP®, 3D-Amino and 3D-Maleimide surface are below the detection limit of 0.1. However, it can be observed that the respective degree of derivatization for these three surfaces is in the same order of magnitude and is significant lower than for the 100 %-PEGMA surface. As we saw in chapter 2, the ligand density of the PEPperCHIP®is sufficient for standard serum diagnostics. This is expected to be valid also for the 3D-Amino and 3D-Maleimide surfaces in terms of amount of available ligands.

3.2.2 Comparison of surface hydrophobicity of different functional surfaces

Contact angles of DIW drops on the four surfaces previously functionalized with maleimidobutyryloxysuccinimide ester were determined as described in 4.7 (p. 80). By comparing these contact angles to contact angles on surfaces after the removal of the Fmoc-group but prior to further functionalization (figure 3.2.1), the rather wide distribution of contact angles per surface type is noticable. The median contact angle of the PEPperCHIP®(70.6°) is considerably higher than

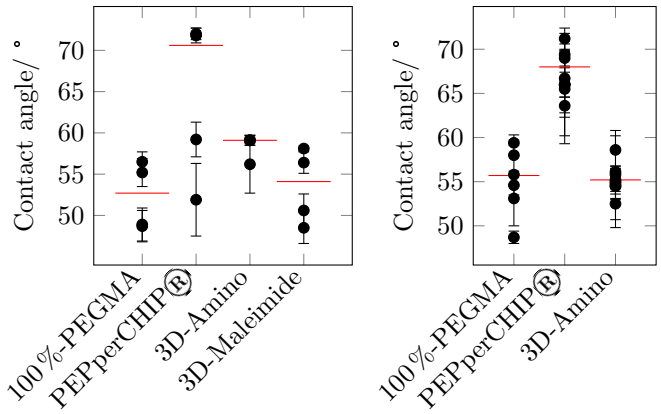

Figure 3.2.1: Contact angles of 5 µl drops of deionized water (DIW) on surfaces functionalized with maleimidobutyryloxysuccinimide ester (left) compared with contact angles of surfaces after removal of the Fmoc-protection group but prior to further functionalization (right). Five contact angles were measured per surface. Dots represent the average contact angle for one surface. Red lines indicate the median contact angle for one type of surface. The number of samples tested for the functionalized surfaces is three, four, four and four and for the surfaces prior to further functionalization six, nine and nine respectively. Surfaces are from various batches.

for the 100 %-PEGMA (52.7°), 3D-Amino (59.1°) or 3D-Maleimide (54.1°) surface. It seems the functionalization does not significantly alter DIW contact angles and thus surface hydrophobicity of the 100 %-PEGMA and 3D-Amino surface. For the PEPperCHIP®, the data is not really conclusive, since the variation in contact angle after functionalization with maleimidobutyryloxy-succinimide ester is rather broad. In order to reproduce assay conditions, it might be advised to derivatize the surfaces utilized for assays at equilibrium for the use in continuous flow assays. If it becomes relevant to reproduce assay conditions from epitope mapping in future studies, the impact of derivatization should be studied in more detail for the PEPperCHIP®.

3.2.3 Adjustment of spot diameters on different surfaces

For spotting, the most effective way to adjust the spot size is depositing a different number of drops onto one position. The correlation of the resulting spot diameter to the number of deposited drops of HA, serum reactive peptide (SRP), FLAG and cMyc peptides spotted at 400 µM was investigated on 3D-Maleimide surfaces and 100 %-PEGMA, PEPperCHIP®and 3D-Amino surfaces derivatized with maleimidobutyryloxysuccinimide ester (figure 3.2.2, p. 47). For the peptide deposition the spotting device was set to 21 °C and a relative humidity of 60 %. The spot pitch was set to 500 µm. Spot diameters are not linearly increasing with the number of drops. The DIW contact angles on the respective surfaces seem not to significantly influence spot diameters. This can be seen at replica 1 and 3 of the PEPperCHIP®, which result in comparable spot diameters for the HA peptide, even though the difference of DIW contact angles of both surfaces is considerably large. The FLAG peptide seems to result in significantly lower spot diameter than the HA or SRP peptide. Also a deviation of approx. 100 µm in spot diameter was observed in between the different replicas. The reason for this is the way in which the FLAG peptide seems to agglomerate on the center of the spot area. Figure 3.2.3 shows fluorescence scans of one drop HA and FLAG spots, visualized by staining with a fluorophore. For the HA peptide, a higher fluorescence intensity can be observed on the spot center, indicating a higher peptide density in this area. For the FLAG peptide however, this center area is smaller and sharply defined. Whereas the forebay of the spot is hardly distinguishable from the background. Depending on the fluorescence intensity of the forebay after labeling, either the whole spot area was detected or just the spot center, which resulted in the variation of observed spot diameters. This effect is not influenced by fluorescence labeling as can be seen in figure 3.2.3 C, which shows label free VSI scans of FLAG spots incubated with anti-FLAG antibody. The influence of the peptide concentration on spot diameter and contact angle of peptide dissolved in spotting buffer on a 3D-Maleimide surface can be seen in figure 3.2.4 on page 48. An increase in peptide concentration from 10 µM to 400 µM seems to increase spot diameter around 60 µm for the HA and SRP peptide. However, no increase was observed for the forebay of the FLAG peptide. Consistent to this, an increase in peptide concentration seems to result in a slight decrease in contact angle of the peptide solution for the HA and SRP but not for the FLAG peptide on a 3D-Maleimide surface.

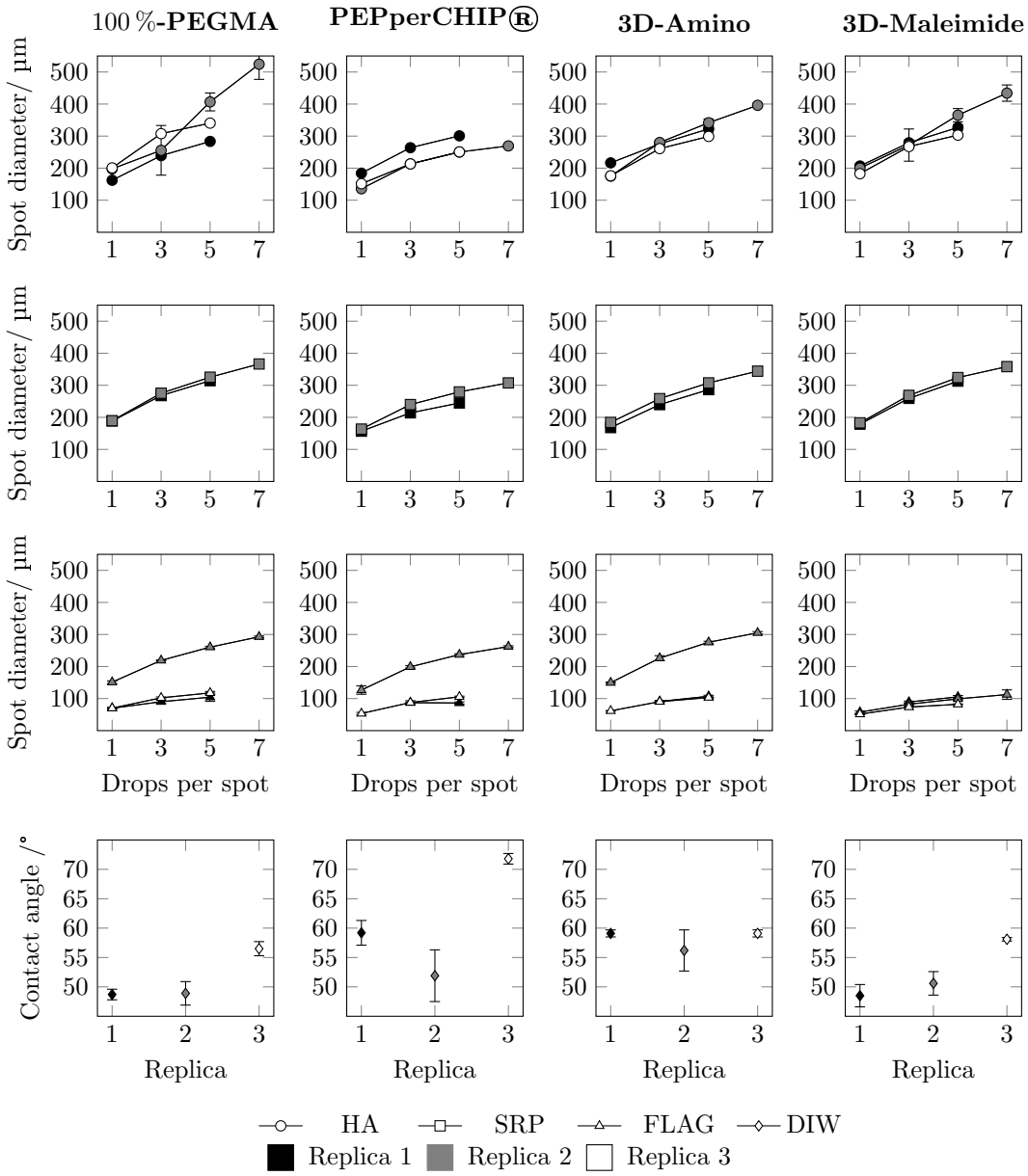

Figure 3.2.2: Spot diameter as a function of the number of deposited drops per spot for three different peptides HA, SRP and FLAG spotted at 400 µM (rows 1 to 4) on the four different surfaces (columns 1 to 4) in up to three replicas (indicated by colour: black, gray, white). Data points represent average spot diameters of approx. 120 spots. Spots were visualized by directly staining the *N*-terminus and free amino groups with (5(6))-5-(and-6)-carboxytetramethylrhodamine (TAMRA) according to section 4.5 page 78 Bottom row: Contact angles of DIW drops of the respective surfaces. Data points represent the average of 5 measured contact angles per surface.

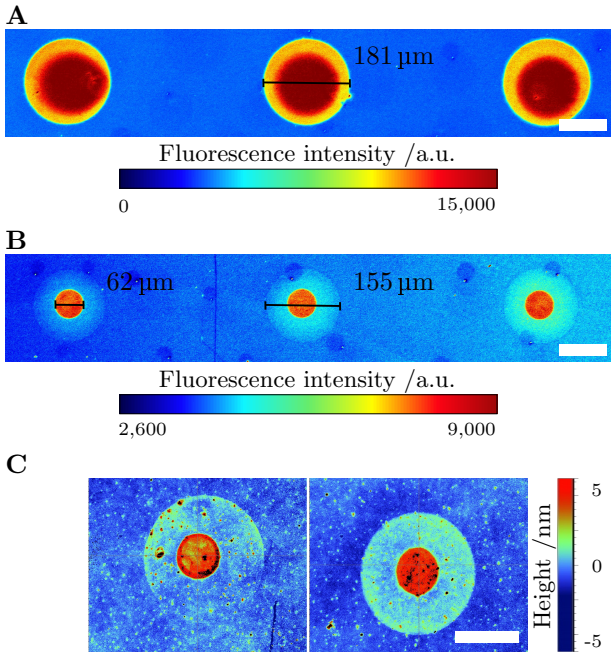

Figure 3.2.3: Visualization of spot shapes of the HA and FLAG peptide. A and B: Fluorescence scans of the HA (A) and FLAG (B) peptide spots (one drop per spot) on a 3D-Amino surface (Replica three from figure 3.2.2). Spots were labeled using TAMRA *N*-hydroxysuccinimide (NHS) ester. Scan: Innoscan, 0.5 µm pixel^{-1}, 532 nm, gain 2. Scale bar represents 100 µm. C: FLAG spots (one drop per spot) on a 3D-Maleimide surface after incubation with anti-FLAG antibody. Measured by VSI. Scale bar represents 100 µm.

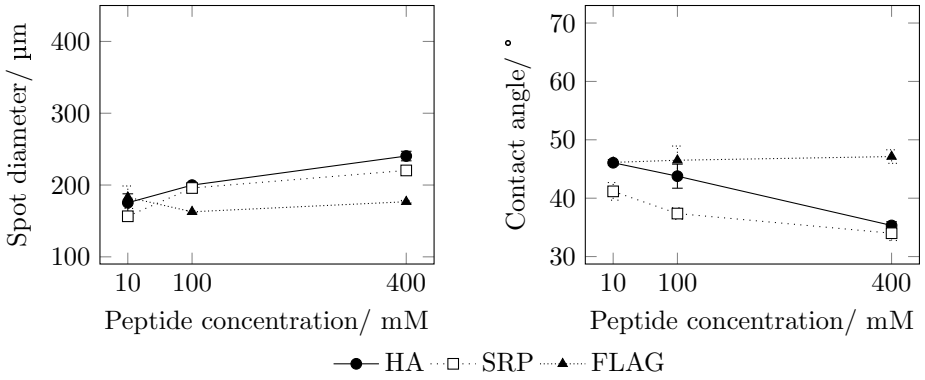

Figure 3.2.4: Correlation of peptide concentration to spot diameter (left) and drop contact angle (right) on 3D-Maleimide surfaces. Concentrations of 10 µM, 100 µM and 400 µM of the peptides HA, SRP and FLAG were prepared by serial dilution and one drop was deposited by spotting on a 3D-Maleimide surface. Data points represent the average spot diameter of 100 spots. For the measurement of contact angle, drops (5 µl) were deposited manually using a pipette. Surfaces of the presented experiments (left and right) are not the same.

When choosing the number of drops to adjust the spot diameter, also the peptide concentration should be considered. By using a different tip for spotting (pico tip), spot diameters of below 100 µm can be achieved, but have not been studied in detail in the scope of this work.

3.2.4 Determination of drop positioning accuracy and spot shape

To minimize drop break down on the surface, the pitch for spotting was set to 500 µm. For four peptide arrays (41 spots per array, including spots of one, three and five drops), the average pitch was determined to be (495 ± 20) µm in x and (503 ± 15) µm in y direction. The average spot diameter for a peptide concentration of 400 µM was determined to be (240 ± 7) µm, (220 ± 2) µm and (177 ± 2) µm for the HA, SRP and FLAG peptide respectively. HA and SRP peptides result in evenly circular spots. The spot appearance appears to depend rather on the peptide type than on the type of surface or surface DIW contact angle.

3.2.5 Considerations on the selection of a functionalized surface

Apart from hydrophobicity and ligand density, the four tested surfaces differ in the time it takes to prepare them for spotting and the related costs for the required chemicals. The 3D-Maleimide surface can be acquired ready to use for 18 € (all costs effective 2018). The 3D-Amino surface needs to be derivatized with maleimidobutyryloxysuccinimide ester which requires 17 h and costs in total of 19 € per slide. For a skilled operator, a maximum of twenty slides can be prepared in one batch. For the PEPperCHIP®, the Fmoc-group needs to be removed prior to derivatization, which prolongs the process time by half an hour (17.5 h) and results in 29 € per surface. It takes eight working days with a total hands on time of approximately 25 h to synthesize the 100 %-PEGMA surface and the cost is about 57 € per surface. Since no significant difference in spot appearance was observed for the four tested surfaces, the 3D-Maleimide surface allows for the fastest and most economic array production and was thus used in further course of development.

3.3 Establishment of VSI as a quality control method

In addition to fluorescence based visualization techniques, VSI was established as a label free method for surface visualization. By comparing the accuracy of measurement of VSI and AFM, the method was validated for its suitability for quality control of peptide arrays. Further, the measurement time in regard of the scan area is compared between AFM, VSI and fluorescence scanning. For the VSI scanning areas in the mm-range, while resolving nanometer high protein layers, is demonstrated. The limit of detection was determined and a further application of VSI is presented, in which the dynamic range of the used fluorescent label is ascertained. The results presented in this section have been published recently by Palermo *et al.* [116].

3.3.1 Comparison of spot topology measured by AFM and VSI

A SOI was identified (see figure 3.3.2 B, p. 52) and the spot topology was measured using both methods. The coordinates of the SOI respective to two edges of the substrate were determined in previous VSI scans. Finding the position for the AFM measurement was therefore facilitated. For a reasonable comparison, the obtained resolution in $\mathrm{nm\,pixel^{-1}}$ should be similarly for both

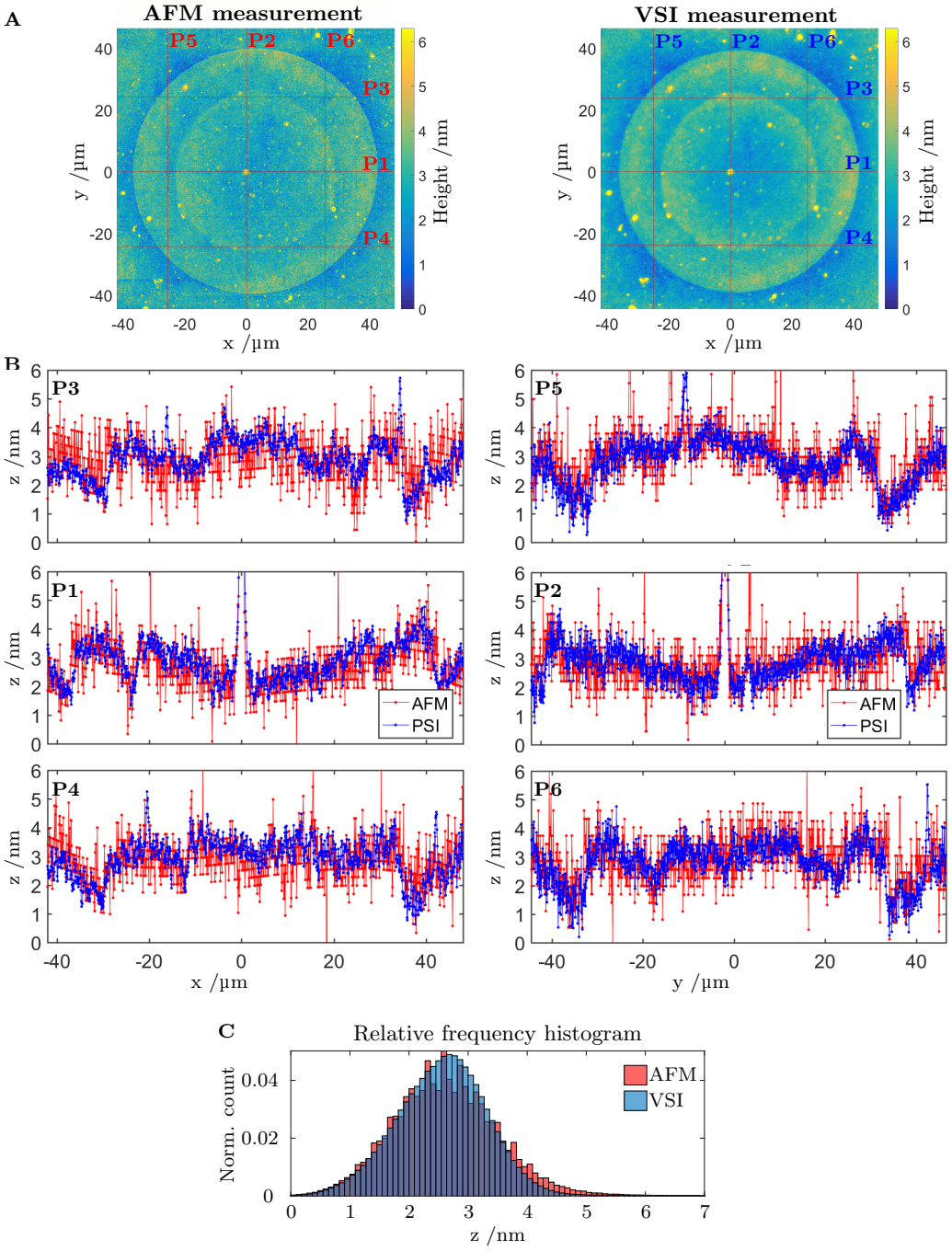

Figure 3.3.1: Comparison of VSI measurement to AFM (z-offset adjusted). A left: Topology of a spot measured by AFM (76.1 nm pixel^{-1} lateral resolution) in Scan Asyst mode. A right: VSI measurement (74.6 nm pixel^{-1} lateral resolution at x50 fold magnification). Red lines indicate measured line profiles depicted in B. Orientation of measurements are rotated 90° to the right, compared to 3.3.2 A and B. B: Line profiles for the AFM and VSI measurement. AFM profiles in red, VSI profiles in blue. Vertically: P5, P2 and P6. Horizontally: P3, P1 and P4. C: Stacked relative frequency histograms of AFM and VSI measurements of the spot of interest (SOI). Reprinted with permision.

methods. After a software update for the AFM device, it was possible to increase the resolution from $181.6 \times 186\,\mathrm{nm\,pixel^{-1}}$ to $76.1 \times 76.1\,\mathrm{nm\,pixel^{-1}}$, which comes close to the resolution for the x50 fold magnification in VSI ($74.6 \times 74.6\,\mathrm{nm\,pixel^{-1}}$). As an example of mismatching resolutions and non square pixel sizes, see section B.6 figures B.6.2 and B.6.3 on page 106 and following. The update also introduced a further scan mode called Scan Asyst. Previously, PeakForce tapping mode was used to scan the rough and rather adhesive array surfaces. This mode is better suited to not damage the substrate surface by direct force control compared to the standard tapping mode. PeakForce tapping is a non-resonant mode with an oscillation frequency below the cantilever resonance. The z-position is modulated by a sine wave to avoid unwanted turning points, whereas standard tapping mode applies a triangular one. The Scan Asyst mode is based on the PeakForce tapping but decouples the cantilever response from the resonance dynamics to automatically adjust all critical imaging parameters. During scanning the z-limit is automatically lowered to some extend and the set-point is adjusted to obtain the minimal required force. The maximum scan area for AFM is a square of 92.52 µm edge length, resulting in 1216 pixel for the before mentioned resolution. The measurement of the whole area takes approximately 90 min. All AFM measurements were conducted by R. Thelen. For the VSI measurement, an area of 96.06 µm by 95.91 µm was scanned at 50 fold magnification by stitching two times, resulting in 1288 pixel by 1286 pixel. Both measurements were flattened and z-offset adjusted (as described in section 4.8.3) and depicted in figure 3.3.1.

The spot topographies obtained in both scans are very similar. However, the VSI scan appears to be minimal higher in contrast compared to the AFM scan. This is confirmed by comparing the shape of the respective histogram (see figure 3.3.1 C), which is slightly slimmer for VSI, and noticeable jagged with a broader tailing for the AFM. As a result, both histograms can not be matched exactly. This was also observed for other spots (see figures B.6.2 and B.6.3 on page 106 and following). To compare absolute height profiles, three vertically and three horizontally profiles were extracted from the respective measurements (see figure 3.3.1 B). The AFM profiles (red) are noticeably more scattered/noisy than the VSI profiles (blue), and for the horizontal profiles the waviness due to flattening is also visible. The AFM profiles superimpose the VSI profiles.
Despite applying completely different measurement principles, both methods produced spot topographies which are sufficiently congruent. Even though, the median local deviations in height of less than 1 nm are in the range of deviations caused by flattening procedures, also environmental influences may impact the measurements. For example, the two devices were not located in the same room and were exposed differently to acoustic noise, vibrations and temperature variations. This effects the AFM scan more significant, due to the considerably longer measurement time. Furthermore, systemic deviations on AFM which increase the measuring uncertainty, are more pronounced on large scan areas compared to areas with sub micron scan range. There are several likely causes for the scattered profiles obtained by AFM. Additionally to the environmental influences just mentioned, the z-limit can not be decreased to the extend required (from $> 10\,\mu\mathrm{m}$

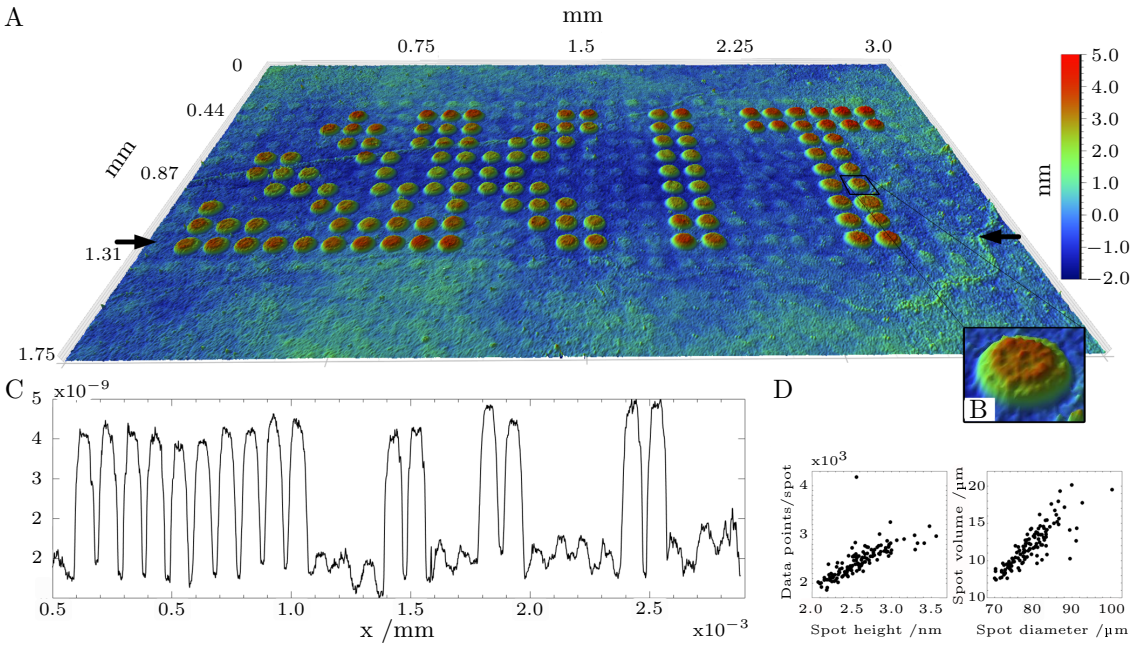

Figure 3.3.2: Large area scan by VSI. Peptide array incubated with human blood serum (1:50) and anti-HA antibody DL550 (13.3 fM over night and subsequently 30 min with secondary antibody (13.3 nM). A: 3D visualization of array topography measured by VSI. Field of view: 3.0 mm × 1.75 mm with 1.4 µm lateral resolution (x 2.75 magnification). B: Magnification of the SOI. C: Height profile across the array in between the black arrows in A. D: Properties of SRP spots. Left: Mean spot height as a function of amount of data points per spot. Right: Spot diameter as a function of spot volume. Reprinted with permission.

to 2 µm) in Scan Asyst mode. This makes up a factor of ten in the noise level and results in a poor approximation of height through roughly resolved pixels. PeakForce Tapping mode allows the z-limits required, but is thereby restricted to a lower lateral resolution. This could be solved with a hardware upgrade to further increase the performance of AFM, but was out of scope of this work.

3.3.2 Scan area

To verify the VSI's ability to resolve nm-high structures, while maintaining a field of view in the mm-millimeter range, the following experiment was conducted. A peptide array, consisting of sixteen sub arrays of 11 x 29 peptide spots each was produced, incubated with antibodies and imaged by VSI. Peptides were deposited onto the functional surface by spotting HA and SRP peptides at a concentration of 400 µM onto a 3D-Maleimide surface. The array was incubated with serum (diluted 1:50) and anti-HA antibody DL550 (13.3 fM) over night and eventually secondary antibody at 13.3 nM (Alexa Fluor 647) was incubated for 30 min. The concentration of anti-HA antibody added was chosen to be two magnitudes lower than the concentration of secondary antibody, to see if anti-HA antibody is still detectable using VSI. While scanning the slide using VSI, the coordinates of each sub array relative to two corners of the 3D-Maleimide slide were determined, and the individual sub arrays were imaged by stitching three measurements together.

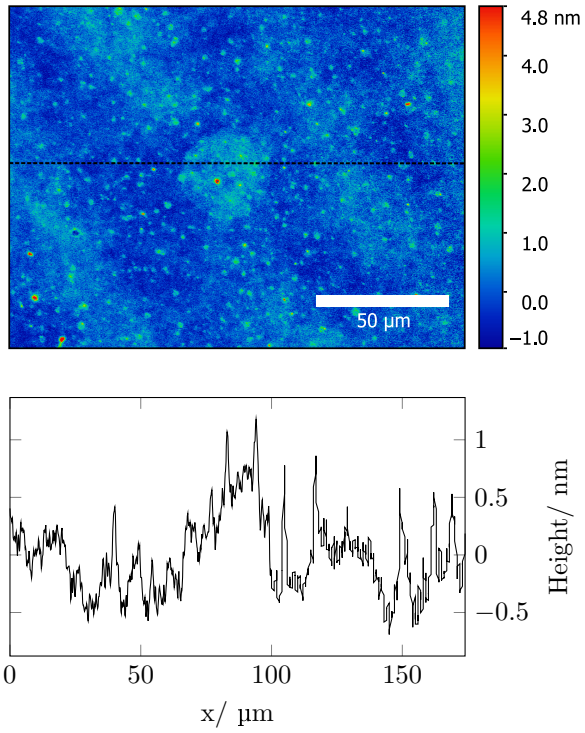

Figure 3.3.3: Example for a spot at the lower limit of detection. Top: VSI scan of a single drop spot of FLAG peptide (400 µM, pico tip) incubated in phosphate buffered saline (PBS) without the addition of antibody (x 27.5 magnification). Scale bar represents 50 µm. Bottom: Height profile along the black dashed line in the VSI scan.

The result of the stitching for one of the sixteen sub arrays can be seen in figure 3.3.2 A. The corresponding fluorescence scan can be found in the appendix (figure B.6.1, page 105). For plane and perfectly aligned surfaces, meaning the FOV is tilted less than $\lambda/4$ relative to the optical axis, no phase shift occurs during measurement. Areas being multiples of the field of view (up to 3 mm x 3 mm, see figure B.6.4 on page 108) can be scanned by stitching individual measurements together without readjusting focus. It was possible to resolve spot heights in a z range of 7 nm while the lateral size of the measurement is in the mm scale.

3.3.3 Time consumption of measurement

Scanning an area of 3 mm x 3 mm in six stitches takes about 4 min. A maximum sized array (20 mm x 70 mm) in 3 mm x 3 mm areas would therefore require a total of 156 scans which would require 10 h and 22 min of pure scan time. Even though a VSI scan is not directly comparable to a fluorescence scan, the latter one takes 45 min per channel (blue, green, red) instead, summing up to 2 h 15 min at 1 µm pixel^{-1} resolution. At this stage, VSI is too time consuming to scan whole maximum sized arrays by default. However, it allows to image a representative area (≈10 %) in 1 h, unbiased by a fluorophore dye or special properties of the substrate.

3.3.4 Automated evaluation of spot size and height

The software operating the VSI device 'Vision 64' allows for automated evaluation of topographies by recognizing features on the substrate surface due to height differences. A detailed evaluation of SRP spot properties is shown in figure 3.3.2 D. Applying a threshold of 1 nm and a minimum of 1000 contiguous pixels, all 125 SRP spots are captured for evaluation. The mean spot height is distributed between 2 nm to 3.5 nm corresponding to 1800 pixel to 4200 pixel, whereas the spot diameter ranges from 70 µm to 100 µm. This rather broad distribution results to some extent from the zero level applied for the calculation, which was averaged for all non-spot areas. The sensitivity of the evaluation could be improved by using local zero levels for each spot. However, the low median height of the HA spots ($\leq$ 1 nm) did not allow for an automated evaluation of spot properties.

3.3.5 Limit of detection

The lower limit of detection for the x 2.75 and x 27.5 fold magnification was found to be at a median layer height of 0.5 nm to 1 nm, depending on the flatness of the surface. For a rather plane surface scanned at x 2.75 magnification, this can be seen in the VSI scan presented in figure 3.3.2 (p. 52). The spots incubated with anti-HA antibody ($\leq$ 1 nm in height) are perceptible in between the plainly visible spots incubated with serum and secondary antibody. In the height profile (figure 3.3.2 C), individual HA spots can barely be distinguished. Figure 3.3.3 shows an example for a spot (FLAG peptide without antibody) scanned at x 27.5 magnification, which is hardly discernible in the scan. However, it is not possible to clearly distinguish the spot from the surface by a line profile since the surface waviness is in the same size as the spot itself. For a perfectly flat surface, the LOD is estimated to be 0.5 nm to 1 nm in height.

3.3.6 Additional application: Determining dynamic range of fluorescence read out

VSI can be used to determine at which dye concentrations quenching of the fluorophore starts to occur. To demonstrate this, three different concentrations of SRP have been spotted onto a 3D-Maleimide surface, arranged in sixteen single arrays. The arrays were incubated with seven dilutions of serum (two arrays per serum) and subsequently secondary antibody. The median spot fluorescence intensity and the median spot height have been determined according to sec. 4.6.1 and 4.8.3 (p. 79 and 81). Due to imperfections of the polymer film, it was not possible to evaluate the 200 µM peptide spots at a serum dilution of 1:800. At a dilution of 1:100 for the 400 µM and 200 µM spots, and 1:50 for the 100 µM spots, no further increase in protein layer height can be observed for higher serum concentrations. Whereas the fluorescence intensity decreases significant for dilutions lower than 1:100. This effect was also observed before in a similar experiment and was also attributed to quenching of the fluorophore at higher concentrations [155]. It remains unclear, why the fluorescence intensity is decreasing for dilutions ranging from 1:50

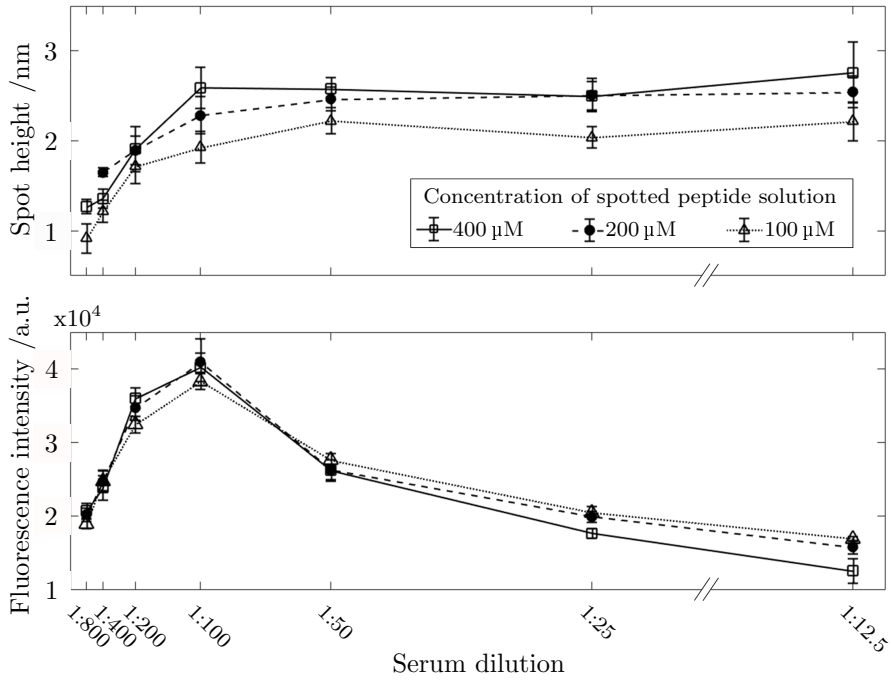

Figure 3.3.4: Median spot height (top) and median spot fluorescence intensity (bottom) for SRP spots (n=9) incubated with serum at different dilutions and secondary antibody at 13.3 nM. Peptides were spotted in three different concentrations: 400 µM, 200 µM and 100 µM onto a 3D-Maleimide surface. Measured by VSI (top) and fluorescence scanning (bottom). For VSI the thresholds were set individually for each dilution to maintain a constant amount of data points per spot. Peptide spots incubated with buffer as negative controls, were not visible in the fluorescence scan or the VSI scan. Reprinted with permission.

to 1:12.5, even though the protein layer height is constant according to the VSI. Maybe the layer heights or packing density of adsorbed proteins increase in the dimension of measurement uncertainty for higher concentrations and cause increased quenching of the fluorophore. For assays comparing absolute fluorescence intensities at equilibrium state for qualitative statements, it seems reasonable to evaluate the dynamic range of fluorophore for the applied concentrations. And when investigating the influence of drying on the protein layer height in more detail, VSI might also be set up for label free quantification in the future.

3.4 Experimental setup for continuous flow assays

A foto of the final experimental setup can be seen in figure 3.4.1. The continuous flow was generated by a syringe pump (Nanopump-Mini, Duratec, Germany). All components being part of the microfluidic system were connected by polytetrafluoroethylene (PTFE) tubing (inner diameter: 0.5 mm, 1/16 inch, Duratec). To inject the sample into the system, a micro-scale sample injector (8125, Rheodyne, USA) was used. By switching the valve of the sample injector manually from load to inject position, the flow is guided through the sample loop and the sample is driven towards the microfluidic channel. Occurring bubbles were eliminated by a bubble trap (Darwin Microfluidics, France). Individual channels were addressed by a motorized valve (MVP 7-8, Hamilton, USA).

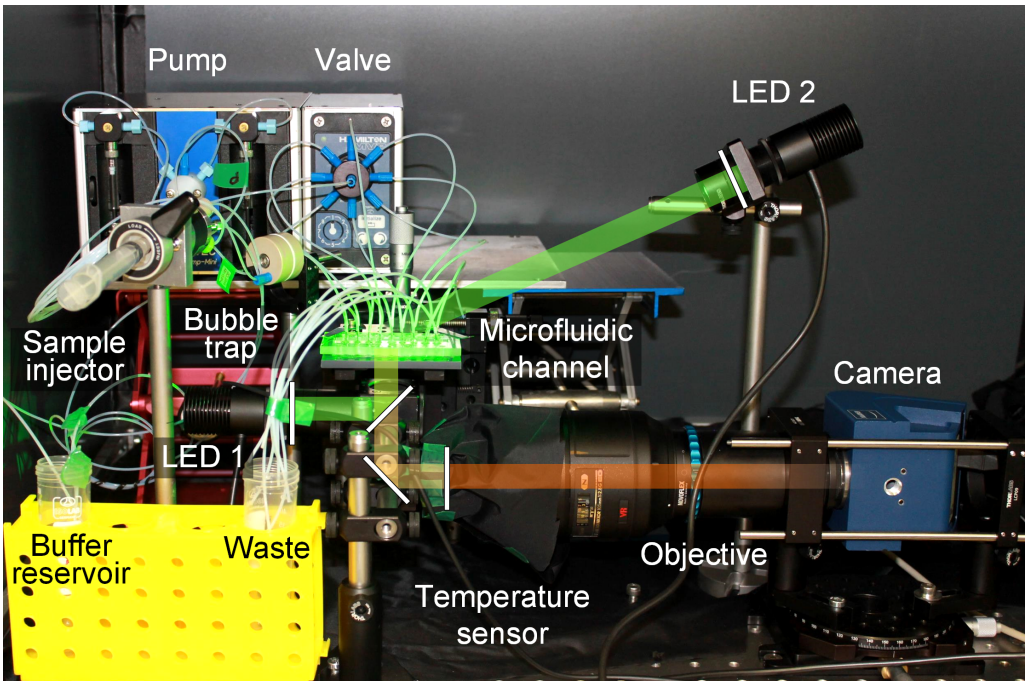

Figure 3.4.1: Experimental setup for the continuous flow incubation of peptide arrays. Coloured bars represent the ray path of light in the setup. White bars indicate filters and mirrors.

Fluorescence in the microfluidic channel was excited by one or two identical LEDs (M530, Thorlabs, USA) at 532 nm. The LED 1 is illuminating the sample from below, as can be seen in figure 3.4.1. Matching band pass filter, mounted to the respective LEDs (depicted as white lines in figure 3.4.1), narrow the by the LED emitted range of wavelengths. The beam is reflected on a dicroitic mirror towards the microfluidic channel. The so excited fluorescence is radiating in all directions. Fluorescence directed towards the bottom of the channel is passing the dicroitic mirror which is transparent for the increased wavelength of the fluorescence and is reflected by a silver mirror into the objective and the camera. Another band pass filter, matching the applied LED, is mounted in between the silver mirror and the objective to narrow down the range of wavelength passing. This increases the filtering of light originating from the LED which otherwise will decrease the sensitivity of fluorescence detection. The excitation from below results in lower background signals, since the LED is not directed directly at the camera. If the top part of the microfluidic channel is not absorbing and transparent, the sample can also be illuminated from above, or both lamps can be used simultaneously. This increases the homogeneity of the exposure in the FOV and also increases the illumination intensity. Fluorescence images were captured by a CCD-camera (ProgRes C5, Jenoptik, Germany) using a AF-S VR Micro-Nikkor IF-ED objective (focal length: 105 mm). The temperature influences the peptide-antibody interaction and plays an important role for the stability of the fluorophores. Therefore, the temperature was logged using a USB temperature sensor (TSP01, Thorlabs, USA) with a resolution of 0.05 °C and accuracy of ±0.3 °C at 25 °C. A LabView program was programmed to control the devices both individually and to execute procedures which involve multiple devices. Except for the sample injection, all processes

like the exchange of running buffer and the incubation of selected channels, can be performed automated using motorized valves.

3.5 Peptide array-PDMS channels using the MicCell-System

Molding structures into PDMS is a widely used method for the rapid production of microfluidic channels [32, 52]. The MicCell System by GeSim was especially developed for the integration of micro arrays into a PDMS channel. The walls and the top of the channel are molded into a PDMS layer, while the actual channel is formed by attaching the peptide array to the PDMS. Different designs on standard sized and 1 inch sized slides were tested in their performance. It was observed, that the channel structures become compressed by the MicCell assemblage. The process window for minimal channel deformation was determined. Further, the background fluorescence of the PDMS layer was reduced.

3.5.1 Fabrication process

The PDMS layer is injection molded. A scheme of the process is depicted in figure 3.5.1. Therefore a cover plate and a channel master structure are mounted to a frame. The cover plate contains threads to connect the tubing as well as the injection inlet and another drill for ventilation. The threads for the connection of the fluidic ports are sealed with filler plugs. The channel master structure is the negative of the later PDMS layer. It can be produced by stereo lithography

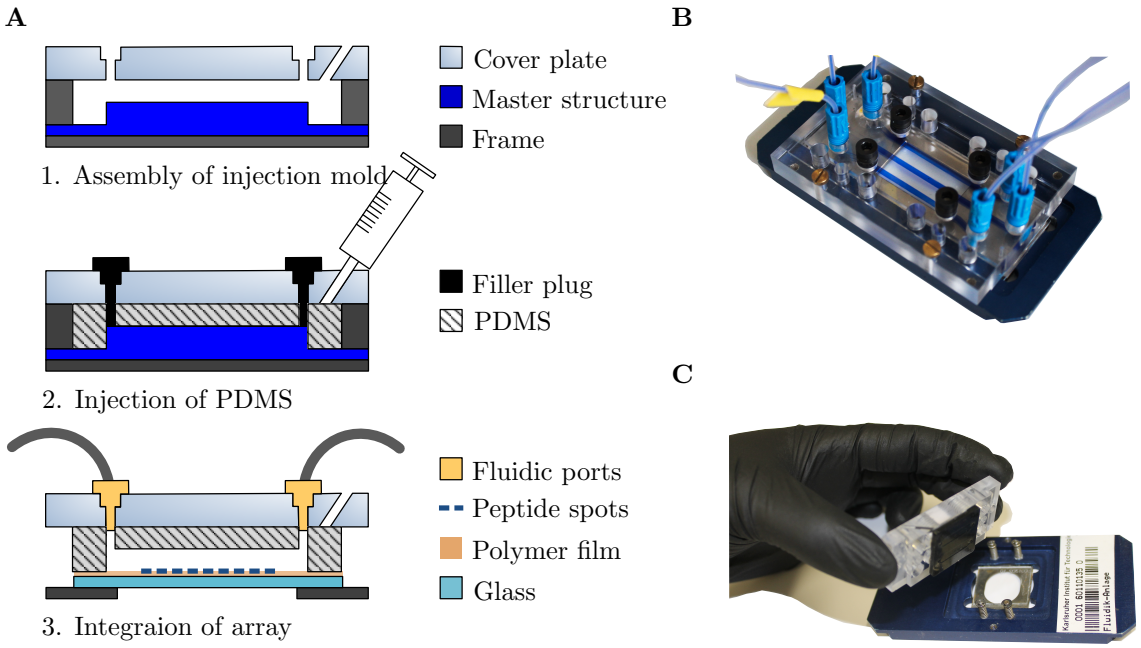

Figure 3.5.1: Production process of a peptide array-PDMS channel using the MicCell System. A: Scheme of the production process. B: Assembly of cover plate, structure bearing PDMS layer and a whole sized peptide array (25 mm by 75 mm). Channels are incubated with a blue dye for better visualization. C: 2 inch design of the MicCell System. PDMS is coloured black to reduce background fluorescence.

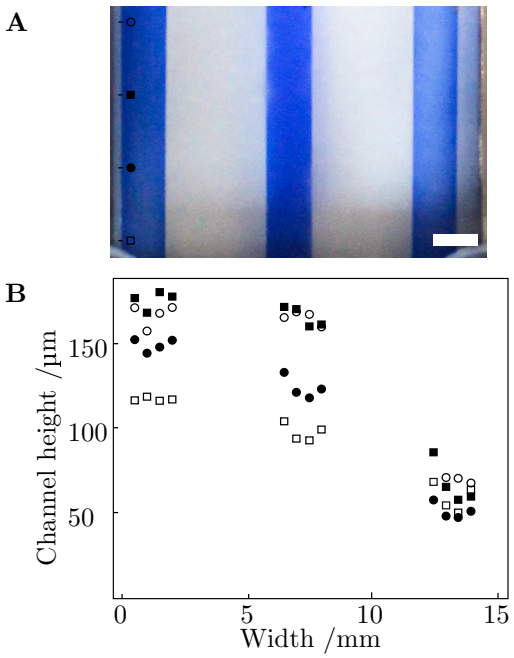

Figure 3.5.2: Height of PDMS channels. Design with three parallel channels. A: Visualization of inhomogeneous channel heights after assembling the MicCell System using blue ink. Channel width is 2 mm, theoretic channel height 150 µm. Plot marks on the left side illustrate the arrangement of measured positions presented in the bottom graph. Scale bar represents 2 mm. B: Measurement of channel height after assembly (10 N cm) at different positions along channel length. Distance in between individual positions is 5 mm. Data points represent the average of two measurements.

methods, 3D printing or micro milling, depending on the required channel aspect ratios or surface roughness. A mixture of monomers and curing agent is injected into the assembly and let either rest for 24 h to 48 h or cure for 2 h to 4 h at 60 °C to 80 °C. When the PDMS is fully cross linked, the cover plate and the attached PDMS layer are carefully removed from the frame and channel master. The peptide array is inserted into a frame onto which the cover plate is mounted. By screwing the cover plate onto the frame, a small pressure is applied to the PDMS and the peptide array to seal the microfluidic channel. The screws are tightened uniformly using a torque-limiting wrench. Finally the filler plugs are exchanged against fluidic ports. The dimensions of the channels mentioned in the following sections, can be found in the appendix (figure B.8.1, p. 109).

3.5.2 Pressure induced deformation of PDMS-layer

To seal the assembly of the MicCell, the PDMS layer is pressed onto the peptide array by screwing the cover plate onto the holding frame. The clamping force needed for sealing depends on the applied flow, but mainly on the channel design in the PDMS layer. It was observed that a distance of 4 mm between channels has to be maintained to prevent leakage from one channel into another. This limits the amount of channels which can be placed on the area of a standard slide.
It was impossible to apply a continuous flow onto the design with four parallel channels with 2 mm spacing, without massive leakage. Even for 18 N cm clamping pressure, which causes observable deformation of the elastic PDMS layer. The deformation at 10 N cm clamping pressure is depicted

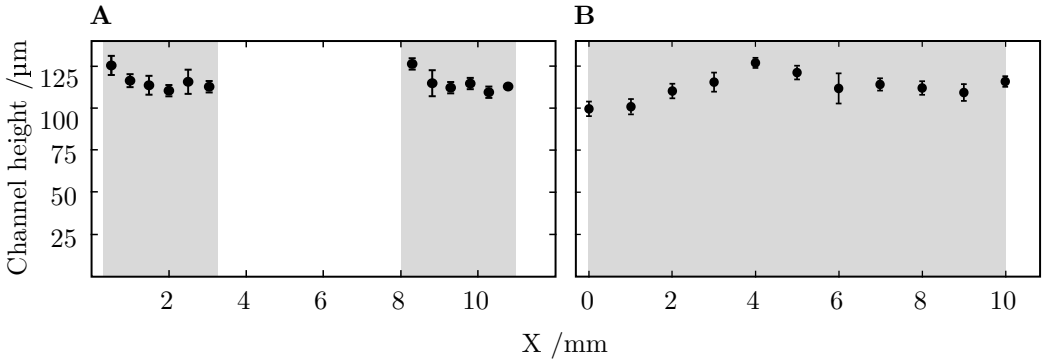

Figure 3.5.3: Heights of the one inch design PDMS channels. Height is measured across the width of the PDMS layer (X). Gray areas mark the location of the actual channel within the PDMS layer. A: Two parallel channels of 3.5 mm width. B: Single channel of 11.6 mm width. Measurement of channel height after assembly (10 N cm) at the center between in and outlet. Data points represent the average of three measurements. Channel width is 3.5 mm, channel height 150 µm. Measurement provided by L.K. Weber.

in figure B.8.2 on page 109. The deformation of the design with three parallel channels, spaced 4 mm apart on the area of a standard slide, can be seen in fig. 3.5.2. Severe deformation was observed for all channel designs on the area of a standard microscope slide (25 mm by 75 mm). The local channel height was determined optically by measuring the distance of focal planes using a microscope (see section 4.10 on page 82).

The deformation due to clamping was found to be least for the design on a one by one inch area. Figure 3.5.3 shows the compression of the respective channel designs. The height profiles for the two parallel channels are compressed about 15 % to 20 %, but are quite comparable. It was assumed that the orientation of the channel to the screws plays a roll in the orientation of deformation.

3.5.3 Leak tightness

Except for the before mentioned channel design with four parallel channels, all designs are found to be leak tight up to a flow rate of 3 ml min^{-1} when screws are tightened until a torque of 10 N cm.

3.5.4 Reduction of background fluorescence

For the capture of the faint fluorescence intensity at the beginning of an incubation, exposure times of several seconds are necessary. During the long exposure, also the low fluorescence emitted by the PDMS layer itself is amplified and results in increased background. For the one inch channel designs also the increase in background fluorescence by stray light refracting from the threads of the fluidic ports plays a role since the threads are partly within the FOV. Therefore, graphene particles were added to the PDMS as introduced by Galla *et al.* [47], to conceal the polymer from light and thus decrease the excitation of fluorescence in the PDMS layer. The maximal mass percentage of graphene particles was found to be 2 %. Higher percentages resulted in reduced viscosity and impeded the injection of blackened PDMS (bPDMS) during casting. Background

fluorescence was reduced by ∼70 % for an exposure time of 8 s and a gain of 8.

3.6 Detection system fluorescence imaging

In the following section fluorescence imaging which is applied for the fluorescence detection is described in more detail. The excitation was tested for its linearity and the temperature dependency of the dyes fluorescence intensity was investigated. Furthermore, the image resolution and the resulting minimal spot size were determined. The sensitivity of the setup was tested on anti-FLAG antibody labelled with Cy3 or DL550 and FLAG peptide. Also the minimal sampling rate was determined.

3.6.1 Fluorescence excitation

To image the increase in fluorescence intensity of peptide spots, which correlates to peptide-antibody binding, the linearity of fluorescence excitation and detection has to be ensured. For excitation from below (LED 1 in figure 3.4.1 p. 56) the power of light at the position of the microfluidic channel was measured using a power meter (PM160, Thorlabs). The detected power was stable at (7.10 ± 0.04) mW approximately 60 min after a cold starting (figure B.7.1, p. 108).

3.6.2 Field of view and Resolution

For maximum magnification, a minimum sized FOV of 5 mm × 3.8 mm can be attained. To fit more than just one 3 mm channel in the FOV, it was adjusted to 16 mm × 12.1 mm. The corresponding imaging resolution was determined to be (6.23 ± 0.11) µm pixel^{-1}. It was calculated by comparing spot diameters in pixels in a fluorescence scan with known resolution to a fluorescence image captured by the setup ($n = 10$). From this follows a minimal spot diameter of 75 µm. To maintain a linear correlation between the intensity of incident light on the CCD and the thus generated pixel gray scale values, the camera gamma value was set to 0.33 according to the manufacturer.

3.6.3 Stability of fluorescence intensity during incubation

Fluorescence is affected by temperature (thermal quenching) and is prone to bleaching effects due to long and intense excitation. For the continuous flow assay a DyLight dye (DyLight 550 NHS ester, Thermo Scientific) was chosen as fluorophore because of its stability compared to rhodamine (5-carboxytetramethylrhodamine succinimidyl ester, Thermo Scientific) or cyanine (Cyanine 3 N-hydroxysuccinimide ester, Abcam) dyes in our experience. In order to evaluate the performance of the fluorophore under assay conditions, the dye was diluted to 1 µM in phosphate buffered saline with 0.05 % Tween 20 (PBS-T) buffer and injected in a microfluidic channel molded into black PDMS (see section 3.5 for more information on PDMS channels). The channel was placed at the sample position and excited using one LED (M530L3, 530 nm) from below, as can be seen in figure

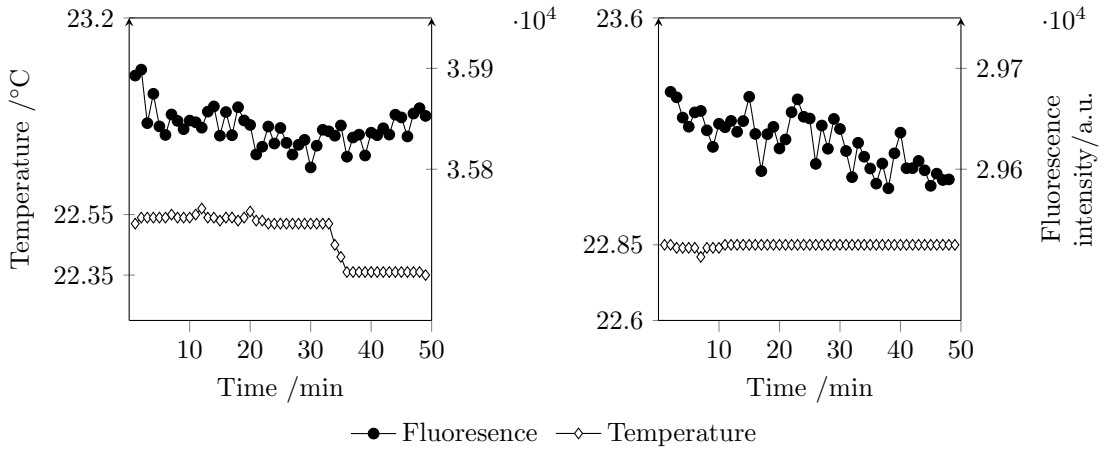

Figure 3.6.1: Fluorescence intensity for 1 µM DyLight550 over time. Time courses for apparently stable temperature ±0.1 °C results in ±100 a.u. stable fluorescence intensity. 100 a.u. correspond to < 0.5 % of the respective initial intensity. Imaging parameters: exposure 5 s, left: gain 10, right: gain 8.

3.4.1 on page 56. The temperature was measured on top of the channel and as reference on the backside of the mounted LED. No flow was applied during the experiment to simulate long time exposure of the dye. The median fluorescence intensity of approximately 50 % of the channel area centered in the field of view was calculated as described in section 4.6.2 Fluorescence imaging on page 79. For the conducted experiments, the absolute increase in temperature over the time of measurement was ranging from < 0.5 °C to 2.5 °C. The respective changes in fluorescence intensity were recorded over a time course of 50 min and the sampling rate was set to one minute. Figure 3.6.1 shows some exemplary progressions. For a temperature apparently stable at ±0.1 °C, the decrease in fluorescence intensity was stable at ±100 a.u.. 100 a.u. correspond to ≈ 0.15 % of the dynamic range of a 16 bit image or ≈ 0.5 % of initial fluorescence intensity (see figure 3.6.1). However, the temperature log is biased by its accuracy of ±0.3 °C. Despite this, no significant decline in fluorescence intensity can be observed for a period of 50 min of exposure. For apparently stable temperatures (±0.1 °C), the fluorescence intensity of the investigated dye can be approximated to be constant, which is the prerequisite for using fluorescence for the detection of interaction in this assay.

The change in fluorescence intensity for a bigger temperature difference is depicted in figure 3.6.2. For an approximately linear increase in temperature, the fluorescence is decreasing also approximately linear. A direct and consistent physical correlation between temperature and fluorescence intensity was supposed in the following. The decline in fluorescence intensity was plotted versus the temperature increase and the respective slope was calculated by linear regression (figure 3.6.2, left). The thus calculated slopes, the decrease in fluorescence in percent to the initial intensity per temperature increase of 1 °C, is plotted versus the temperature difference (Δ_T) (exclusively increase) occurred during the measurement (figure 3.6.2, right). It appears, as if the decline in fluorescence intensity increases with a decline in temperature increase (Δ_T) during the measurement. A preliminary correction factor was obtained to be $1.64\% \cdot \Delta_T + 0.5\%$. However, the accuracy of

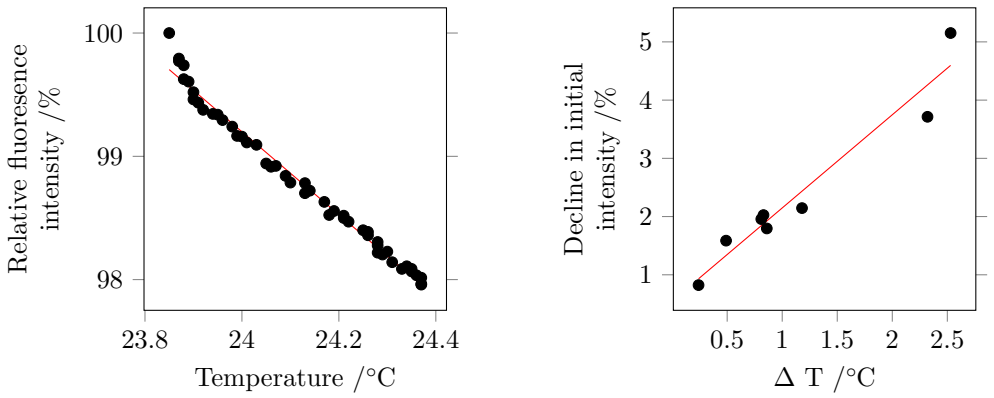

Figure 3.6.2: Fluorescence intensity for 1 µM DyLight550 over time for different, non stable temperature courses. Imaging parameters: exposure 5 s gain 8. Left: Temperature increases about 0.5 °C during the experiment, while fluorescence intensity decreases about 2 %. Right: Decline in fluorescence intensity in percent of the initial intensity per temperature increase as function of temperature difference during measurement. Coefficient of determination (r^2) > 0.94 for all measurements. Red line: $f(x) = 1.6x + 0.5$ obtained by linear regression.

the temperature sensor of ±0.3 °C should be kept in mind. A more accurate temperature sensor and more measurements are required to determine a statistical relevant correlation and account for outlier. A meticulous determination of this correlation could deliver a correction factor, which is needed in case of temperature increases during measurements.

3.6.4 Sensitivity and time intervals for imaging

The limit of detection depends strongly on the intensity of the fluorescence, which is emitted by a single protein and thus on the ratio of fluorophore per protein as well as on the fluorophore itself. The lowest concentration tested was 1.3 nM of anti-FLAG M1 Cy3 antibody on 400 µM FLAG spots (see figure 3.6.3). However, the ratio of fluorophore per antibody could not be determined due to the low batch quantity. This also applied to another batch of anti-FLAG antibody, labelled with DL550. The lowest detectable concentration was 30 nM (see figure 3.6.4). To capture these minute fluorescence intensities, long exposure times are needed. From experience, exposure times in the range of 8 s and a gain of 8 resulted in detectable increase of fluorescence intensity for different batches of antibodies.

The minimal sampling rate for the experiment presented in figure 3.6.4 was found to be 60 s. Even tough, the exposure time was set to 8 s, the time for downloading the image from the camera onto the PC, and saving it, took the remaining 52 s. Setting shorter sampling rates resulted in camera crashes. As can be seen in figure 3.6.4, the duration of the initial binding phase in which the intensity increases linearly was about 5 min. Depending on the velocity of interaction, this sampling rate might not represent the signal increase appropriately.

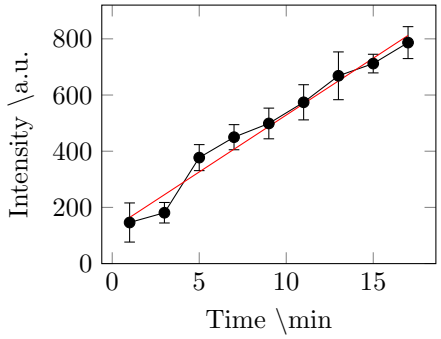

Figure 3.6.3: Background corrected mean fluorescence intensity of six 400 µM FLAG spots (three drops per spot) incubated with 1.3 nM anti-FLAG M1 Cy3 antibody over time. The spots were located in the center of the channel. Temperature was stable at (24.5 ± 0.3) °C during incubation. Channel: 1 inch design with a single channel. Flow rate was set to 200 µl/ min corresponds to a flow velocity of about 2 mm s^{-1}, assuming a constant height of 125 µm for the compressed channel. The exposure time was 9 s at a gain of 8. Sampling rate was set to 2 min.

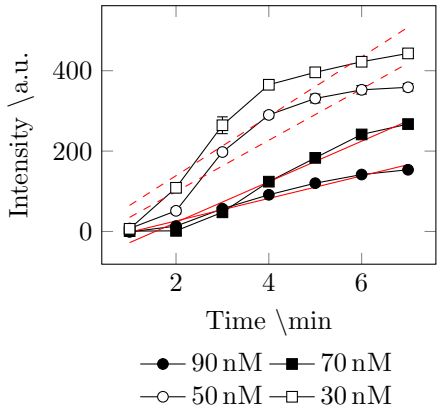

Figure 3.6.4: Background corrected mean fluorescence of 400 µM FLAG spots incubated with different concentrations of anti-FLAG M1 DL550 antibody over time. Temperature was stable at (24.7 ± 0.5) °C during incubation. Channel: 1 inch design with two parallel channels. Experiments have been conducted on two peptide arrays. The fill colour of the marks indicate association to the respective array. Flow rate was set to 50 µl/ min corresponding to a flow velocity of about 2 mm s^{-1}, assuming a constant height of 120 µm for the compressed channel. The exposure time was 8 s at a gain of 8. Sampling rate was set to 1 min.

3.7 Peptid array-glass channels by adhesive layer bonding

This approach minimizes the compression of channels, and the tight bond formed between the peptide array and the glass substrate allows for minimal lateral space in the micrometer range. The feasibility of creating sealed microfluidics by bonding two glass substrates with an intermediate layer of Ordyl dry film resist was first presented by Vulto *et al.* [171] and since then applied in various ways to bond glass-glass microfluidic channels [157, 172] or to structure other materials like poly(methyl methacrylate) (PMMA) [168] or polycarbonate (PC) [153] for channel fabrication. The difference of this approach to standard glass-glass bonds is the chemical composition of the surface on which the peptide array is synthesized. A polymer film is crafted onto a glass substrate containing functional groups, which allow the coupling of amino acid monomers or whole peptides.

Four different functionalized surfaces used for the most popular synthesis strategy of peptide arrays were investigated. Since the channel fabrication normally involves high temperatures (150 °C), the impact of the production process on the peptide array was investigated. The process parameters for bonding and post bond baking needed to be altered to significant lower temperatures, since degradation may occur during high temperature process steps. To connect the channels to tubes, a simple and compact interface (see figure 3.4.1on page 56, B), which can be placed in a fluorescence microscope or integrated into more complex microfluidic networks to perform fluorescence immunoassays, was designed.

3.7.1 Fabrication process

The fabrication process is illustrated in figure 3.7.1 and the detailed protocol can be found in section 4.11 on page 82. It involves the production of a peptide array and the clean room fabrication of sealed microfluidic channels based on a dry film resist an lithography. First, a glass substrate is cut to microscope slide format. Chromium marks are patterned on the substrate to mark the positions where holes, serving as fluidic ports, are laser drilled into it. The substrate is then cleaned and the dry film resist is laminated on top. Before and after exposure, short bakes are conducted (soft bake, post exposure bake (PEB)). The resist is developed and the substrate is cleaned for being joined with the peptide array. Therefore, a peptide array and the structured substrate are placed on top of each other, with the functional side of the peptide array facing towards the patterned adhesive layer of the resist. Under vacuum and applying pressure, both substrates are bonded at elevated temperature. Finally a post bond bake (PBB) is performed for 1 h under protection gas. Vacuum and protection gas are used to impede hydrolysis of the functional surface, which is accelerated at elevated temperatures.

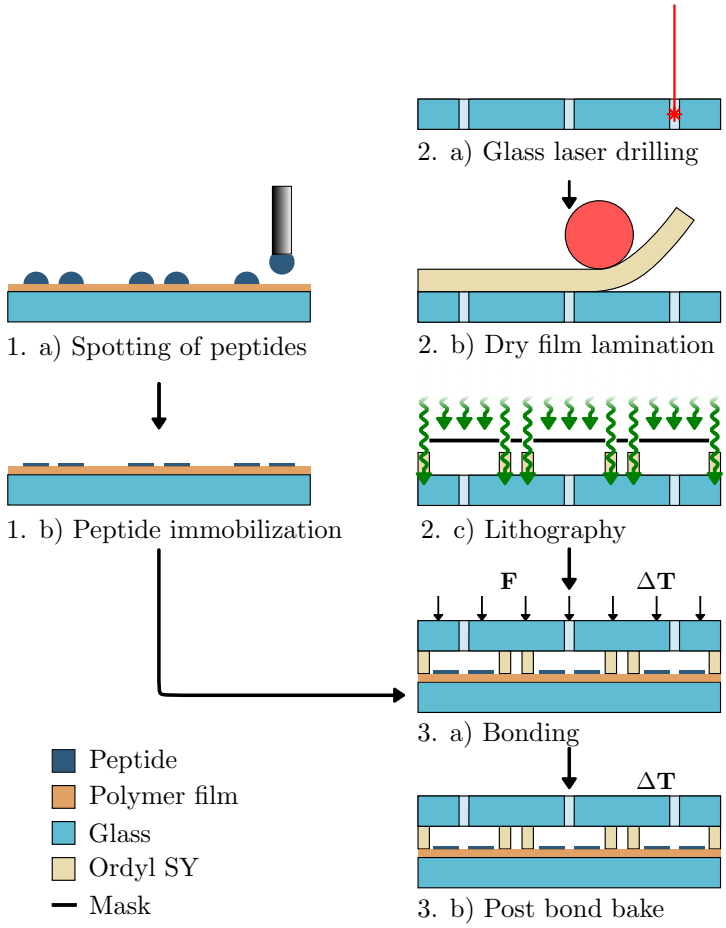

Figure 3.7.1: Fabrication process for adhesive layer bonding. 1. Peptide array production. 1. a) Peptides deposited in array format by spotting onto a functionalized surface. 1. b) Unreacted peptides are washed away and the free linker on the surface is blocked to prevent further reaction. 2. Preparation of glass substrate. 2. a) Holes are laser drilled into a glass substrate to serve as fluidic in- and outlets. 2. b) A negative dry film resist is laminated onto the pre-treated glass substrate. 2. c) A mask is applied and the resist is exposed and not cross linked residues are removed by washing. 3. Joining of the glass substrate and the peptide array. 3. a) Peptide array and pre-structured glass substrate are bonded together to form a microfluidic channel. 3. b) After bonding a post bond bake is performed. The resulting channel consists of the a glass top layer, the functionalized glass slide of the peptide array as bottom layer, and the structured film resist as side walls that define the channel geometries. Based on a figure by M. Meissner.

3.7.2 Impact of baking steps on peptide arrays

Temperatures for bonding reported in literature range from 80 °C [64] to 195 °C [171], followed by a PBB or hard bake at 150 °C. The elevated temperatures during this bake further increase the cross linking of the resist. Reported temperatures for PBB range from 120 °C [43] to 195 °C [137], most commonly being 150 °C [171, 64, 172]. In all protocols concerning the bonding of two substrates, a temperature of 150 °C was applied during PBB, which is supposed to further improve cross-linking of the resist but probably also serves to out-gass the solvents contained in the resist. However, peptide arrays are heat-sensitive, therefore the temperature for bonding and post bond baking is the challenging parameter addressed in this experiment. To investigate the thermal stability of the peptides, bakes at different temperatures were conducted (see figure 3.7.2). Therefore, peptide arrays were prepared containing HA-peptide and SRP using 3D-Maleimide surfaces. The variability due to spotting was minimized by using functionalized surfaces from the same batch, performing the spotting and further wet chemical steps for peptide immobilization in one experiment under the same environmental conditions and cutting the generated peptide arrays into pieces to further minimize inter substrate variations, whereas one piece per substrate was used as reference. After baking at different temperatures, arrays were incubated with human serum over night and subsequently with anti-HA DL800 and anti-IgG DL680 for 1 h and scanned in a fluorescence scanner (sec. 4.2 on p. 76). The median fluorescence intensity per spot was averaged over the entire array. Even though the inter array deviation in fluorescence intensity is quite high, the mean intensity tends to decrease for increasing temperatures. Arrays exposed to 100 °C also tend to exhibit decreased fluorescence intensities. Since heat input is essential for fabrication, a compromise must be made between minimizing surface damage and best possible bonding conditions.

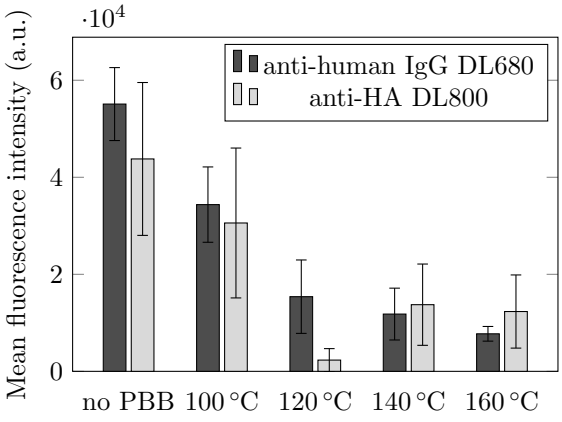

Figure 3.7.2: Mean fluorescence intensities after performing a bake at different temperatures. The bake was conducted for 1 h at different temperatures under argon atmosphere.

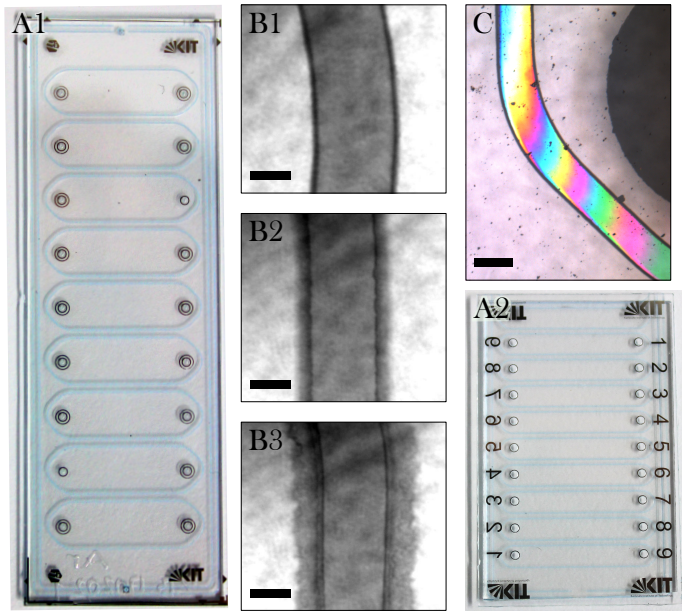

Figure 3.7.3: Images of whole peptide chips in different designs and individual structures. A: Ready to use peptide chips, exposed at 200 mJ cm^{-2}, bonded at 100 °C, 735 N cm^{-2} for 30 min onto 3D-Maleimide. PBB at 100 °C for 1 h. Design: A1: 6 mm channel width, A2: 3 mm channel width. B: Microscopy images of the bonded Ordyl structures on glass for different exposure doses. B1: 150 mJ cm^{-2}, B2: 250 mJ cm^{-2} B3: 350 mJ cm^{-2}. Scale bars indicate 100 µm. C: Thinning failure due to small distance of hole to Ordyl structure. Scale bar represents 200 µm.

3.7.3 Optimization of process parameters

To minimize the heat induced thinning failures caused by the flow of Ordyl into the laser drilled holes during lamination and soft bake (see figure 3.7.3 C), the distance between the holes in the glass and the Ordyl structures was set to ≈1 mm. Further, a low temperature for lamination and soft bake (80 °C) and maximal hole diameters of 500 µm resulted in defect free channel formation. Since doses above 250 mJ cm^{-2} resulted in increasing overexposure for front side exposed glass on glass bonds, as can be seen in figure 3.7.3 B1-B3, the range of doses tested on 3D-Maleimide surfaces was limited to 150 mJ cm^{-2} to 225 mJ cm^{-2}. For these doses tested in front side configuration (150, 175, 200 and 225 mJ cm^{-2} on 3D-Maleimide surfaces) good results could be achieved, with 200 mJ cm^{-2} resulting in minimal defects. In order to estimate the magnitude of the fracture strength, simple pull tests were randomly conducted. The observed failure was cohesive for all samples and occurred at the interface Ordyl/ peptide array. It was not possible to detect significant differences in fracture strength among the different doses tested on 3D-Maleimide or for the three other surfaces exposed at 200 mJ cm^{-2}. The average fracture strength on 3D-Maleimide for all samples investigated was measured to be (305 ± 50) N cm^{-2}. This corresponds to a theoretical pressure resistance of maximal 4.9 bar per channel ($w \times h \times l$, $(3 \times 0.11 \times 17.5)$ mm^3).
For the bonding process, pressures ranging from 220 N cm^{-2} to 735 N cm^{-2} were tested at 100 °C for 30 min and a 1 h post bonding bake at 100 °C was performed. No influence of the applied pressure was observed. Thus it was found, that at 2950 N cm^{-2} structures are destroyed by flattening.

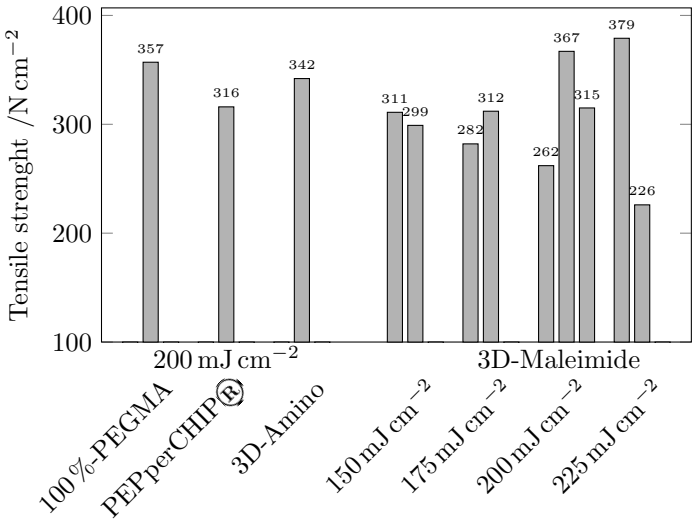

Figure 3.7.4: Pull tests on random samples for the estimation of magnitude of fracture strength for peptide chips exposed at 200 mJ cm^{-2} on different functional surfaces or exposed at different doses on 3D-Maleimide surfaces.

3.7.4 Compatibility of functional surfaces to adhesive layer bonding

To investigate the compatibility of peptide arrays with the Ordyl process, different functionalized surfaces were tested. The PEPperCHIP®, the 3D-Amino and the 100 %-PEGMA surfaces were tested as representatives of the carboxyl group reactive type of surfaces, 3D-Maleimide surface was tested as representative of thiol reactive type of surfaces. Process parameters optimized for the 3D-Maleimide surface were applied (exposure dose: 200 mJ cm^{-2}, bonding pressure: 735 N cm^{-2}, bonding temperature: 100 °C, bonding duration: 30 min, PBB temperature: 100 °C, PBB duration: 1 h). The structure quality was determined by optical inspection. No defects were observed for the 100 %-PEGMA and 3D-Amino surface, one defect in one channel-structure was observed in the PEPperCHIP®(see Appendix figure B.9.1 A, page 110) and two minor defects in two channel-structures in the 3D-Maleimide surface (see Appendix figure B.9.1). Defects did not compromise leakage of the channels. Fracture strengths were found to be 202 N cm^{-2}, 203 N cm^{-2}, 219 N cm^{-2} and 228 N cm^{-2} respective for the 3D-Maleimide, PEPperCHIP®, 3D-Amino and 100 %-PEGMA surface.

3.7.5 Observations on flow profiles

Channels were suspect to optical inspection, since height measurement as described in section 4.10 is not applicable on the peptide chip. The flow profiles showed to be parabolic (figure B.9 B) and no significant difference in channel height was observed judging from the shade of the ink across channels (figure B.9 C).

3.7.6 Automatized incubation of the peptide chip

A simple and easy to assemble interface was designed to connect the microfluidic channels on the chip to the tubing (see figure 3.4.1on page 56 B). The setup shown in figure 3.4.1 A1 on p. 56, was used to excite and detect fluorescence signals originating from binding events of fluorescently labelled sample antibodies to peptide spots. A sensitive fluorescence microscope with a camera capable of taking time laps images is also suitable to perform the experiment. Incubation process, imaging and data processing was automatized and controlled using LabView. Auto fluorescence of Ordyl did not interfere with the imaging, since the field of view was adjusted to the channel under investigation. Furthermore, no leakage was observed at the maximum pump rate possible (corresponding to $750\,\mu l\,min^{-1}$) for the syringes applied.

3.8 Conclusion

An experimental setup to perform continuous flow assays on peptide arrays and preliminary studies for the establishment of concentration analysis was realized. In this context, a method for the production of peptide arrays was established as well as a method for label-free quality control for the development of the production method. Two possibilities to integrate peptide arrays into microfluidic channels were tested. Furthermore, it was shown, that the fluorophore selected for signal detection remained stable under the experimental conditions.

For the fast fabrication of peptide arrays spotting has been established. The 3D-Maleimide surface turned out to be the most economic in preparation time and pricing among the surfaces tested. Its ligand density was found to be comparable to the of the PEPperCHIP®, albeit its surface hydrophobicity is considerably lower. Spot diameter for the HA peptide at 400 µM vary about 5, 7, 12 and 25 µm for one, three, five and seven drops per spot respectively. For a FOV of 16 mm × 12.1 mm these variations correspond to 1, 2, 2 and 5 pixel.

It was demonstrated that VSI is a very sensitive method to visualize peptide arrays unbiased by a fluorophore dye. Median local deviations in z of height profiles measured by VSI vary less than 1 nm from those measured by AFM. Given that the measuring principles are completely different, and that measurements were performed in different rooms and thus under non constant environmental conditions, the obtained height profiles are astonishing comparable. Spots can be resolved down to 1 nm spot height on a FOV of 174 µm × 131 µm as well as on 1.74 mm × 1.31 mm. Under optimal conditions this allows to visualize not only minute antibody layers adsorbed to a peptide spot but also bare peptide spots, without any antibody treatment. The z resolution remains preserved also for larger FOV which can be obtained by stitching. Stitching to obtain a scan area of up to 3 mm × 3 mm was demonstrated without further re focussing while resolving spots with median heights < 5 nm in about 4 min. Even though default scanning of a whole array using VSI is still too time consuming compared to a fluorescence scan at a comparable resolution, VSI

allows to image areas of special interest or a representative area ((≈10 %) in under 1 h, unbiased by a fluorophore dye. Additionally a method for the evaluation of the dynamic range of fluorescence labelled protein was presented. This will allow for assays to compare absolute fluorescence intensities and might also be set up for label free quantification in the future. However, therefore the influence of drying on the protein layer height and density has to be investigated in more detail.

A set up has been designed for the automated incubation of peptide arrays with sample and for fluorescence imaging. The FOV was adjusted to 16 mm × 12.1 mm to depict more than just one 3 mm channel at the same time. This resulted in a resolution of $(6.23 \pm 0.11)\,\mu\mathrm{m\,pixel}^{-1}$. The LED should be turned on ∼ 1 h prior fluorescence imaging to obtain a constant illumination power. The fluorescence intensity of the tested dye DL550, is stable for constant temperature (±0.1 °C at around 24 °C) for up to 50 min under assay conditions. The stability over a broader time range was the precondition for the use of a fluorophore dye for the detection of binding antibodies. In the future, the set up could be extended by an active temperature regulation. For this fluorophore, the lowest detectable antibody concentration was 30 mM anti-FLAG DL550. However, the degree of labeling varies from batch to batch of antibodies. To develop a standard as part of further assay development, the degree of labeling needs to be correlated to a fluorescence intensity.

Two different channel fabrication methods have been investigated for the incorporation of peptide arrays. The PDMS method was improved by adding up to ∼ 2 % (*w/w*) graphene particles prior to polymerization. This reduced the background fluorescence by approximately 70 % for the long exposure times (8 s, a gain of 8), which are required to detect minute fluorescence signals. The channel containing PDMS layer is clamped onto the peptide array. The so assembled channels proved to be leak tight up to a flow of $3\,\mathrm{ml\,min}^{-1}$ when screws were tightened until a torque of 10 N cm. The advantages of the PDMS channels are their applicability for rapid prototyping through the easy and fast production. However, the restriction of channel design was determined to be a minimum distance of 4 mm in between channels. This space is needed as seal face. Also the channels are being deformed by clamping. This showed to be noticeable for the 1 inch design and severe for the designs of the area on a standard sized microscope glass slide (25 mm × 75 mm). The PDMS system is thus adequate for all applications where the channel cross section (and with it the flow velocity) does not need to be reproducible intra array, for example automated incubations for epitope mapping, or by using just one channel for one assay. However, the limitations for these applications have jet to be determined in detail.

The second type of channel fabrication involves the lithographic structuring of an adhesive layer and subsequent bonding of glass to the peptide array. Glass has the advantage of being more rigid and better suited to optical detection methods. As adhesive layer, the dry film resist Ordyl SY355 was used. The process window was determined to be quite broad with exposure doses ranging from $150\,\mathrm{mJ\,cm}^{-2}$ to $220\,\mathrm{mJ\,cm}^{-2}$ and bonding pressures ranging from $220\,\mathrm{N\,cm}^{-2}$ to $735\,\mathrm{N\,cm}^{-2}$. Also,

flood exposure can be performed with just minimal tapering of the structure, making it simple enough for most labs with clean room capabilities. Since the peptide array is temperature and oxygen sensitive, 100 °C should not be exceeded during fabrication and all process steps involving the peptide array should be performed under vacuum or protective gas. The magnitude of the fracture strength was estimated to be $(305 \pm 50)\,\mathrm{N\,cm^{-2}}$ on 3D-Maleimide surfaces. As expected, this is significantly less than values reported for glass-glass bonding using Ordyl ($(1300 \pm 236)\,\mathrm{N\,cm^{-2}}$ [64]), but was found adequate for common moderate pressure driven microfluidics. Channels of the peptide chip are theoretically resistant to a pressure of up to 4.9 bar, and proved to be leak proof for a flow rate of up to $750\,\mathrm{\mu l\,min^{-1}}$.
The process described should be transferable to all types of micro arrays, extending the range of applications from mere peptide arrays to DNA, RNA and protein arrays. Furthermore, spatially resolved, high throughput assays can be performed that are capable of determining kinetic rates.

3.9 Outlook

In the next step, the antibody-peptide interaction of the epitopes $_{929}$ExxEVIVxK$_{937}$, PALT(A)xET and PEFxGSxP should be investigated. The experimental setup developed for this purpose proved to be functional and the prerequisites for the analysis of antibody concentration were created. It remains to calibrate the fluorescence intensity using fluorescently labelled antibodies with known dye to protein ratio. A defined amount of these antibodies can be spiked into the actual serum sample as standard prior to labelling it. Improvements on the setup could be the establishment of a temperature control to actively adjust the temperature in the microfluidic channel. Also an upgrade of the camera for the imaging could reduce the intervals in between images taken due to a faster download to the computer. Further the fabrication process of microfluidic channels by adhesive layer bonding could be extended to incorporate sensors for monitoring temperature, pH or ionic strength. By adding actuators, valves, and a more complex microfluidic network, it would be possible to fabricate lab-on-chip or lab-on-disc systems.

4 Materials and Methods

4.1 Peptide array synthesis

In this work, different functionalized surfaces have been used for the synthesis of peptide arrays. For peptide arrays produced by immobilization of peptides by spotting, either 3D-Maleimide surfaces (PolyAn, Germany) were used or 2D-Amino surfaces (PolyAn, Germany), PEPperSlide®10 % PEGMA /90 % PMMA (Pepperprint, Germany) and 100 % PEGMA surfaces have been functionalized with maleimidobutyryloxysuccinimide ester (VWR, USA).

4.1.1 Synthesis of 100% PEGMA surfaces

Protocol according to J. Striffler [162].

Cleaning and activation Glass slides were placed in a glass chamber (place for 10 slides, volume 200 ml) and shaked in 1 M potassium hydroxide (Sigma Aldrich, USA) in Isoporopanol (Sigma Aldrich, USA) for 3 h, to generate hydroxyl groups. Subsequently glass slides were rinsed with deionized water and Ethanol (Sigma Aldrich, USA), dried in an argon gas flow and directly reacted with the silane solution.

Silanization Cleaned and activated glass slides were placed in a glass chamber in an desiccator under inert gas and incubated with a mixture of 2.4 % deionized water, 2.9 % (3-aminopropyl)-triethoxysilane (APTES) (Sigma Aldrich, USA) in ethanol for 6 to 16 h. After incubation, glass slides were rinsed in ethanol, washed three times in dichlormethane (DCM) (VWR, USA) in an ultrasonic bath for 5 min. Afterwards glass slides were heated in an oven to 120 °C for 45 min and subsequently stored at 4 °C under inert gas.

Nucleophile substitution Silanized glass slides were placed in a glass chamber in an desiccator under inert gas. DCM was cooled to 0 °C and in a counter flow of inert gas one equivalent α-bromoisobutyrylbromid (BIBS) (Sigma Aldrich, USA) (0.1 mM) and six equivalents *N,N*-diisopropylethylamin (DIPEA) (VWr, USA) was added. The solution was shortly mixed and incubated with glass slides for 6 to 16 h. For washing, the glass slides were placed in a glass chamber and shaked 6 to 16 h in DCM and subsequently 2×2 min in methanol (Sigma Aldrich, USA).

The glass slides were dried in an argon gas flow and stored under inert gas at 4 °C until further processing.

Polymerisation of 100 % PEGMA Glass slides were placed in a glass chamber in an desiccator under inert gas. A Schlenk flask was evacuated and loaded with argon three times and 75 ml PEGMA (VWR, USA), 75 ml deionized water and 75 ml methanol were added at counter flow of inert gas. Further, 1.7 g 2.2-bipyridyl (Bipy) (VWR, USA) was added and mixed till dissolved completely. Subsequently 0.94 mg Copper(I)bromide (VWR, USA) was added and mixed for 5 min. The mixture was poured into the glass chamber and incubated for 6 to 16 h. For washing the slides were washed 3×5 min with deionized water and 2×2 min with methanol. Possible residues were removed by applying ultrasound in DCM for 2×2 min. The glass slides were dried in an argon gas flow and stored under inert gas at 4 °C until further processing.

Amidation and esterification in *N,N*-diisopropylcarbodiimide (DIC) and *N*-methylimidazole (NMI) Polymerized glass slides were placed in a glass chamber in an desiccator under inert gas. In a Schlenk flask, a 0.2 M solution of the amino acid β-alanine (Iris Biotech, Germany) in DMF (VWR, USA) was prepared. 1.2 equivalents of DIC (VWR, USA) (0.24 M) were added in counter flow of inert gas and stirred for 5 min. Then two equivalents of NMI (Sigma Aldrich, USA) (0.4 M) were added, also in counter flow of intert gas and stirred for 1 min before pouring into the glass chamber. The desiccator was incubated and flooded with inert gas three times, and the slides were incubated for 16 h. For washing, slides were shaked 3 x 5 min in DMF, 2 x 3 min in methanol, subsequently dried in a gas flow of inert gas and stored at 4 °C until further processing.

Acetylation of free amino and hydroxyl groups After coupling or immobilisation of a peptide or amino acid, the functionalized glass slides were placed in a glass chamber in a dessicator and incubated with a mixture of 10 % (v/v) acetic anhydride (VWR, USA), 20 % (v/v) DIPEA and 70 % (v/v) DMF for 16 h to acetylate the free hydroxyl groups. After the peptide is synthesized (before removal of protection groups) a second acetylation of about 2 to 4 h is performed, to acetylate free amino groups. For washing the functionalized glass slides are shaked 2×2 min in DMF, 2×2 min in methanol, rinsed in DMF and dried in a gas flow of inert gas and stored at 4 °C until further processing.

Removal of side chain protection groups After immobilisation of a complete peptide, the functionalized glass slides were placed in a glass chamber into a dessicator and swollen in DCM for 30 min. Next, they were shaked in a mixture of 51 % (v/v) Trifluoracetic acid (Sigma Aldrich, USA), 3 % (v/v) triisobutylsilane (TIBS) (VWR, USA) and 2 % (v/v) deionized Water in DCM for 3×30 min. In case of turbidity of the surface, incubation time was terminated. For washing functionalized glass slides were shaked 2×5 min in DCM, 5 min in DMF, 30 min in a mixture of 5 % (v/v) DIPEA in DMF, 3×5 min in DMF and 2×3 min in methanol. Afterwards slides were rinsed in DCM and dried in a gas flow of inert gas and stored at 4 °C until further processing.

Removal of Fmoc-protection groups The Fmoc-protection group is removed to deprotect the *N*-terminal amino group of the amino acid or peptide. The functionalized glass slides were placed in a glass chamber into a dessicator and incubated for 20 min with a mixture of 20 % (v/v) Piperidin (VWR, USA) in DMF.

UV/Vis Photospectrometry of the piperidine dibenzofulvene adduct In the removal of the Fmoc-protection group the intermediate piperidine dibenzofulvene adduct is formed which is equivalent to the surface bound amino acid or peptide previously bearing the Fmoc-group. By comparing the absorption at 301 nm of the deprotection solution to a blank the concentration of PDFA can be determined according to Lambert-Beer's law [35, 14, 142]. A molar extinction coefficient of $\varepsilon = 5129\,\mathrm{l\,mol^{-1}\,cm^{-1}}$ was determined by M. Beyer [13, 14]. However, no absolute quantities can be obtained by this method, since different molar extinction coefficients have been reported by other groups [41]. This might be correlated to the PDFA to dibenzofulvene/piperidine equilibrium [142, 56]. Nevertheless, the obtained values can be compared to those obtained in the same manner [142, 13, 17]. The supernatant was pipetted in a cuvette and extinction at 301 nm was measured in a photometer (VIS Spectralphotometer, Jenway). By applying the law of Lambert-Beer, where n is the amount of PDFA in moles, A the area of the substrates surface, E the measured extinction and V the volume of the deprotection solution, ε the extinction coefficient and d the path length of the cuvette, the grade of functionalization (DG) was determined [142].

$$DG = \frac{n}{A} = \frac{E \cdot V}{\varepsilon \cdot d \cdot A} \tag{4.1.1}$$

4.1.2 Peptide array synthesis by spotting

For the synthesis of peptide arrays by spotting, presynthesized peptides containing an *C*-terminal cysteine where immobilized onto maleimid functionalized surfaces. Therefore 3D Maleimid surfaces were used or amino functionalized surfaces (2D Amino Surface or 100 % PEGMA surface) were further functionalized with maleimidobutyryloxysuccinimide ester.

Functionalisation of 100 % PEGMA surfaces with maleimidobutyryloxysuccinimide ester To immobilize or couple a peptide with the spotting method employing a thio reaction, the glass slides need to be functionalized with maleimidobutyryloxysuccinimide ester. For the 100 %-PEGMA surfaces and the PEPperCHIP®(Pepperprint) Fmoc-protection groups have to be removed first, to guarantee accessibility of amino groups (see paragraph 4.1.1 Removal of Fmoc-protection groups). Surfaces were placed in a petri dish into a desiccator. According to the protocol of Dr. J. Stiffler, 2.5 ml of a mixture of 0.1 M maleimidobutyryloxysuccinimide ester in DMF was pipetted onto one surface to be functionalized, while a second one is placed, face down, on top of the first one. The desiccator was evacuated and loaded with inert gas for three times and the mixture is left to react for 16 h. For washing, slides were carefully detached from each other and shaked 3×5 min in DMF, 2×3 min in methanol, rinsed in DCM and dried in a gas flow of inert

gas and stored at 4 °C until further processing.

Maleimide-click-reaction of Fmoc-D-Cys-OH from solution Maleimide functionalized substrates are swollen in PBS-T for 10 min. Fmoc-D-Cys-OH (Iris Biotech, Germany) is dissolved in PBS-T (0.5 % v/v Tween20 (Sigma Aldrich, USA) in PBS (Sigma Aldrich, USA)) to a concentration of 42 mM. Glass slides were placed in a petridish into a desiccator. 0.25 ml of the solution was pipetted onto one surface, while a second one was placed, face down, on top of the first one. The desiccator was evacuated and loaded with inert gas for three times and the mixture was left to react for 16 h. For washing, slides were carefully detached from each other and shaked 3×5 min in DIW, 2×3 min in methanol, rinsed in DCM and dried in a gas flow of inert gas and stored at 4 °C until further processing.

Deposition of peptides onto 3D Maleimide surfaces Peptides were dissolved in PBS containing up to 10 % glycerol (99 % (Alfa Aeser, Germany) and set to concentrations ranging from 50 nM to 400 nM. The spotting was conducted using a NanoPlotter 2.1 (GeSiM, Radeberg, Germany) using the Nano Tip J A70-401 20 310 for spot diameters >100 µm and Pico Tip J A070-402 p00738A for spot diameters <100 µm. Humidity in the spotting chamber was set to 60 % and temperature to 21 °C. After spotting, the slides were dried for 2 h in an argon flooded vial at room temperature and subsequently blocked in PBS containing 0.4 % 2-mercaptoethanol (Merck, Germany). The washing was performed at 70 RPM on an orbital shaker (Orbital Shaker DOS-20S, Elmi Ltd., Lettland) for 3 min with PBS, 3 min deinoized water, 5 min acetonitirile (VWR Chemicals, USA) containing 0.1 % trifluoroacetic acid (TFA) (99 %) (Honeywell Chemicals, USA), 5 min DMF containing 0.5 % DIPEA, 3×5 min DMF and 2×3 min methanol. Slides were dried in an argon gas stream and stored at 4 °C until further usage.

4.2 Incubation of peptide arrays with antibodies

4.2.1 Antibodies

The donation of serum by a human individual was approved by the state chamber of physicians of Baden-Wuerttemberg (reference number: F-2011-044 and F-2011-044#A1) and informed consent was obtained. To detect bound serum antibodies, a secondary antibody (goat) anti-human ($F_C\gamma$) AF647 (Jackson Immunoresearch, USA) was used at a concentration of 13.3 nM. Monoclonal anti-HA antibody, (provided by Dr. Gerd Moldenhauer (DKFZ, Heidelberg)), diluted to 1 µg µl^{-1} was conjugated to the fluorophores DL550 NHS esters (DyLight 550 NHS ester, Thermo Fisher Scientific, USA), DL680 NHS ester (DyLight 680 Micro scale Antibody Labeling Kit, Thermo Fisher Scientific, USA) or Cy3 (Lightning-Link Cy3 labeling kit, Innova Biosciences, UK) according to the instructions. Also degree of labeling, which is the ratio of fluorophore per protein, was determined if possible according to the instructions.

4.2.2 Incubation at equilibrium state

For all incubation and washing steps the peptide arrays are mounted into PEPperCHIP®incubation trays (PEPperPrint, Heidelberg, Germany), which allow for the subdivision of microscope glass slides into individual sub units. The tray stands on an orbital shaker with a rotation speed of 140 RPM (Orbital Shaker DOS-20S, Elmi Ltd., Lettland). For storage, the dry arrays are kept under argon atmosphere at 4 °C. The assay consists of two incubation steps, each followed by a fluorescence scan. To exclude unspecific interactions between secondary antibodies and peptides, a pre-staining of the array with secondary antibodies is performed, before incubation with the serum.

Swelling and blocking Each step starts with a swelling of the array for 10 min in PBS-T (pH 7.4). When incubated for the first time, the arrays are blocked for 30 min in Rockland buffer (Rockland Immunochemicals Inc., USA) to minimize unspecific binding. Afterwards, the arrays are washed shortly with PBS-T. In the scope of this work, two other blocking reagents were also tested: SmartBlock (Candor, Germany) and caseine blocking buffer 10x (Sigma Aldrich, USA).

Incubation For the pre-staining, the arrays are incubated with secondary DL680 and DL800 conjugated anti-human antibodies (Goat anti-human IgG-Fcγ DL680 and goat anti-human IgM-Fcμ, Biomol, Hamburg, Germany), diluted to 0.2 µg ml^{-1} in PBS-T with 10 % v/v blocking buffer for 30 min. For the main-staining, arrays are incubated with serum diluted 1:500 for the epitope mapping and 1:100 for the substitution analysis in PBS-T with 10 % v/v blocking buffer over night at 4 °C. For the detection of bound serum antibodies, the arrays are washed shortly with PBS-T and incubated with secondary antibodies as described above. The secondary antibody mixture additionally contains DL800 conjugated (fluorescently labeled using a DyLight 800 Microscale Antibody Labeling Kit, Thermo Fisher Scientific, Rockford, USA) monoclonal anti-HA antibodies (provided by Dr. Gerd Moldenhauer, DKFZ, Heidelberg) diluted to 1 µg ml^{-1} and/or monoclonal anti-FLAG M2 antibodies (Sigma Aldrich, USA) diluted to 0.2 µg ml^{-1}. After each incubation step, the arrays are washed shortly with PBS-T and 0.1 mmol dm^{-3} tris(hydroxymethyl)aminomethane (TRIS) (Sigma Aldrich, USA), dried with Argon and scanned at the respective wavelength.

4.2.3 Incubation in a microfluidic channel at continuous flow

All buffers used for washing, blocking and incubation were degassed and filtered sterile (membrane filter type 154, 0.2 µm pore size, Sartorius) using a bottle top filter (Nalgene, Thermo Scientific). In the first step the microfluidic channel is filled with PBS-T with 0.05 % Tween20 (PBS-T) (Sigma Aldrich) and the array is pre swollen for 10 min under flow with a volume flow rate of 600 µl/ min. Next, the system is blocked with Rockland buffer for 30 min to prevent any unspecific binding of antibodies in the system. The channel is then washed for 10 min with assay buffer (PBS-T containing 10 % *v/v* blocking buffer). The incubation of arrays with antibodies is realized at a flow

velocity of $2\,\mathrm{mm\,s^{-1}}$, resulting in Reynolds numbers of approx. 0.6 for all the microfluidic channels of the 1 inch design. Characteristic lengths were calculated for a rectangular cross sections [6].

4.3 Determination of antibody titer by ELISA

IgG anti-toxin antibody levels were determined for tetanus, diphtheria and pertussis by IgG ELISA IgG kits (Tetanus IgG ELISA, Diphtheria IgG ELISA and Pertussis IgG ELISA with Pertussis IgG Quantification kit, Sekisui Virotech GmbH, Germany) according to protocol. Evaluation was done according to the instructions; titers were calculated by the mean of three different dilutions in duplicates.

4.4 Isolation of specific antibodies

To isolate antibodies binding to the identified epitope $_{923}$IHLVNNESSEVIVHK$_{937}$ 16 ml of serum 11 were purified using a two-step batch chromatography. The first step involved protein G as ligand, the second step a pre-synthesized peptide immobilized on the chromatography resin. The isolated antibodies were tested in a tetanus IgG ELISA for their ability to interact with the native toxin. 16 ml of serum 11 were purified using the NAP Protein G Spin kit (Thermo Scientific, USA) according to protocol. The first four fractions were pooled and a buffer exchange to PBS was performed with the ZebaSpin Desalting kit 7K MWCO (Thermo Scientific, USA) according to the protocol. For the subsequently chromatography step the SulfoLink Immobilization Kit for Peptides (Thermo Scientific, USA) was used according to protocol. The pre-synthesized peptide (IHLVNNESSEVIVHK-βA-D-βA-polyethylene glycol-C_{COOH}) was purchased by Peps4LS (Germany). The βA-D-βA-spacer was chosen over the usual GSGS-spacer, since it used in all peptides printed by PEPperPRINT. To increase the solubility and further decrease steric effects an additional polyethylene glycol-spacer was chosen. The column was loaded six times with 3 ml of serum each time. The concentration of antibodies after purification (second and third fraction pooled) was determined to be $0.053\,\mathrm{mg\,ml^{-1}}$ by optical density measurement at 280 nm in a Jenway 7305 spectrophotometer (Bibby Scientific, UK). After elution, the buffer was exchanged to PBS as described before. The tetanus ELISA was conducted using isolated antibodies diluted 1:2 and 1:10 as described in section 4.3.

4.5 Incubation of peptide arrays with fluorophore

To visualize surface bound peptides, arrays were incubated with (5(6))-TAMRA (5-(and-6)-carboxytetramethylrhodamine succinimidyl ester, Thermo Scientific), a NHS ester conjugated fluorophore. The NHS ester is reacting with the amino groups of the peptides as well as with unreacted amino groups in the synthesis film. Therefore, the array was swollen for 10 min in PBS-T, blocked with Rockland buffer (RB) for 30 min, washed 3×1 min in RB-PBS-T (1:10) and was then incubated

with (5(6))-TAMRA at 1.8 µM in PBS-T for 2 h. Subsequently the array was washed 3×1 min in RB-PBS-T (1:10), shortly in 0.1 mM TRIS, dried with an argon gas stream and scanned at 532 nm.

4.6 Fluorescence image acquisition and analysis

4.6.1 Fluorescence scanning

Fluorescence scanning for the DL800 and DL680 was performed using an Odyssey scanner (LI-COR Biosciences, USA) with a resolution of 21 µm pixel^{-1}. The fluorophores Alexa Fluor 647 and DL550 were scanned using the Innoscan AL1100 (Innopsys, France) at resolutions ranging from 1 µm pixel^{-1} to 10 µm pixel^{-1} and laser power set to low. Emmissionfilters used for DL550: 582 ± 37 5nm, and for Alexa Fluor 647: 677 ± 22 5nm. Resulting 16 bit gray scale images were analyzed with the PepSlide Analyzer (Sicasys Software GmbH, Germany) or if the array was produced by spotting using the software Mapix 7.4.1 (Innopsys, France). A grid matching the array and containing the information about position and amino acid sequence of each spot is positioned onto the fluorescence image. The gray scale values of all pixels inside a spot of this predefined grid are measured as raw intensities. For background correction, global background controls were applied. For this method, control spots (an array of 4 to 10 spots) are placed outside of the array content and the average gray scale value of these spots is defined as global background. The median and mean foreground intensities for each spot were determined by subtracting the global background from the raw intensities. The foreground median intensities of spot duplicates are averaged. Dust on the surface of the arrays results in outliers which can be identified by differences in the signal intensities of spot duplicates. The average intensity of such spots is set to zero under the following two conditions: (1) the intensities of spot duplicates differ by more than 65 % in the average spot intensity and (2) the intensities of spot duplicates are higher than 50 % of the average intensity of all spots of the array. Additionally, the fluorescence scans were revised manually for outliers that are not detected by the before described criteria.

4.6.2 Fluorescence imaging

For fluorescence imaging the camera ProgRes C5 (Jenoptics, Germany) was used. The camera posses a 2/3 inch CCD sensor with a maximal resolution of 2580 x 1944 pixel. The image is captured as RGB with 12 bit colour depth in each channel (red, green, blue). Exposure duration can be adjusted up to 180 s. The camera is connected to the computer via fire wire. According to the manufacturer, the gamma value of the camera was set to 0.33 for all measurements to guarantee a linear correlation between the intensity of incident light on the CCD and the thus generated pixel gray scale values. The duration of exposure and the gain value were adapted to suit the respective experiment. Depending on the exposure time and the following time required

to download the image to the computer, the intervals of image capturing can be set. After the image is captured, the RGB images are splitted into the single colour channels and a bias and flat field correction is performed for the red channel using ImageJ. The fluorescence intensity is calculated as the median grey scale value of all pixels of one peptide spot. Finally, the median intensity of designated background control areas is subtracted from the intensity of the peptide spots. Therefore the ImageJ plugin 'Microarray Profile KIT' by D. Häringer was used. It allows to define and position a grid of circles on the image, and calculates the median gray scale values within these circles. The adaptation of a C++ makro by D. Markato und L.K. Weber allowed for the automatization of the process. The thus generated tables containing row, column, time step, minimum, maximum, median and background corrected median intensity were further processed in matlab.

4.7 Measurement of contact angle

The contact angle of a drop on a flat surface provides information about its hydrophobicity. Measurements were conducted on the OCA 25 (DataPhysics, Germany) using the software SCA20. Drops were dispensed in 5 µl DIW or a solution of peptide and PBS. Evaluation of contact angles on drops was conducted according to the Youg-Laplace method. For every surface, five drops were dispensed along the longitudinal edge of the substrate and measured.

4.8 Evaluation of spot morphology

For the evaluation of spot morphology, unbiased by fluorescence markers, a method using VSI was established and compared to AFM.

4.8.1 Vertical Scanning Interferometry

Spot topology was imaged by the ContourGT-K by Bruker, using vertical scanning interferometry in VXI mode for higher z-resolution at ambient conditions. The green light source was selected, back scan was set to 3 µm and the number of measurements to average was set to three at auto resolution. To reduce noise and improve image quality, the the device was operated on a vibration-dampening table. The field of view was 1.75 mm × 1.3 mm and 96 µm × 72 µm for x 2.75 and x 50 magnification. To image an array with the area of 3 mm by 1.75 mm, three measurements were automatically stitched together, applying an overlap of 23 %. Measurements were flattened in Vision64, applying a operational F-Filter using the tilt only option. Additionally dust particles were masked via histogram. Median spot heights were obtained by the multiple region option, where the leveling was set to auto, and the threshold for height and number of contiguous pixels was set depending on the analysis conducted.

4.8.2 Atomic force microscopy

All AFM measurements were performed under ambient conditions with a Bruker Dimension Icon AFM. The measurements were conducted in scan assist mode using Scanasyst-Air cantilevers (Bruker, USA) with resonance frequency of about 150 kHz and scan speed of 0.15 Hz. The offline image flattening and analysis was performed with the NanoScope Analysis 8.4 software.

4.8.3 Data processing

The image data obtained by AFM and VSI were processed as described in the following to determine compare the results of both methods and determine median spot heights.

Comparison of AFM and VSI measurements For the comparison of spot topologies measured with AFM and VSI, the respective measurements were imported into Gwyddion 2.49 [105]. Minimal z-values were set to zero and a third degree polynomial background correction was conducted. Data sets were exported as text files and further processed in Matlab 16a. For alignment, the position of a prominent feature in the middle of the spot was used as zero point. Measurements were set up to be congruent to each other by applying reference marks next to the features of interest, so no rotational correction was needed in post processing. Histograms were plotted using the Matlab histogram function. Considering the respective resolution, line profiles were extracted, intersecting the spots vertically and horizontally.

Determining spot heights for VSI measurements For each level of serum dilution, nine spots were measured using VSI as described above. The medium spot heights were determined using the multiple region option in Vision64, which identifies all areas matching threshold criteria in height and amount of contiguous pixels. Thresholds for each dilution level were set to maintain a constant amount of pixels per spot.

4.9 Molding of PDMS

The production of the PDMS molds was carried out with the MicCell molding station by GeSim. The two-component system Sylgard 184 (Dowsil, USA) was mixed in a ratio of 1:10 (curing agent to polymer), vented and injected into the station using a syringe (SOFT-JECT 5 ml, Henke Sass Wolf) onto which a precision tip (.020X.5 purple, Nordson EFD) was mounted. To blacken the PDMS, ferric oxide particles (Eisenoxid schwarz, SilikonFabrik) were added to a weight percentage of 2 % before ventilation. The molding station consists of a holder to which a master structure (SOG Master from GeSim or produced lithographically by Proform AG) is screwed from below and the cover plate from the top (see figure 3.5.1 p. 57). The inlets and outlets were kept free by filler plugs. After completion of the polymerization (about 12 h to 48 h at room temperature or 2 h to 4 h at 80 °C), the master structure and the frame can be removed. The channel is closed by attaching a glass slide or peptide array on the PDMS layer.

4.10 Measurement of channel height of assembled PDMS channels

The MicCell system, consisting of cover plate, PDMS layer containing the channel structure, a glass slide and a frame, was measured under an INM 200 microscope from Leica. Measured was the height difference in focal plane in between the glass channel bottom to the PDMS channel ceiling. Measurements were carried out in multiplicates to determine a user-specified standard deviation. The vertical measurement inaccuracy of the microscope stage is 4 µm.

4.11 Adhesive layer bonding

To integrate a peptide array in a microfluidic channel, adhesive layer bonding of a pre-structured polymer film resist (Ordyl SY355, Elga Europe, Italy) was adapted. The resulting channel consists of the glass top layer, the functionalized glass of the peptide array as bottom layer, and the structured film resist as side walls. Chromium marks were patterned onto the cover glass to allow positioning of the three parts relative to each other. These marks indicate the positions of the microfluidic in- and outlets for the subsequent laser drilling and serve during substrate bonding for the alignment of the peptide array and the pre-structured glass substrate. The sheet resist was laminated onto the cover sheet with the already laser drilled in-/outlets and was structured using lithography, forming the walls of the microfluidic channel. Side walls were 200 µm wide, 110 µm high and the wall to wall distance was 100 µm. At the end the peptide array was bonded as channel bottom layer to the structured sheet resist and in a last step a post bond bake was conducted.

4.11.1 Preparation of glass substrate

To facilitate positioning for laser drilling and bonding of the glass substrates, alignment marks were patterned by an etching process. A 50 nm thick chromium layer was vapor deposited (Univex 450, Leybold, Germany) onto 500 µm thick soda-lime glass substrates (B20057, Siegert Wafer, Germany). A 500 nm layer of AZ 1505 (Microchemicals, Germany) was deposited onto the chrome layer by spin coating, according to the standard recipe. The resist was structured by photolithography and the chromium etching was performed by immersing the substrates into TechniStrip Cr01 (Microchemicals, Germany) for 45 s. The remaining AZ-1505 was stripped in AZ 400K Developer. Structuring of the alignment marks is similarly possible by lift-off processing using the ma-N 1420 negative tone resist (Micro Resist Technology, Germany), resulting in a lower processing complexity without requiring chromium etchant. Vias, serving as fluidic ports, were drilled by an ultrashort pulse laser (Tangerine, Amplitude Systems, France) at a wavelength of 1030 nm, 400 fs pulse length, 8.2 W laser power, repetition rate of 200 kHz and a scan speed of 200 mm s^{-1}. The area of a circle was ablated completely while rastering a hatch pattern.

4.11.2 Structuring of the adhesive layer

The previously marked and drilled glass substrates were rinsed in isopropyl alcohol (Sigma Aldrich, USA) and ultra pure water to remove residues from laser drilling and then further cleaned in an oxygen plasma (4-Tec, Dressler, Germany). Two layers of the negative tone dry film resist Ordyl SY355 (55 µm, Elga Europe, Italy) were then laminated onto the glass substrates at 80 °C, roller speed of 4.4 mm s^{-1} using an office laminator (GMP Photone laminator, GMP, United Kingdom). A soft bake was performed at 80 °C for 2 min on a hotplate. After a wait time of 15 min the resist was exposed to 200 mJ cm^{-2} at 365 nm wavelength in front-side configuration. After removing the top protection foil of the dry film resist, the substrate was subjected to a PEB at 85 °C for 1 min. The substrate was developed by submerging in Ordyl SY300 Developer (Elga Europe, Italy) and sonication (Sonorex Super 10P, Bandelin, Germany) for up to 4 min and then rinsed in isopropyl alcohol and ultra pure water.

4.11.3 Bonding of the peptide array to the glass substrate

To seal the microfluidic channels, the peptide array was bonded to the glass-Ordyl structure at elevated temperatures. Therefore, a hot wafer bonding machine with unstructured, perfectly smooth and even mold inserts was used (EVG 510 HE, EVG, Germany). The peptide array and the prestructured glass substrate were placed in contact on top of each other, with the functionalized side of the peptide array facing towards the patterned adhesive layer of the Ordyl. Bonding was performed in vacuum (≈1 mbar) with a chuck temperature of 100 °C and a pressure of 735 N cm^{-2} for 30 min. Finally the post bond bake was performed at 100 °C for 1 h under argon protection gas to further cross link the resist. This post bond bake could most likely also be realized by prolonging the bond duration, but for a production perspective the bond time should be kept minimal to increase production throughput and therefore to use the cheaper oven based post bond bake. Ready peptide chips were stored at 4 °C under argon gas until usage.

4.11.4 Optical inspection

Structure quality was evaluated by visualization in a microscope (INM 20, Leica, Germany) at five fold magnification. Images were captured by a camera (Color View, Olympus Soft Imaging Solutions, Japan) using the software AnalySIS (Olympus, Japan).

4.11.5 Investigation of fracture strength of bonds

The fracture strength of the bond was examined in pulling tests (Load Frame 5569A, Instron, USA). For mounting the samples into the frame, copper cylinders (⌀: 25 mm) were glued on the flat top and bottom side of the peptide chip using UHU Plus Endfest 300 (UHU, Germany). The glue was cured under argon atmosphere at room temperature for 24 h, in order not to falsify the process-related fracture strength by further heating. The cylinders were pushed into the top mount and the sample was hanging freely while the bottom mount was approached and fixed tension-free. The

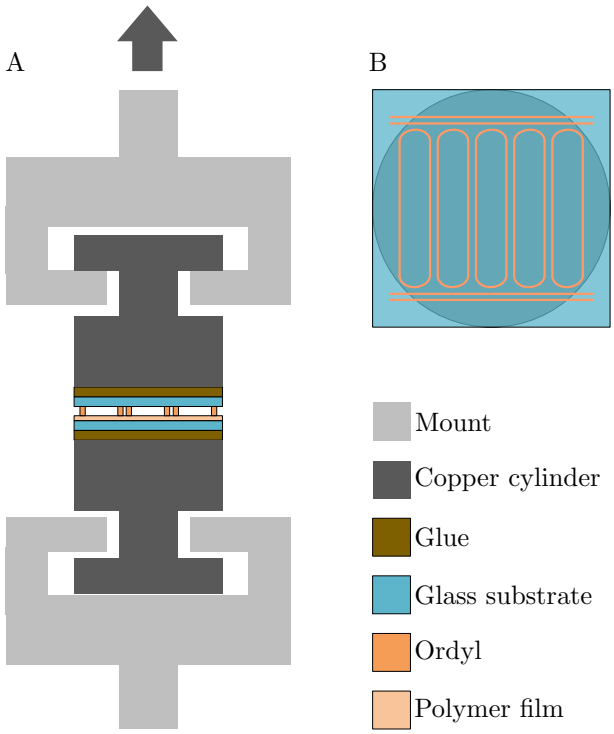

Figure 4.11.1: Measurement setup for pull tests. A: The peptide chip is glued to copper cylinders which are slided into the top mount and the sample was hanging freely while the bottom mount was approached and fixed tension-free. B: Top view of the bonded chip glued onto a copper cylinder.

experiment was performed at a loading speed of $10\,\mathrm{N\,s^{-1}}$ and samples were prepared in duplicates and triplicates, except for the 3D-Amino, PEPperCHIP®and 100 %-PEGMA surfaces, where just one experiment each was conducted.

Appendix

A.2 Incubation Process

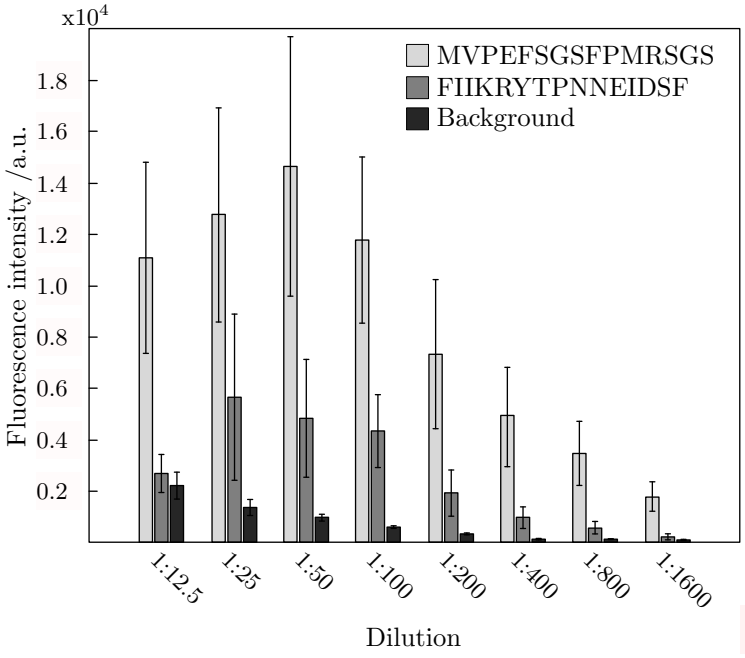

Figure A.2.1: Median fluorescence intensity of two different peptides compared to the background for different serum dilutions. Peptide array was divided into sixteen incubation areas and incubated with eight different dilutions of serum in duplicates followed by $0.2\,\mu g\,ml^{-1}$ secondary antibody. Each area contained nineteen spots per peptide. The background corrected median fluorescence intensity was averaged for all 38 spots per dilution. The median fluorescence intensity of the background was determined by averaging 38 control spots which were placed in between peptide spots. Scan: Innoscan AL1100 at 635 nm, intensity 6. Peptides came up in an epitope mapping with the tetanus toxin content for serum 19.
The concentration of the sample antibody and the secondary antibody affect the absolute intensity of fluorescence signals. Increasing concentrations result in increasing spot fluorescence intensities, but also lead to an unwanted increase in background intensity.

A.3 Epitope mapping

Table A.3.1: IgG antibody titer estimation for tetanus, pertussis and diphtheria by ELISA. Titers are expressed in international units (IU) per ml^{-1}, according to WHO standard. "n.d." stands for "not determined". According to international standards for standard ELISA full protection against a toxin is given for titers $\geq 0.1\,IU\,ml^{-1}$ whereas titers $< 1\,IU\,ml^{-1}$ are correlated with long-term protection [2]. Anti-tetanus IgG titers were published in [117]. Reprinted with permission.

Serum Nr.	**Tetanus** IU ml^{-1}	**Pertussis** IU ml^{-1}	**Diphtheria** IU ml^{-1}
1	4.1	n.d.	0.9
2	5.9	72	4.2
3	1.8	n.d.	0.2
4	2.5	35	1.5
5	2.0	7	0.8
6	0.8	n.d.	0.3
7	1.6	72	0.9
8	7.9	19	2.6
9	2.9	131	0.3
10	0.8	12	0.4
11	1.0	7	0.1
12	0.2	9	0.03
13	2.2	n.d.	0.8
14	2.0	34	0.9
15	0.9	18	0.6
16	1.0	14	0.3
17	4.8	9	0.4
18	3.3	22	0.8
19	0.8	40	0.6

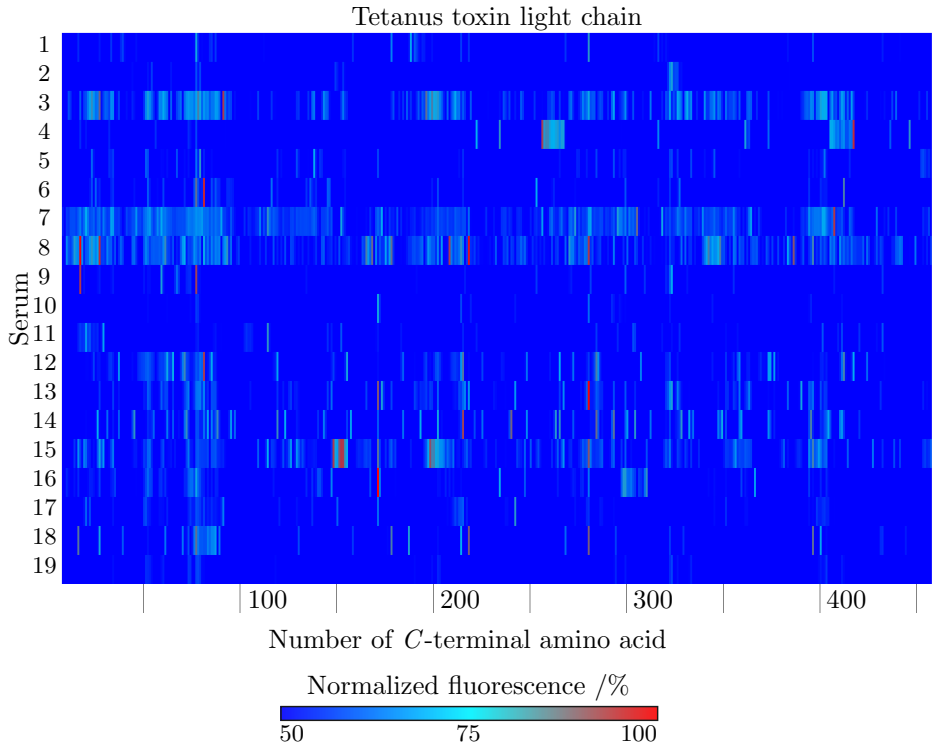

Figure A.3.1: Heat map of the linear epitope mapping for the tetanus toxin heavy chain amino acids 1 to 457 for nineteen sera of vaccinated Europeans using 15mere peptides with an overlap of fourteen amino acids. Peptides are numbered according to the number of the peptides *C*-terminal amino acid in the toxin sequence. Each row represents the fluorescence intensities of one serum. Fluorescence intensities were normalized to the respective maximum intensity of each serum. Reprinted with permission [117].

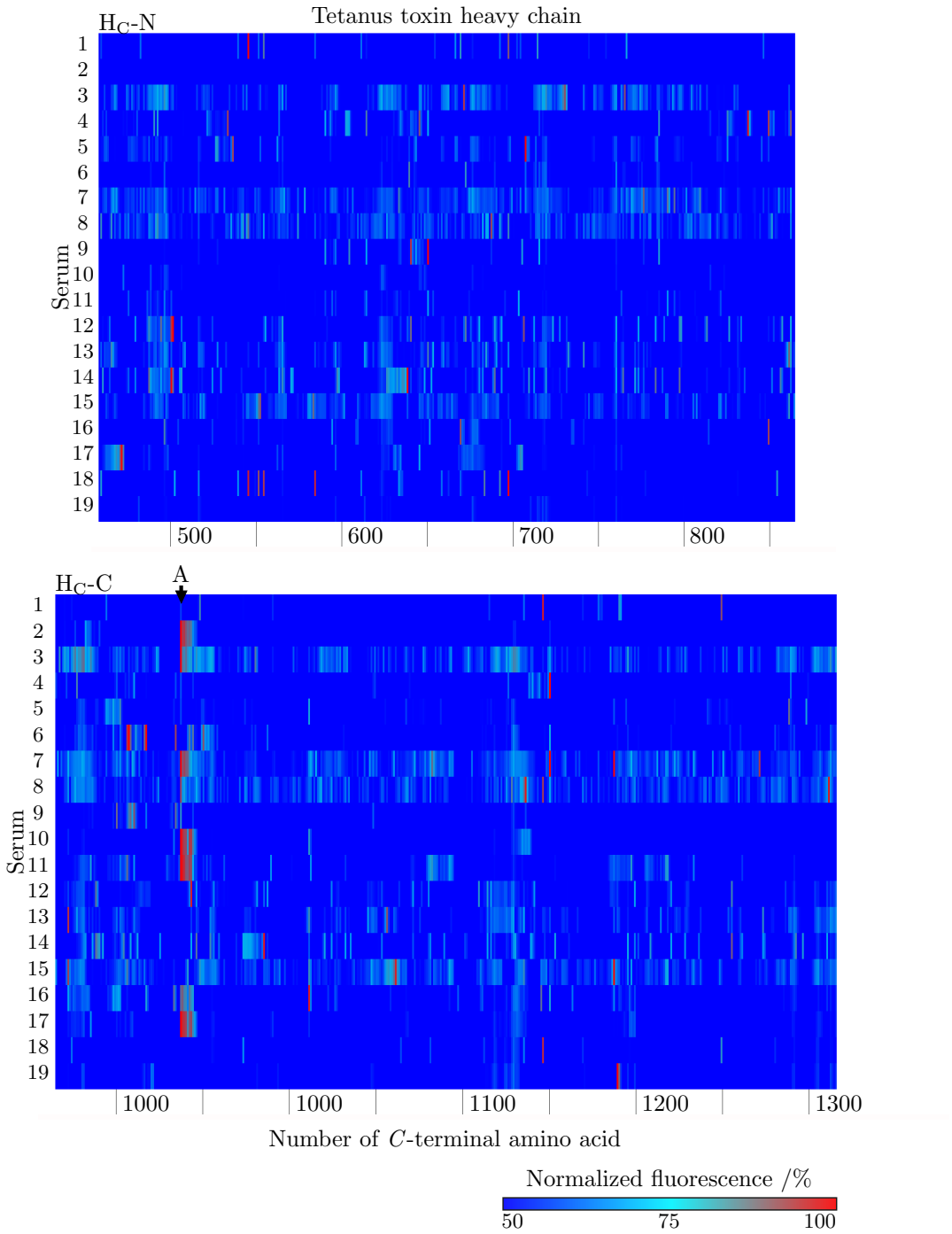

Figure A.3.2: Heat map of the linear epitope mapping for the tetanus toxin heavy chain amino acids 458 to 1315 for nineteen sera of vaccinated Europeans using 15mere peptides with an overlap of fourteen amino acids. Peptides are numbered according to the number of the peptides *C*-terminal amino acid in the toxin sequence. Each row represents the fluorescence intensities of one serum. Fluorescence intensities were normalized to the respective maximum intensity of each serum. Each row represents the fluorescence intensities of one serum. A Prominent band of consecutive peptide spots is marked with the letter 'A'. Heat map on the basis of [117]. Reprinted with permission.

A.4 Substitution analysis

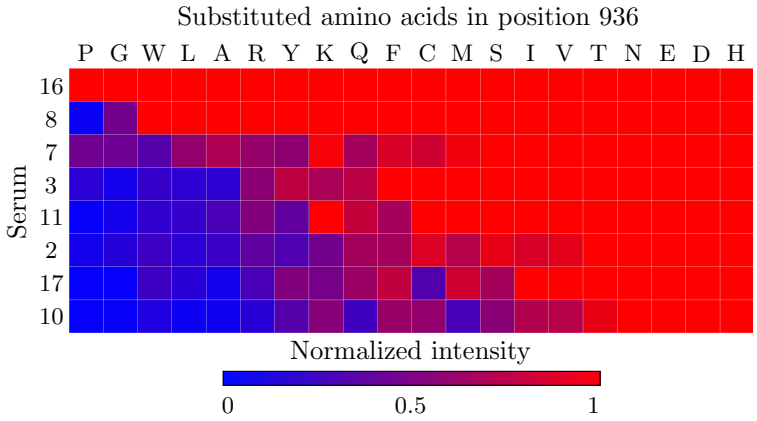

Figure A.4.1: Normalized fluorescence intensities for the substituted amino acids in position H_{936} of $_{923}$IHLVNNESSEVIVHK$_{937}$. Intensities were normalized to the respective maximum intensity for the position H_{936} for each serum. For serum 16, the subsitution of H_{936} does not result in the loss of fluorescence intensity and is thus not regarded as part of the fingerprint for this serum. For the other sera the role of H_{936} is not stringent.

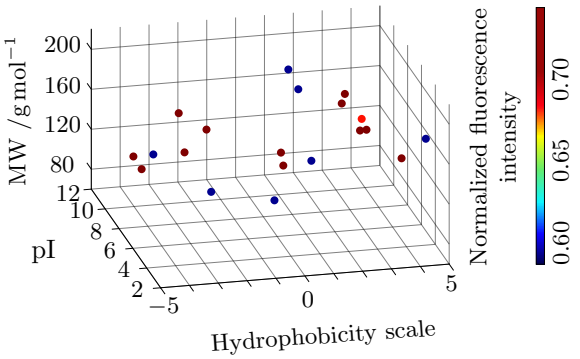

Figure A.4.2: Correlation of chemical properties of amino acids to the normalized fluorescence intensity at the position 936 of the epitope $_{923}$IHLVNNESSEVIVHK$_{937}$. Colored dots represent the nineteen amino acids. Fluorescence intensities were normalized to the respective maximum intensity for the position H_{936} for the eight sera. The normalized intensities were averaged over all sera for each amino acid respectively. Chemical properties considered are the molecular weight (MW) correlating with the size of the amino acid side chain, the isoelectrical point (pI) correlating with the charge at neural pH and a hydropathic value according to the scale of Kyle and Doolittle [80] correlating with the hydrophilicity (values < 0) or hydrophacity (values > 0) of the respective amino acid. No correlation between chemical properties to fluorescence inentisty can be observed.

Table A.4.1: Correlation of the peptides and sera used in the substitution analysis of the pertussis toxin. The assignment was chosen upon maximal interaction.

Peptide	Sequence	Serum
P1	$_{173}$YYDYEDATFETYALT$_{187}$	5, 14
P2	$_{167}$VSKEEQYYDYEDATF$_{181}$	2, 4, 5, 7, 10, 11, 12, 14, 18, 19
P3	$_{161}$ISVRVHVSKEEQYYD$_{175}$	4, 5, 10, 12, 14, 18
P4	$_{155}$LIYVAGISVRVHVSK$_{169}$	4, 5, 10, 12, 14, 18
P5	$_{136}$PYEGRYRDMYDALRR$_{150}$	2, 10, 11, 12, 18
P6	$_{49}$TPGWSIYGLYDGTYL$_{63}$	2, 4, 5, 7, 12, 14, 18, 19
P7	$_{53}$SIYGLYDGTYLGQAY$_{67}$	2, 4, 9, 12
P8	$_{57}$LYDGTYLGQAYGGII$_{71}$	2, 4, 9, 12

Table A.4.2: Hits of the protein database query for the identified fingerprint [DE]-x-x-E-[IV]-I-[IV]-[CDEHIMNSTV]-K. The table shows the organism in which the protein was found, the protein on which the motif is located and the amino acid position and the exact sequence. The query was conducted with the following settings: include splice variants (Swiss-Prot); exclude fragments; Hits for motif on all UniProtKB/Swiss-Prot (release 2016_11 of 30-Nov-16: 553231 entries) database sequences found 47 hits in 47 sequences. All hits within the same protein of the same organism are shown in the same row. Hits in different versions of the same protein were deleted. Reprinted with permission [117].

Organism	Protein	Query result	Motif & aa position
Aeropyrum pernix	Exosome complex component	sp(Q9YC05) RRP42_AERPE (276 aa)	177-185 EtgEIIISK
Alteromonas mediterranea	Elongation factor 4 (EF-4)	sp(B4RVA8) LEPA_ALTMD (598 aa)	173-181 DvlEVIVNK
Archaeoglobus fulgidus	30S ribosomal protein S12	sp(O28387) RS12_ARCFU (142 aa)	94-102 EhdEVIVEK
Caenorhabditis briggsae	Probable RING finger protein 207 homolog	sp(Q60MF5) RN207_CAEBR (836 aa)	745-753 EndEIIVEK
Caenorhabditis elegans	DNA repair protein rad-50	sp(O44199) RAD50_CAEEL (1298 aa)	708-716 EkeEIIIVK
Caenorhabditis elegans	Sentrin-specific protease	sp(Q09353) SENP_CAEEL (697 aa)	114-122 EenEVIIEK
Caenorhabditis elegans	Uncharacterized protein ZK177.4	sp(09372) YS44_CAEEL (655 aa)	64-72 EirEIIVSK
Clostridium acetobutylicum	DNA-directed RNA polymerase subunit beta	sp(Q97EG9) RPOB_CLOAB (1241 aa)	298-306 EssEVIVHK

Continued on next page

Table A.4.2 Query results for the tetanus fingerprint ExxEVIVxK - continued

Organism	Protein	Query result	Motif & aa position
Clostridium tetani	Tetanus toxin	sp(P04958) TETX_CLOTE (1315 aa)	929-937 EtgEIIVEK
Deinococcus geothermalis	Acyl carrier protein (ACP)	sp(Q1J195) ACP_DEIGD (76 aa)	6-14 EvkEVIVDK
Dictyostelium discoideum	Vesicle-associated membrane protein 7A	sp(Q54NW7) VAM7A_DICDI (216 aa)	153-161 EkiEIIVDK
Emericella nidulans	Ribosome-releasing factor 2, mitochondrial	sp(Q5BB57) RRF2M_EMENI (921 aa)	299-307 EhdEIIVEK
Enterococcus faecium	DNA-directed RNA polymerase subunit beta	sp(Q8GCR6) RPOB1_ENTFC (1208 aa)	306-314 EtgEIIVEK
Finegoldia magna	DNA-directed RNA polymerase subunit beta	sp(B0S2E5) RPOC_FINM2 (1202 aa)	831-839 DtgEIIVHK
Flavobacterium psychrophilum	Protein translocase subunit SecA	sp(A6GX63) SECA_FLAPJ (1116 aa)	833-841 DtcEVIVEK
Homo sapiens	A-kinase anchor protein 4 (AKAP-4)	sp(Q5JQC9) AKAP4_HUMAN (854 aa)	66-74 75-83 EekEIIVIK
Homo sapiens	Xin actin-binding repeat-containing protein 2	sp(4UGR9) XIRP2_HUMAN (3374 aa)	647-655 EseEVIIEK
Human rhinovirus 14	Genome polyprotein	sp(P03303) POLG_HRV14 (2179 aa)	572-580 EleEVIVEK
Human rhinovirus 3	Genome polyprotein	sp(Q82081) POLG_HRV3 (2178 aa)	572-580 EleEVIVEK
Ignicoccus hospitalis	30S ribosomal protein S3	sp(A8AA20) RS3_IGNH4 (241 aa)	181-189 EgvEVIISK
Lactobacillus salivarius	DNA-directed RNA polymerase subunit beta	sp(Q1WVA5) RPOB_LACS1 (1199 aa)	307-315 DtgEIIVNK
Lecanicillium sp.	Nonribosomal peptide synthetase vlms	sp(A0A024F910) VLMS_LECSP (8903 aa)	1760-1768 DleEVIINK
Methanocaldococcus jannaschii	Uncharacterized protein MJ0538	sp(Q57958) Y538_METJA (260 aa)	176-184 DrdEIIINK

Continued on next page

Table A.4.2 Query results for the tetanus fingerprint ExxEVIVxK - continued

Organism	Protein	Query result	Motif & aa position
Mus musculus	A-kinase anchor protein 4 (AKAP-4)	sp(Q60662) AKAP4_MOUSE (849 aa)	66-74 75-83 EekEIIVIK
Mus musculus	Zinc fingers and homeoboxes protein 3	sp(Q8C0Q2) ZHX3_MOUSE (951 aa)	171-179 EgtEIIITK
Mycoplasma capricolum subsp. capricolum	Alanine–tRNA ligase	sp(Q2SSW4) SYA_MYCCT (896 aa)	728-736 DqaEIIIDK
Neosartorya fumigata	Nonribosomal peptide synthetase 13	sp(Q4WAW3) FTMA_ASPFU (2211 aa)	477-485 DnaEVIVEK
Oceanobacillus iheyensis	DNA-directed RNA polymerase subunit beta	sp(Q8ETY7) RPOC_OCEIH (1203 aa)	856-864 EtgEVIVEK
Petrotoga mobilis	GTP 3',8-cyclase	sp(A9BF51) MOAA_PETMO (323 aa)	207-215 EfkEIIIDK
Physcomitrella patens subsp. patens	Retinoblastoma-related protein	sp(A9SVH7) RBR_PHYPA (1116 aa)	1013-1021 DemEVIIIK
Rattus norvegicus	A-kinase anchor protein 4 (AKAP-4)	sp(O35774) AKAP4_RAT (847 aa)	74-82 EekEIIVIK
Rattus norvegicus	Zinc fingers and homeoboxes protein 3	sp(Q80Z36) ZHX3_RAT (951 aa)	170-178 EgtEIIITK
Saccharomyces cerevisiae	Adaptor-related protein complex 3 subunit delta	sp(Q08951) AP3D_YEAST (932 aa)	889-897 DteEVIVIK
Schizosaccharomyces pombe	ESCRT-I complex subunit vps23	sp(Q7Z992) SST6_SCHPO (487 aa)	260-268 EqnEIIITK
Xenopus laevis	Cingulin	sp(Q9PTD7) CING_XENLA (1360 aa)	304-312 DsrEIIVEK
Yarrowia lipolytica	Ras-like GTP-binding protein RYL2	sp(P41925) RYL2_YARLI (209 aa)	164-172 EvfEVIITK

Table A.4.3: Hits of the protein database query for the identified fingerprint [PV]-[ASG]-[LAM]-[TS]-[ASGDEF]-[AGSVIL]-E-[TVI]-[GS]. The table shows the organism in which the protein was found, the protein on which the motif is located and the amino acid position and the exact sequence. The query was conducted with the following settings: include splice variants (Swiss-Prot); exclude fragments; Hits for motif on all UniProtKB/Swiss-Prot (release 2016_11 of 30-Nov-16: 553231 entries) database sequences found 48 hits in 48 sequences. All hits within the same protein of the same organism are shown in the same row. All hits within the same protein of the same organism are shown in the same row. Rows containing hits on the same protein of different organisms were merged into one.

Organism	**Protein**	**Query result**	**Motif & aa position**
Pseudomonas savastanoi pv. phaseolicola	3-phosphoshikimate 1-carboxyvinyltransferase (EC 2.5.1.19) (5-enolpyruvylshikimate-3-phosphate synthase)	sp(Q48N21) AROA_PSE14	190 -198 VALTGSEIG
Pseudomonas syringae pv. tomato (strain ATCC BAA-871 / DC3000)		sp(Q888I3) AROA_PSESM	190-198 VALTGSEIG
Pseudomonas syringae pv. syringae (strain B728a)		sp(Q4ZY26) AROA_PSEU2	190-198 VALTGSEIG
Archaeoglobus fulgidus	30S ribosomal protein S12	sp(O28387) RS12_ARCFU	94-102 EhdEVIVEK
Yersinia enterocolitica serotype O:8 / biotype 1B (strain NCTC 13174 / 8081)	Succinylglutamate desuccinylase (EC 3.5.1.96).	sp(A1JS32) ASTE_YERE8	14-22 PSLTSGETS
Halobacterium salinarum (strain ATCC 29341 / DSM 671 / R1)	Probable deoxyhypusine synthase (DHS) (EC 2.5.1.46	sp(B0R5L2) DHYS_HALS3	202-210 PALTDAEIG
Halobacterium salinarum (strain ATCC 700922 / JCM 11081 / NRC-1) (Halobacterium halobium)		sp(Q9HPX2) DHYS_HALSA	202-210 PALTDAEIG
Pyrobaculum aerophilum (strain ATCC 51768 / IM2 / DSM 7523 / JCM 9630 / NBRC 100827)	D-aminoacyl-tRNA deacylase (EC 3.1.1.96) (D-tyrosyl-tRNA(Tyr) deacylase)	sp(Q8ZVE0) DTDA_PYRAE	129-137 VSATFIEVG
Pyrobaculum calidifontis (strain JCM 11548 / VA1)		sp(A3MWS2) DTDA_PYRCJ	130-138 VSATFLEVG
Aspergillus flavus (strain ATCC 200026 / FGSC A1120 / NRRL 3357 / JCM 12722 / SRRC 167)	Probable endo-1,3(4)-beta-glucanase AFLA_105200 (EC 3.2.1.6)	sp(B8N7S7) EGLX_ASPFN	530-538 PAATSIETG
Aspergillus oryzae (strain ATCC 42149 / RIB 40) (Yellow koji mold)	(Mixed-linked glucanase AFLA_105200)	sp(Q2UIE6) EGLX_ASPOR	530-538 PAATSIETG

Continued on next page

Table A.4.3 – Query results for the polio motif PALTAxET- continued

Organism	Protein	Query result	Motif & aa position
Oryza sativa subsp. japonica (Rice)	Jasmonic acid-amido synthetase JAR1 (EC 6.3.2.-) (Auxin-responsive GH3-like protein 5) (OsGH3-5) (Indole-3-acetic acid-amido synthetase GH3.5) (Jasmonate-amino acid synthetase JAR1) (Protein JASMONATE RESISTANT 1) (OsJAR1)	sp(Q6I581) GH35_ORYSJ	381-389 VGLTEVEVG
Hahella chejuensis (strain KCTC 2396)	Maltoporin (Maltose-inducible porin)	sp(Q2SQ17) LAMB_HAHCH	193-201 VGASSLEVG
Paracoccidioides brasiliensis	pH-response transcription factor pacC/RIM101	sp(Q8J257) PACC_PARBR	581-589 PSMSFAEVG
Coxsackievirus A21 (strain Coe)	Genome polyprotein (Cleaved into: P3; Protein 3AB; P2; P1;	sp(P22055) POLG_CXA21	618-626 PALTAVET
Coxsackievirus A24 (strain EH24/70)	Capsid protein VP0 (VP4-VP2); Capsid protein VP4 (P1A)	sp(P36290) POLG_CXA24	622-630 PALTAVETG
Coxsackievirus A9 (strain Griggs)	(Virion protein 4); Capsid protein VP2 (P1B) (Virion protein 2);	sp(P21404) POLG_CXA9	597-605 PALTAVETG
Coxsackievirus B1 (strain Japan)	Capsid protein VP3 (P1C) (Virion protein 3); Capsid protein	sp(P08291) POLG_CXB1J	599-607 PALTAAETG
Coxsackievirus B3 (strain Nancy)	VP1 (P1D) (Virion protein 1); Protease 2A (P2A) (EC 3.4.22.29)	sp(P03313) POLG_CXB3N	599-607 PALTAAETG
Coxsackievirus B3 (strain Woodruff)	(Picornain 2A) (Protein 2A); Protein 2B (P2B); Protein 2C	sp(Q66282) POLG_CXB3W	599-607 PALTAAETG
Coxsackievirus B4 (strain E2)	(P2C) (EC 3.6.1.15); Protein 3A (P3A); Viral protein	sp(Q86887) POLG_CXB4E	597-605 PALTAVETG
Coxsackievirus B4 (strain JVB / Benschoten / New York/51)	genome-linked (VPg) (Protein 3B) (P3B); Protein 3CD (EC	sp(P08292) POLG_CXB4J	597-605 PALTAVETG
Coxsackievirus B5 (strain Peterborough / 1954/UK/85)	3.4.22.28); Protease 3C (P3C) (EC 3.4.22.28); RNA-directed	sp(Q03053) POLG_CXB5P	597-605 PALTAAETG
Coxsackievirus B6 (strain Schmitt)	RNA polymerase (RdRp) (EC 2.7.7.48))	sp(Q9QL88) POLG_CXB6S	597 -605 PALTAVETG
Echovirus 5 (strain Noyce)		sp(Q9YLJ1) POLG_EC05N	599-607 PALTAVETG
Echovirus 6 (strain Charles)		sp(Q66474) POLG_EC06C	597-605 PALTAAETG
Echovirus 9 (strain Barty)		sp(Q66577) POLG_EC09B	598-606 PALTAAETG
Echovirus 9 (strain Hill)		sp(Q66849) POLG_EC09H	598-606 PALTAAETG
Echovirus 11 (strain Gregory)		sp(P29813) POLG_EC11G	598-606 PALTAVETG

Continued on next page

Table A.4.3 – Query results for the polio motif PALTAxET- continued

Organism	Protein	Query result	Motif & aa position
Echovirus 12 (strain Travis)		sp(Q66575) POLG_EC12T	597-605 PALTAAETG
Echovirus 30 (strain Bastianni)		sp(Q9WN78) POLG_EC30B	597-605 PALTAVETG
Poliovirus type 1 (strain Mahoney)	Genome polyprotein (Cleaved into: P1; Capsid protein VP0 (VP4-VP2); Capsid protein VP4 (P1A) (Virion protein 4); Capsid protein VP2 (P1B) (Virion protein 2); Capsid protein VP3 (P1C) (Virion protein 3); Capsid protein VP1 (P1D) (Virion protein 1); P2; Protease 2A (P2A) (EC 3.4.22.29) (Picornain 2A) (Protein 2A); Protein 2B (P2B); Protein 2C (P2C) (EC 3.6.1.15); P3; Protein 3AB; Protein 3A (P3A); Viral protein genome-linked (VPg) (Protein 3B) (P3B); Protein 3CD (EC 3.4.22.28); Protease 3C (P3C) (EC 3.4.22.28); RNA-directed RNA polymerase (RdRp) (EC 2.7.7.48) (3D polymerase))	sp(P03300) POLG_POL1M	621-629 PALTAVETG
Poliovirus type 1 (strain Sabin)	Genome polyprotein (Cleaved into: P3; Protein 3AB; P1;	sp(P03301) POLG_POL1S	621-629 PALTAVETG
Poliovirus type 2 (strain Lansing)	Capsid protein VP0 (VP4-VP2);	sp(P06210) POLG_POL2L	620-628 PALTAVETG
Poliovirus type 2 (strain W-2)	Capsid protein VP4 (P1A) (Virion protein 4); Capsid protein VP2 (P1B) (Virion protein 2);	sp(P23069) POLG_POL2W	620-628 PALTAVETG
Poliovirus type 3 (strains P3/Leon/37 and P3/Leon 12A[1]B)	Capsid protein VP3 (P1C) (Virion protein 3); Capsid protein VP1 (P1D) (Virion protein 1); P2; Protease 2A (P2A) (EC 3.4.22.29) (Picornain 2A) (Protein 2A); Protein 2B (P2B); Protein 2C (P2C) (EC 3.6.1.15); Protein 3A (P3A); Viral protein genome-linked (VPg) (Protein 3B) (P3B); Protein 3CD (EC 3.4.22.28); Protease 3C (P3C) (EC 3.4.22.28); RNA-directed RNA polymerase (RdRp) (EC 2.7.7.48) (3D polymerase) (3Dpol) (Protein 3D) (3D))	sp(P03302) POLG_POL3L	618-626 PALTAVETG

Continued on next page

Table A.4.3 – Query results for the polio motif PALTAxET- continued

Organism	Protein	Query result	Motif & aa position
Swine vesicular disease virus (strain H/3 '76) (SVDV)	Genome polyprotein (Cleaved into: P3; Protein 3AB; P2; P1; Capsid protein VP0 (VP4-VP2); Capsid protein VP4 (P1A) (Virion protein 4); Capsid protein VP2 (P1B) (Virion protein 2); Capsid protein VP3 (P1C) (Virion protein 3); Capsid protein VP1 (P1D) (Virion protein 1); Protease 2A (P2A) (EC 3.4.22.29) (Picornain 2A) (Protein 2A); Protein 2B (P2B); Protein 2C (P2C) (EC 3.6.1.15); Protein 3A (P3A); Viral protein genome-linked (VPg) (Protein 3B) (P3B); Protein 3CD (EC 3.4.22.28); Protease 3C (P3C) (EC 3.4.22.28); RNA-directed RNA polymerase (RdRp) (EC 2.7.7.48) (3D polymerase) (3Dpol) (Protein 3D) (3D)]	sp(P16604) POLG_SVDVH	597-605 PALTAAETG
Swine vesicular disease virus (strain UKG/27/72) (SVDV)		sp(P13900) POLG_SVDVU	597-605 PALTAAETG
Bartonella bacilliformis (strain ATCC 35685 / KC583)	Peptide chain release factor 1 (RF-1)	sp(A1URS5) RF1_BARBK	150-158 VSLSDSEVG
Actinobacillus succinogenes (strain ATCC 55618 / 130Z)	23S rRNA (uracil(747)-C(5))-methyltransferase RlmC (EC 2.1.1.189) (23S rRNA(m5U747)-methyltransferase)	sp(A6VKU5) RLMC_ACTSZ	264-272 VALTGIEIS
Haemophilus parasuis serovar 5 (strain SH0165)	23S rRNA (uracil(747)-C(5))-methyltransferase RlmC (EC 2.1.1.189) (23S rRNA(m5U747)-methyltransferase)	sp(B8F5M9) RLMC_HAEPS	267-275 VALTGIEIS
Shewanella frigidimarina (strain NCIMB 400)	Serine/threonine transporter SstT (Na(+)/serine-threonine symporter)	sp(Q07ZL7) SSTT_SHEFN	198-206 VAATFAETG
Shewanella oneidensis (strain MR-1)		sp(Q8ECL5) SSTT_SHEON	198-206 VAATFAETG
Shewanella sp. (strain ANA-3)		sp(A0KV41) SSTT_SHESA	198-206 VAATFAETG
Shewanella sp. (strain MR-4)		sp(Q0HKG6) SSTT_SHESM	198-206 VAATFAETG
Shewanella sp. (strain MR-7)		sp(Q0HWR8) SSTT_SHESR	198-206 VAATFAETG

Continued on next page

Table A.4.3 – Query results for the polio motif PALTAxET- continued

Organism	Protein	Query result	Motif & aa position
Shewanella sp. (strain W3-18-1)		sp(A1RI59) SSTT_SHESW	198-206 VAATFAETG
Homo sapiens (Human)	Ankyrin repeat domain-containing protein SOWAHD (Ankyrin repeat domain-containing protein 58) (Protein sosondowah homolog D)	sp(A6NJG2) SWAHD_HUMAN	272-280 VGATAVETS
Sinorhizobium fredii (strain NBRC 101917 / NGR234)	Serine–tRNA ligase (EC 6.1.1.11) (Seryl-tRNA synthetase) (SerRS) (Seryl-tRNA(Ser/Sec) synthetase)	sp(C3MBU2) SYS_SINFN	287-295 VSLTDAETS

Table A.4.4: Hits of the protein database query for the motif [VPI]-P-E-F-x-[GDS]-[STA]-x-[PVAS]. The table shows the organism in which the protein was found, the protein on which the motif is located and the amino acid position and the exact sequence. The query was conducted with the following settings: include splice variants (Swiss-Prot); exclude fragments; Hits for motif on all UniProtKB/Swiss-Prot (release 2016_11 of 30-Nov-16: 553231 entries) database sequences found 37 hits in 37 sequences. All hits within the same protein of the same organism are shown in the same row. All hits within the same protein of the same organism are shown in the same row. Rows containing hits on the same protein of different organisms were merged into one.

Organism	Protein	Query result	Motif & aa position
Methanosarcina acetivorans (strain ATCC 35395 / DSM 2834 / JCM 12185 / C2A)	Phosphoenolpyruvate carboxylase (PEPC) (PEPCase) (EC 4.1.1.31)	sp(Q8TMG9) CAPPA_METAC) (526 aa)	400-408 PPEFiGTgA
Arabidopsis thaliana (Mouse-ear cress)	CDT1-like protein a, chloroplastic (AtCDT1a)	sp(Q9SJW9) CDT1A_ARATH (571 aa)	354-362 PPEFaSTpA
Zea mays (Maize)	DNA (cytosine-5)-methyltransferase 2 (EC 2.1.1.37) (Chromomethylase 2) (DNA cytosine methyltransferase MET5) (Zea methyltransferase5) (Zmet5)	sp(Q9ARI6) CMT2_MAIZE) (915 aa)	138-146 VPEFiGSpV
Zea mays (Maize)	DNA (cytosine-5)-methyltransferase 3 (EC 2.1.1.37) (Chromomethylase 3) (DNA methyltransferase 105)	sp(Q8LPU5) CMT3_MAIZE (915 aa)	138-146 VPEFiGSpV
Bos taurus (Bovine)	Lambda-crystallin homolog (EC 1.1.1.45) (L-gulonate 3-dehydrogenase) (Gul3DH)	sp(Q8SPX7) CRYL1_BOVIN) (321 aa)	272-280 VPEFsGAtA

Continued on next page

Table A.4.4 – Query results for the *S. aureus* motif PEFxGSxP - continued

Organism	Protein	Query result	Motif & aa position
Mus musculus (Mouse)	Lambda-crystallin homolog (EC 1.1.1.45) (L-gulonate 3-dehydrogenase) (Gul3DH)	sp(Q99KP3) CRYL1_MOUSE	269-277 VPEFsGAtV
Sus scrofa (Pig)	Lambda-crystallin homolog (EC 1.1.1.45) (L-gulonate 3-dehydrogenase) (Gul3DH)	sp(Q8SQ26) CRYL1_PIG) (322 aa)	272-280 IPEFsGAvA
Oryctolagus cuniculus (Rabbit)	Lambda-crystallin (EC 1.1.1.45) (L-gulonate 3-dehydrogenase) (Gul3DH)	sp(P14755) CRYL1_RABIT) (319 aa)	269-277 IPEFsGAtV
Staphylococcus aureus (strain USA300)	Extracellular matrix protein-binding protein emp.	sp(Q2FIK4) EMP_STAA3) (340 aa)	328-336 VPEFkGSlP
Staphylococcus aureus (strain NCTC 8325)	Extracellular matrix protein-binding protein emp.	sp(Q2G012) EMP_STAA8) (340 aa)	328-336 VPEFkGSlP
Staphylococcus aureus (strain bovine RF122 / ET3-1)	Extracellular matrix protein-binding protein emp.	sp(Q2YWL4) EMP_STAAB) (339 aa)	327-335 VPEFkGSiP
Staphylococcus aureus (strain COL)	Extracellular matrix protein-binding protein emp.	sp(Q5HHM6) EMP_STAAC) (340 aa)	328-336 VPEFkGSlP
Staphylococcus aureus (strain Newman)	Extracellular matrix protein-binding protein emp.	sp(A6QF98) EMP_STAAE (340 aa)	328-336 VPEFkGSlP
Staphylococcus aureus (strain Mu50 / ATCC 700699)	Extracellular matrix protein-binding protein emp.	sp(Q99VJ2) EMP_STAAM (340 aa)	328-336 VPEFkGSlP
Staphylococcus aureus (strain N315)	Extracellular matrix protein-binding protein emp.	sp(Q7A6P4) EMP_STAAN) (340 aa)	328-336 VPEFkGSlP
Staphylococcus aureus (strain MSSA476)	Extracellular matrix protein-binding protein emp.	sp(Q6GB43) EMP_STAAS (340 aa)	328-336 VPEFkGSlP
Staphylococcus aureus	Extracellular matrix protein-binding protein emp. (40 kDa vitronectin-binding cell surface protein)	sp(P0C6P1) EMP_STAAU) (340 aa)	328-336 VPEFkGSlP
Staphylococcus aureus (strain MW2)	Extracellular matrix protein-binding protein emp.	sp(Q8NXI8) EMP_STAAW) (340 aa)	328-336 VPEFkGSlP

Continued on next page

Table A.4.4 – Query results for the *S. aureus* motif PEFxGSxP - continued

Organism	Protein	Query result	Motif & aa position
Bos taurus (Bovine)	Integral membrane protein 2B (Immature BRI2) (imBRI2) (Transmembrane protein BRI) (Bri) [Cleaved into: BRI2, membrane form (Mature BRI2) (mBRI2); BRI2 intracellular domain (BRI2 ICD); BRI2C, soluble form; Bri23 peptide (Bri2-23) (ABri23) (*C*-terminal peptide) (P23 peptide)]	sp(Q3T0P7) ITM2B_BOVIN) (266 aa)	134-142 VPEFaDSdP
Gallus gallus (Chicken)	Integral membrane protein 2B (Transmembrane protein E3-16)	sp(O42204) ITM2B_CHICK (262 aa)	129-137 VPEFaDSdP
Homo sapiens (Human)	Integral membrane protein 2B (Immature BRI2) (imBRI2) (Protein E25B) (Transmembrane protein BRI) (Bri) [Cleaved into: BRI2, membrane form (Mature BRI2) (mBRI2); BRI2 intracellular domain (BRI2 ICD); BRI2C, soluble form; Bri23 peptide (Bri2-23) (ABri23) (*C*-terminal peptide) (P23 peptide)]	sp(Q9Y287) ITM2B_HUMAN) (266 aa)	134-142 VPEFaDSdP
Macaca fascicularis (Crab-eating macaque)	Integral membrane protein 2B (Immature BRI2) (imBRI2) (Transmembrane protein BRI) (Bri) [Cleaved into: BRI2, membrane form (Mature BRI2) (mBRI2); BRI2 intracellular domain (BRI2 ICD); BRI2C, soluble form; Bri23 peptide (Bri2-23) (ABri23) (*C*-terminal peptide) (P23 peptide)]	sp(Q60HC1) ITM2B_MACFA) (266 aa)	134-142 VPEFaDSdP

Continued on next page

Table A.4.4 – Query results for the *S. aureus* motif PEFxGSxP - continued

Organism	Protein	Query result	Motif & aa position
Mus musculus (Mouse)	Integral membrane protein 2B (Immature BRI2) (imBRI2) (Protein E25B) (Transmembrane protein BRI) (Bri) [Cleaved into: BRI2, membrane form (Mature BRI2) (mBRI2); BRI2 intracellular domain (BRI2 ICD); BRI2C, soluble form; Bri23 peptide (Bri2-23) (ABri23) (*C*-terminal peptide) (P23 peptide)].	sp(O89051) ITM2B_MOUSE) (266 aa)	134-142 VPEFaDSdP
Pan troglodytes (Chimpanzee)	Integral membrane protein 2B (Immature BRI2) (imBRI2) (Transmembrane protein BRI) (Bri) [Cleaved into: BRI2, membrane form (Mature BRI2) (mBRI2); BRI2 intracellular domain (BRI2 ICD); BRI2C, soluble form; Bri23 peptide (Bri2-23) (ABri23) (*C*-terminal peptide) (P23 peptide)]	sp(A5A6H8) ITM2B_PANTR) (266 aa)	134-142 VPEFaDSdP
Sus scrofa (Pig)	Integral membrane protein 2B (Immature BRI2) (imBRI2) (Transmembrane protein BRI) (Bri) [Cleaved into: BRI2, membrane form (Mature BRI2) (mBRI2); BRI2 intracellular domain (BRI2 ICD); BRI2C, soluble form; Bri23 peptide (Bri2-23) (ABri23) (*C*-terminal peptide) (P23 peptide)]	sp(Q52N47) ITM2B_PIG) (266 aa)	134-142 VPEFaDSdP
Rattus norvegicus (Rat)	Integral membrane protein 2B (Immature BRI2) (imBRI2) (Transmembrane protein BRI) (Bri) [Cleaved into: BRI2, membrane form (Mature BRI2) (mBRI2); BRI2 intracellular domain (BRI2 ICD); BRI2C, soluble form; Bri23 peptide (Bri2-23) (ABri23) (*C*-terminal peptide) (P23 peptide)].	sp(Q5XIE8) ITM2B_RAT) (266aa)	134-142 VPEFaDSdP

Continued on next page

Table A.4.4 – Query results for the *S. aureus* motif PEFxGSxP - continued

Organism	Protein	Query result	Motif & aa position
Pongo abelii (Sumatran orangutan)	Integral membrane protein 2B (Immature BRI2) (imBRI2) (Transmembrane protein BRI) (Bri) (Cleaved into: BRI2, membrane form (Mature BRI2) (mBRI2); BRI2 intracellular domain (BRI2 ICD); BRI2C, soluble form; Bri23 peptide (Bri2-23) (ABri23) (*C*-terminal peptide) (P23 peptide))	sp(Q5R876) ITM2B_PONAB	134-142 VPEFaDSdP
Mus musculus (Mouse)	Nitric oxide-associated protein 1	sp(Q9JJG9) NOA1_MOUSE) (693 aa)	127-135 VPEFpDAsV
Leptosphaeria maculans (Blackleg fungus) (Phoma lingam)	Dipeptidase sirJ (EC 3.4.13.19) (Sirodesmin biosynthesis protein J)	sp(Q6Q886) SIRJ_LEPMC) (394 aa)	264-272 VPEFsSAdP
Bos taurus (Bovine)	Signal transducer and activator of transcription 5A (Mammary gland factor)	sp(Q95115) STA5A_BOVIN (794 aa)	703-711 VPEFvSAsA
Sus scrofa (Pig)	Signal transducer and activator of transcription 5A	sp(Q9TUZ1) STA5A_PIG) (799 aa)	708-716 VPEFvSAsS
Ovis aries (Sheep)	Signal transducer and activator of transcription 5A (Mammary gland factor)	sp(P42231) STA5A_SHEEP) (794 aa)	703-711 VPEFvSAsA
Bos taurus (Bovine)	Signal transducer and activator of transcription 5B	sp(Q9TUM3) STA5B_BOVIN) (787 aa)	708-716 VPEFvSAsA
Sus scrofa (Pig)	Signal transducer and activator of transcription 5B	sp(Q9TUZ0) STA5B_PIG) (787 aa)	708-716 VPEFvSAsS
Caenorhabditis elegans	Protein unc-80 (Uncoordinated protein 80)	sp(Q9XV66) UNC80_CAEEL) (3263 aa)	1492-1500 IPEFlDAgA
Ictalurid herpesvirus 1 (strain Auburn) (IcHV-1) (Channel catfish herpesvirus)	Uncharacterized protein ORF52	sp(Q00121) VG52_ICHVA) (318 aa)	274-282 PPEFiDAaV
Saccharomyces cerevisiae (strain ATCC 204508 / S288c) (Baker's yeast)	Uncharacterized protein YMR317W	sp(Q04893) YM96_YEAST (1140 aa)	63-71 VPEFtSSsS

A.5 Validation of antibody specificity towards the native toxin

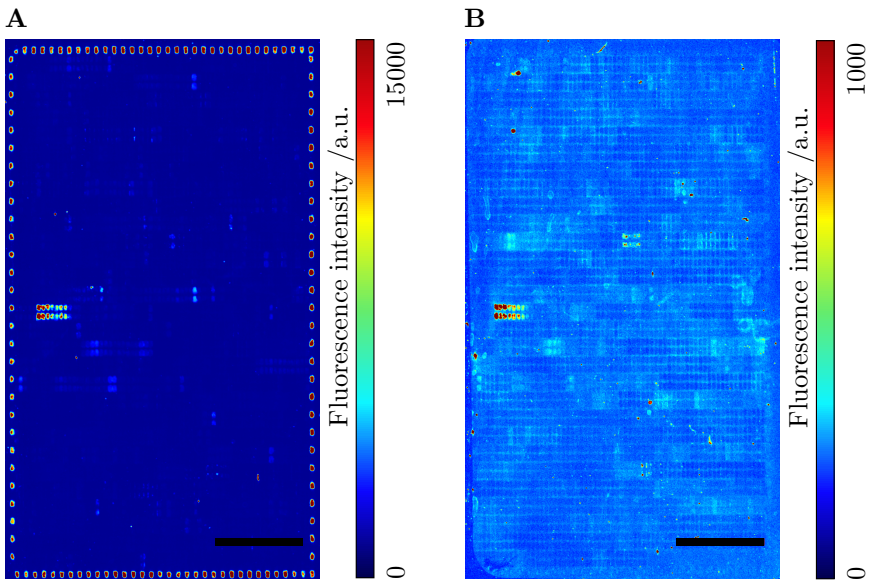

Figure A.5.1: Fluorescence scan of serum 11 before (left) and after (right) isolation of epitope-specific antibodies. Incubated on a peptide array containing the epitope mapping content. No distinct interaction, except with the epitope used for isolation of serum antibodies, can be observed. Especially striking is the loss of interaction with the control frame. Scale bar represents 0.5 cm. Reprinted with permission.

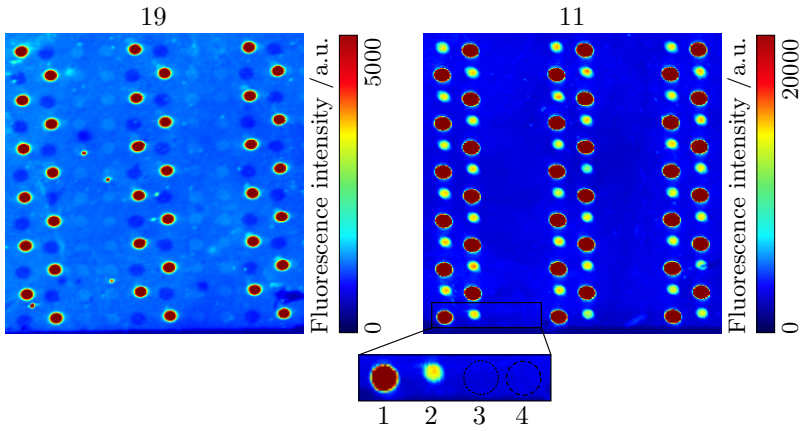

Figure A.5.2: Exemplary fluorescence scans of the validation of serum antibody interaction with four different peptides. 1: MVPEFSGSFPMR positive control [176]. 2: $_{923}$IHLVNNESSEVI**V**VH**K**$_{937}$, antigenic peptide used for the isolation of antibody species. 3: IHLVNNESSEVIVH**R**: first negative control. 4: IHLVNNESSEVI**A**HK, second negative control. Amino acids differing from the sequence of 1 are highlighted through bold letters. Both negative controls were identified in the substitution analysis to prevent the binding of the corresponding antibody species. Arrays consisted of 36 spots per peptide; peptides were pre-synthesized and spotted onto functionalized maleimide surfaces. The array on the left was incubated with serum 19 as negative control; the array on the right was incubated with serum 11. Reprinted with permission.

B.6 Establishment of a quality control method using VSI

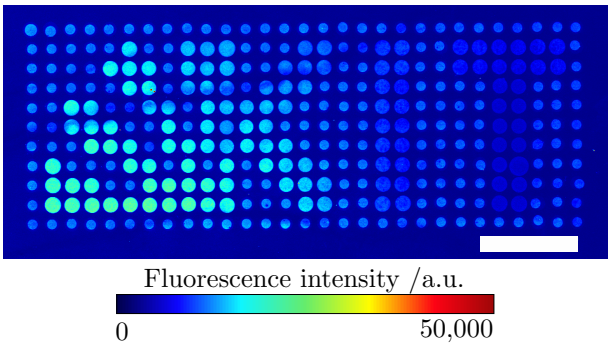

Figure B.6.1: Overlay of the fluorescence scans of the sub array depicted in figure 3.3.2 (page 52), containing the pattern of 11 x 29 spots incubated with serum (1:50), secondary antibody (labelled with AF647) and anti-HA DL550. Scans were conducted using the Innoscan fluorescence scanner at a resolution of 2 µm pixel^{-1}. 635 nm: gain 10. 532 nm: gain 10. Scale bar represents 500 µm. Reprinted with permission.

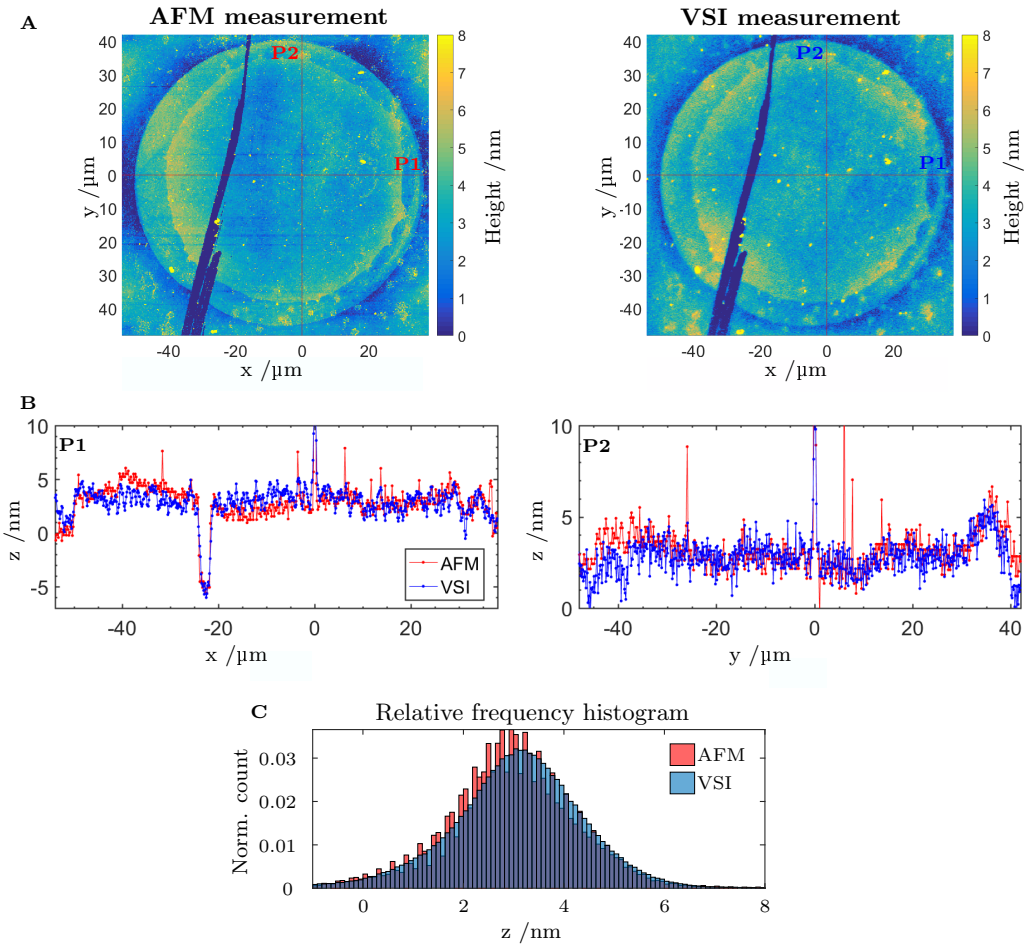

Figure B.6.2: Comparison of VSI measurement to AFM (z-offset adjusted). A left: Topology of SOI measured by AFM (Lateral resolution is not square: x 181.6 nm pixel^{-1}, y 186 nm pixel^{-1}). Peak force tapping mode was used as measuring mode since the array surface is soft and tends to contaminate the cantilever, which leads to a failing feedback and cantilever consumption. Peak force tapping mode is non-resonant since the oscillation frequency is kept below the cantilever resonance. The mode also allows direct force control and thus minimizes lateral forces which may result in damage of the substrate. The z-position is modulated by a sine wave instead of a triangular one to avoid unwanted turning points. However, artifacts, appearing as scratches in direction of cantilever movement, can be seen in the AFM measurement. A right: Topology of SOI measured by VSI (135.3 nm pixel^{-1} lateral resolution at x ten fold magnification. VSI data result from one single measurement at 25 fold magnification and was not stitched. Red lines indicate measured line profiles depicted in B. B: Line profiles for the AFM and VSI measurement. AFM profiles in red, VSI profiles in blue. Vertically: P2. Horizontally: P1. C: Stacked histograms of AFM and VSI measurements of the SOI. The higher resolution of the VSI is reflected in the histogram in higher pixel counts. From these measurements it can not be concluded whether the differences in the line profiles is due to different binning or a result of measurement deviation. Also the positioning of the profiles is a potential cause of error, since it was done manually and may vary within ± 5 pixel. Reprinted with permission.

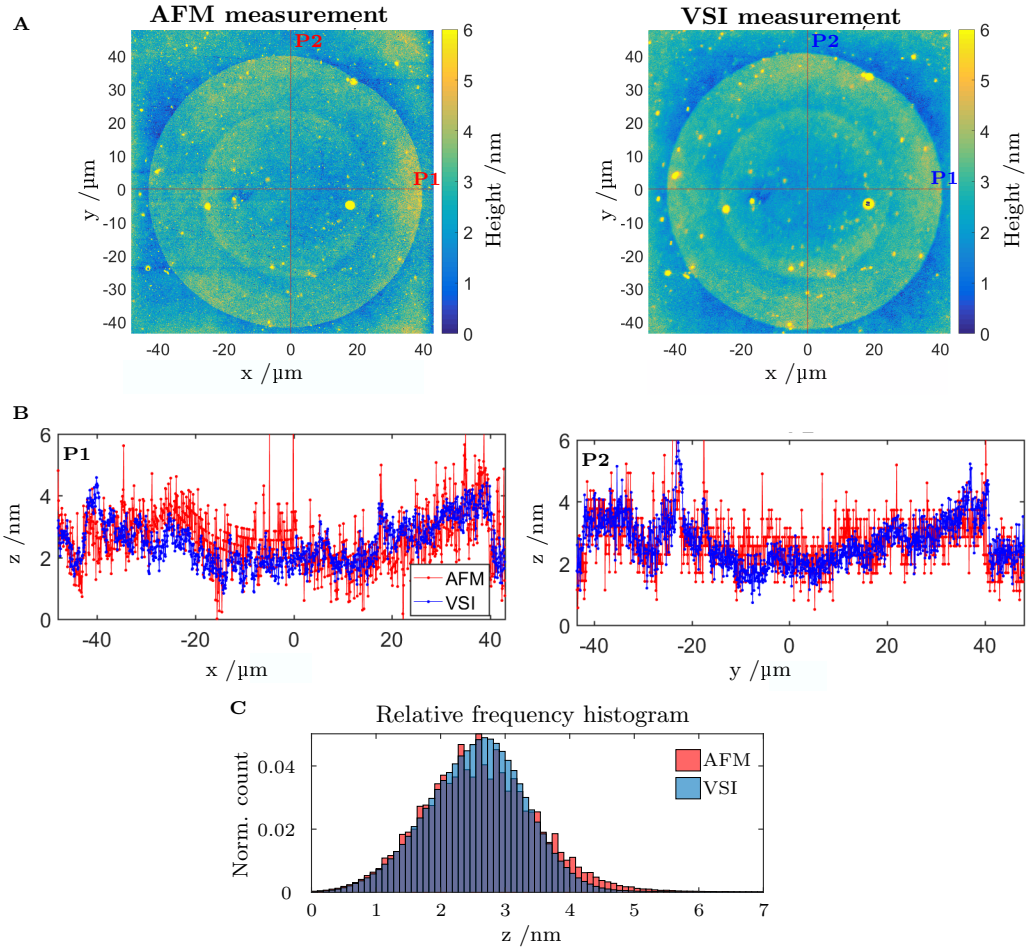

Figure B.6.3: Comparison of VSI measurement to AFM (z-offset adjusted). A left: Topology of a spot measured by AFM (76.1 nm pixel^{-1} lateral resolution). A software update enabled a new measuring mode: Scan Asyst mode. This mode utilizes peak force tapping but decouples the cantilever response from resonance dynamics to automatically adjust all critical imaging parameters and a real-time feedback loop constantly monitors and adjusts the gain. During scanning, the z-limit is automatically lowered, the set-point is automatically adjusted to minimal forces required and also the scan-rate is automatically controlled. As already seen in figure B.6.2, artifacts appearing as scratches in direction of the cantilever movement are present in the AFM measurement. A right: VSI measurement (74.6 nm pixel^{-1} lateral resolution at x 25 fold magnification). Red lines indicate measured line profiles depicted in B. Orientation of measurements are rotated 90° to the right, compared to 3.3.2 A and B. B: Line profiles for the AFM and VSI measurement. AFM profiles in red, VSI profiles in blue. Vertically: P2. Horizontally: P1. The influence of flattening is more dominant for AFM (obtained data points describe a curve). C: Stacked histograms of AFM and VSI measurements of the spot. The histogram representing the AFM measurement is closer to the VSI one than in B.6.2 due to better matching resolution. However, the AFM histogram is slightly broader and considerably noisier. Reprinted with permission.

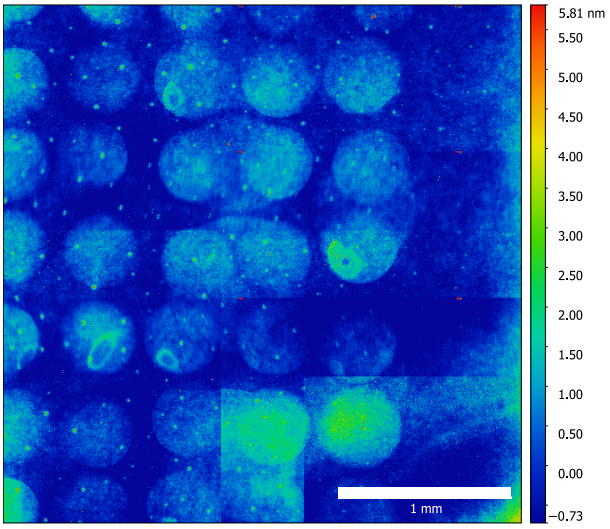

Figure B.6.4: VSI scan of an area of 3 mm x 3 mm using x 27.5 magnification and stitching six times. Visible are poorly positioned HA spots incubated with anti-HA antibody. Due to flattening and minor spot heights of about 1 nm to 1.5 nm, the overlap of stitched areas can be seen clearly in the lower right corner of the scan. Scale bar represents 1 mm. Scan acquisition took approximately 4 min.

B.7 Experimental setup

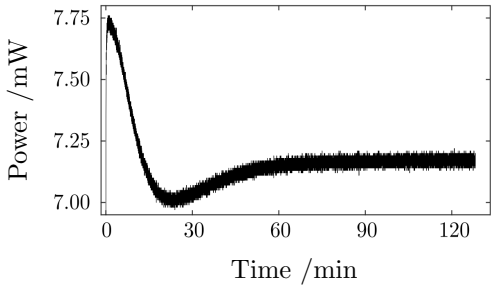

Figure B.7.1: LED power at sample position over time for exposure from below (LED 1 figure 3.4.1, p. 56). Power was measured using the PM160 power meter by Thorlabs. Measured power was stable after approximately 60 min.

B.8 Peptide array-PDMS channels

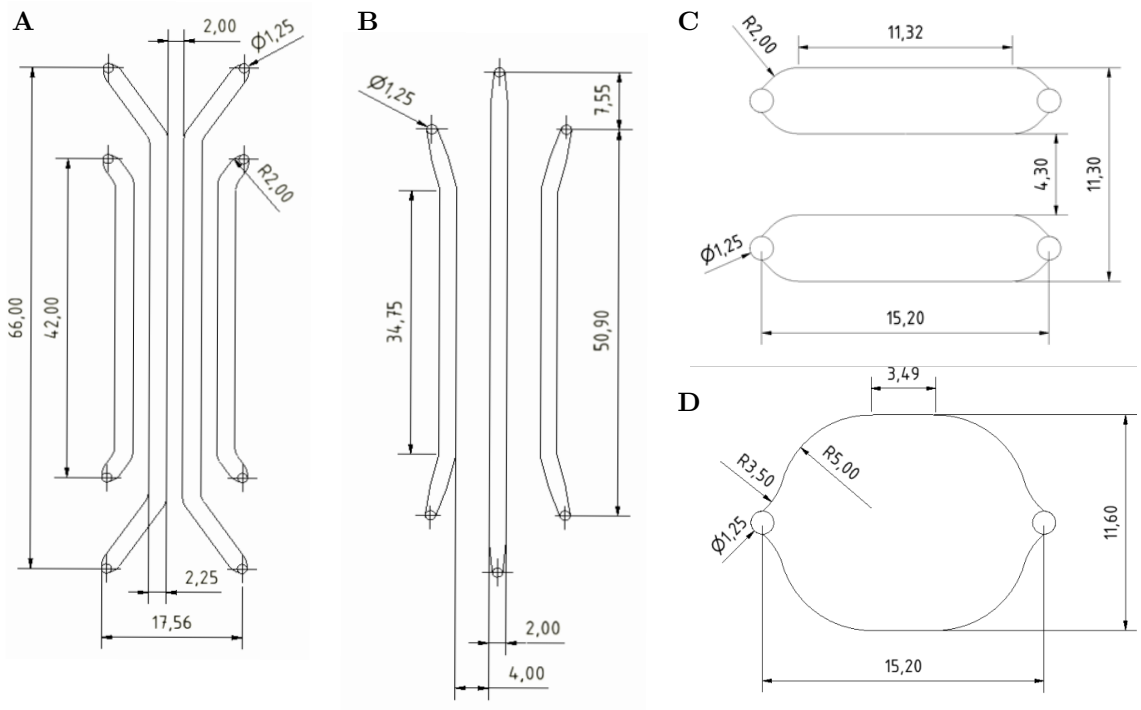

Figure B.8.1: Dimensions of different channel designs. Four (A) and three (B) channels on the area of a standard sized microscope glass slide (25 mm by 75 mm. Two (C) and one (D) channel on the area of 2.51 cm by 2.51 cm (1 inch by 1 inch).

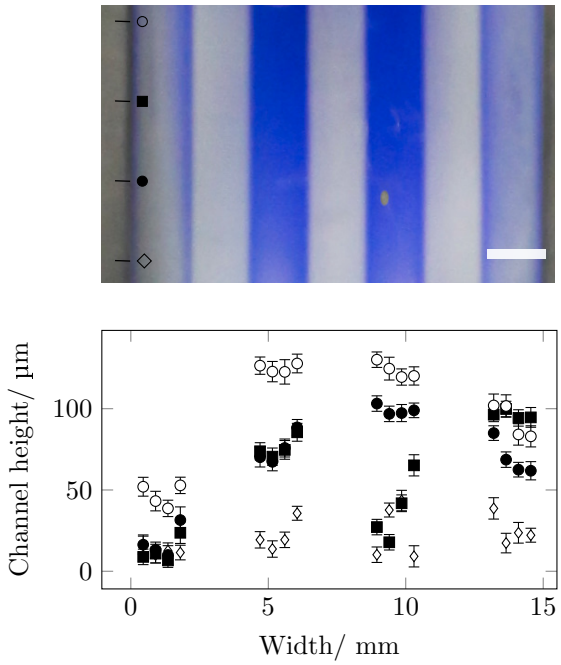

Figure B.8.2: Height of PDMS channels. Top: Visualization of inhomogeneous channel heights after assembling the MicCell System using blue ink. Channel width is 2.25 mm, channel height 150 µm. Plot marks on the left side illustrate the order of measured positions presented in the bottom graph. Scale bar represents 2 mm. Bottom: Measurement of channel height after assembly (10 N cm) at different positions along channel length. Distance in between individual positions is 5 mm. Data points represent the average of four measurements.

B.9 Peptide array-glass channels

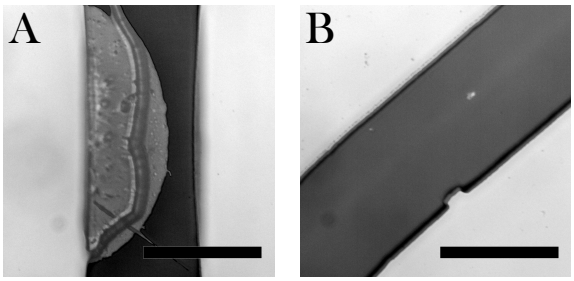

Figure B.9.1: Defects in the adhesive layer after bonding glass to functionalised surfaces. A: PEPperCHIP. B: 3D-Maleimide. Scale bar represents 200 µm.

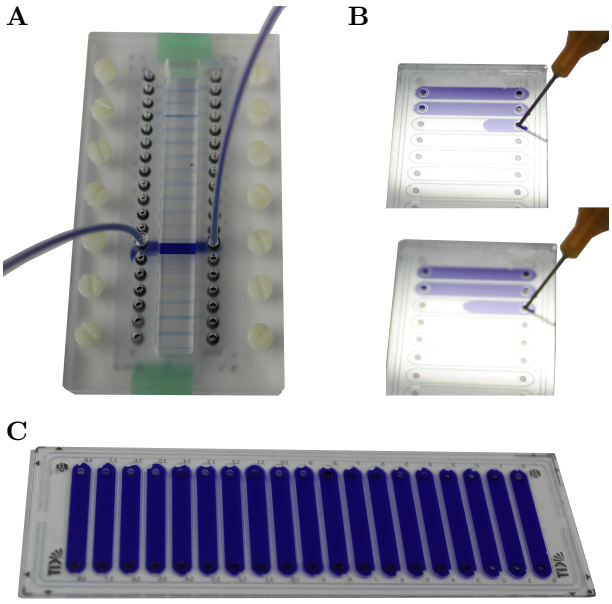

Figure B.9.2: Peptide chip (3 mm design) filled with blue ink for visualisation. A: Peptide chip mounted into the interface. B: Visualisation of flow profile for channel filling. C: Peptide chip, all channels filled with blue ink.
.

Bibliography

[1] A. M. Pappenheimer Jr. “Diphtheria toxin”. In: *Annual review of biochemistry* 46.1 (1977), pp. 69–94.

[2] E. A. *Map le P.A.C.* World Health Organization. 1994.

[3] A. Aderem and R. J. Ulevitch. “Toll-like receptors in the induction of the innate immune response”. In: *Nature* 406.6797 (2000), p. 782.

[4] S. Akita, N. Umezawa, N. Kato, and T. Higuchi. “Array-based fluorescence assay for serine/threonine kinases using specific chemical reaction”. In: *Bioorganic & medicinal chemistry* 16.16 (2008), pp. 7788–7794.

[5] J. J. Archelos, M. K. Storch, and H.-P. Hartung. “The role of B cells and autoantibodies in multiple sclerosis”. In: *Annals of Neurology: Official Journal of the American Neurological Association and the Child Neurology Society* 47.6 (2000), pp. 694–706.

[6] K.-D. Arndt, W. Bahmann, L. Barfels, J. Bauer, H. Bernstein, G. Böge, U. Borutzki, B. Heinrich, M. Kampf, A. Kemnitz, et al. *Handbuch Maschinenbau: Grundlagen und Anwendungen der Maschinenbau-Technik*. Heidelberg: Springer-Verlag, 2014.

[7] P. Askelöf, K. Rodmalm, G. Wrangsell, U. Larsson, S. B. Svenson, J. L. Cowell, A. Unden, and T. Bartfai. “Protective immunogenicity of two synthetic peptides selected from the amino acid sequence of Bordetella pertussis toxin subunit S1.” In: *Proceedings of the National Academy of Sciences* 87.4 (1990), pp. 1347–1351.

[8] B. Autran, F. Triebel, M. Viguier, M. Jolivet, P. Falmagne, and P. Debre. “Monoclonal B-cell response to diphtheria toxoid: evidence for cross-reactive epitopes”. In: *Immunology* 60.4 (1987), p. 531.

[9] H. Bannwarth, B. Kremer, and A. Schulz. *Basiswissen Physik, Chemie und Biochemie: Vom Atom bis zur Atmung - für Biologen, Mediziner und Pharmazeuten*. Springer-Lehrbuch. Heidelberg: Springer-Verlag, 2007. ISBN: 9783540712398.

[10] C. E. Bell and D. Eisenberg. “Crystal structure of nucleotide-free diphtheria toxin”. In: *Biochemistry* 36.3 (1997), pp. 481–488.

[11] A. M. Belu, D. J. Graham, and D. G. Castner. “Time-of-flight secondary ion mass spectrometry: techniques and applications for the characterization of biomaterial surfaces”. In: *Biomaterials* 24.21 (2003), pp. 3635–3653.

[12] U. Beutling, K. Städing, T. Stradal, and R. Frank. "Large-scale analysis of protein–protein interactions using cellulose-bound peptide arrays". In: *Protein–Protein Interaction*. Springer, 2008, pp. 115–152.

[13] M. Beyer. "Entwicklung und Anwendung neuartiger Trägeroberflächen zur kombinatorischen Peptidsynthese mit Aminosäure-Tonerpartikeln". PhD thesis. University of Heidelberg, 2005.

[14] M. Beyer, T. Felgenhauer, F. R. Bischoff, F. Breitling, and V. Stadler. "A novel glass slide-based peptide array support with high functionality resisting non-specific protein adsorption". In: *Biomaterials* 27.18 (2006), pp. 3505–3514.

[15] G. S. Bixler, R. Eby, K. M. Dermody, R. M. Woods, R. C. Seid, and S. Pillai. "Synthetic peptide representing a T-cell epitope of CRM197 substitutes as carrier molecule in a Haemophilus influenzae type B (Hib) conjugate vaccine". In: *Immunobiology of Proteins and Peptides V*. Springer, 1989, pp. 175–180.

[16] O. Bleher, A. Schindler, M.-X. Yin, A. B. Holmes, P. B. Luppa, G. Gauglitz, and G. Proll. "Development of a new parallelized, optical biosensor platform for label-free detection of autoimmunity-related antibodies". In: *Analytical and bioanalytical chemistry* 406.14 (2014), pp. 3305–3314.

[17] I. Block. "Herstellung und Anwendung von hochkomplexen Peptidbibliotheken". PhD thesis. University of Heidelberg, 2009.

[18] C. von Bojnicic-Kninski, V. Bykovskaya, F. Maerkle, R. Popov, A. Palermo, D. S. Mattes, L. K. Weber, B. Ridder, T. C. Foertsch, A. Welle, et al. "Selective Functionalization of Microstructured Surfaces by Laser-Assisted Particle Transfer". In: *Advanced Functional Materials* 26.39 (2016), pp. 7067–7073.

[19] F. Breitling, F. Loffler, C. Schirwitz, Y.-C. Cheng, F. Markle, K. Konig, T. Felgenhauer, E. Dorsam, F. Ralf Bischoff, and A. Nesterov-Muller. "Alternative setups for automated peptide synthesis". In: *Mini-Reviews in Organic Chemistry* 8.2 (2011), pp. 121–131.

[20] S. Buus, J. Rockberg, B. Forsström, P. Nilsson, M. Uhlen, and C. Schafer-Nielsen. "High-resolution mapping of linear antibody epitopes using ultrahigh-density peptide microarrays". In: *Molecular & Cellular Proteomics* 11.12 (2012), pp. 1790–1800.

[21] L. A. Carpino and G. Y. Han. "9-Fluorenylmethoxycarbonyl amino-protecting group". In: *The Journal of Organic Chemistry* 37.22 (1972), pp. 3404–3409.

[22] E. de Castro, C. J. A. Sigrist, A. Gattiker, V. Bulliard, P. S. Langendijk-Genevaux, E. Gasteiger, A. Bairoch, and N. Hulo. "ScanProsite: detection of PROSITE signature matches and ProRule-associated functional and structural residues in proteins". In: *Nucleic acids research* 34.suppl_2 (2006), W362–W365.

[23] J. Cello, A. Samuelson, P. Stålhandske, B. Svennerholm, S. Jeansson, and M. Forsgren. "Identification of group-common linear epitopes in structural and nonstructural proteins of enteroviruses by using synthetic peptides." In: *Journal of clinical microbiology* 31.4 (1993), pp. 911–916.

[24] *Characterization of Rituximab by Conformational Epitope Mapping and Epitope Substitution Scan.* accessed: Application Note. PEPperPRINT. Dec. 2018.

[25] M. H. Chiu and E. J. Prenner. "Differential scanning calorimetry: an invaluable tool for a detailed thermodynamic characterization of macromolecules and their interactions". In: *Journal of Pharmacy and Bioallied Sciences* 3.1 (2011), p. 39.

[26] J.-W. Choi, D.-K. Kang, H. Park, A. J. deMello, and S.-I. Chang. "High-throughput analysis of protein–protein interactions in picoliter-volume droplets using fluorescence polarization". In: *Analytical chemistry* 84.8 (2012), pp. 3849–3854.

[27] P. Chong, G. Zobrist, C. Sia, S. Loosmore, and M. Klein. "Identification of T-and B-cell epitopes of the S2 and S3 subunits of pertussis toxin by use of synthetic peptides." In: *Infection and immunity* 60.11 (1992), pp. 4640–4647.

[28] S. A. Cockle. "Identification of an active–site residue in subunit S1 of pertussis toxin by photocrosslinking to NAD". In: *FEBS Letters* 249.2 (1989), pp. 329–332.

[29] T. M. Cook, R. T. Protheroe, and J. M. Handel. "Tetanus: a review of the literature". In: *British Journal of Anaesthesia* 87.3 (2001), pp. 477–487.

[30] R. A. Copeland, D. L. Pompliano, and T. D. Meek. "Drug–target residence time and its implications for lead optimization". In: *Nature reviews Drug discovery* 5.9 (2006), p. 730.

[31] M. Cretich, F. Damin, G. Pirri, and M. Chiari. "Protein and peptide arrays: recent trends and new directions". In: *Biomolecular engineering* 23.2-3 (2006), pp. 77–88.

[32] M. Cretich, G. Di Carlo, C. Giudici, S. Pokoj, I. Lauer, S. Scheurer, and M. Chiari. "Detection of allergen specific immunoglobulins by microarrays coupled to microfluidics". In: *Proteomics* 9.8 (2009), pp. 2098–2107.

[33] B. M. Diethelm-Okita, D. K. Okita, L. Banaszak, and B. M. Conti-Fine. "Universal epitopes for human CD4+ cells on tetanus and diphtheria toxins". In: *The Journal of infectious diseases* 181.3 (2000), pp. 1001–1009.

[34] G. Duveneck, M. Pawlak, D. Neuschäfer, E. Bär, W. Budach, U. Pieles, and M. Ehrat. "Novel bioaffinity sensors for trace analysis based on luminescence excitation by planar waveguides". In: *Sensors and Actuators B: Chemical* 38.1-3 (1997), pp. 88–95.

[35] J. Eichler, M. Bienert, A. Stierandova, and M. Lebl. "Evaluation of cotton as a carrier for solid-phase peptide synthesis." In: *Peptide research* 4.5 (1991), pp. 296–307.

[36] M. Ewald, P. Fechner, and G. Gauglitz. "A multi-analyte biosensor for the simultaneous label-free detection of pathogens and biomarkers in point-of-need animal testing". In: *Analytical and bioanalytical chemistry* 407.14 (2015), pp. 4005–4013.

[37] N. F. Fairweather and V. A. Lyness. “The complete nucleotide sequence of tetanus toxin”. In: *Nucleic acids research* 14.19 (1986), pp. 7809–7812.

[38] J. R. Falsey, M. Renil, S. Park, S. Li, and K. S. Lam. “Peptide and small molecule microarray for high throughput cell adhesion and functional assays”. In: *Bioconjugate chemistry* 12.3 (2001), pp. 346–353.

[39] M. J. Feldstein, J. P. Golden, C. A. Rowe, B. D. MacCraith, and F. S. Ligler. “Array biosensor: optical and fluidics systems”. In: *Biomedical microdevices* 1.2 (1999), pp. 139–153.

[40] B. Fields, D. Knipe, P. Howley, and D. Griffin. *Fields virology. 5th.* Philadelphia: Wolters Kluwer Health/Lippincott Williams & Wilkins, 2007.

[41] G. Fields and R. Noble. “Solid phase peptide synthesis utilizing 9-fluorenylmethoxycarbonyl amino acids.” In: *International journal of peptide and protein research* 35.3 (1990), pp. 161–214.

[42] C. Fotinou, P. Emsley, I. Black, H. Ando, H. Ishida, M. Kiso, K. A. Sinha, N. F. Fairweather, and N. W. Isaacs. “The crystal structure of tetanus toxin Hc fragment complexed with a synthetic GT1b analogue suggests cross-linking between ganglioside receptors and the toxin”. In: *Journal of Biological Chemistry* 276.34 (2001), pp. 32274–32281.

[43] P. Frank, J. Schreiter, S. Haefner, G. Paschew, A. Voigt, and A. Richter. “Integrated microfluidic membrane transistor utilizing chemical information for on-chip flow control”. In: *PloS one* 11.8 (2016), e0161024.

[44] R. Frank. “Spot-synthesis: an easy technique for the positionally addressable, parallel chemical synthesis on a membrane support”. In: *Tetrahedron* 48.42 (1992), pp. 9217–9232.

[45] R. Frank. “The SPOT-synthesis technique: synthetic peptide arrays on membrane supports - principles and applications”. In: *Journal of immunological methods* 267.1 (2002), pp. 13–26.

[46] C. E. Fricks and J. M. Hogle. “Cell-induced conformational change in poliovirus: externalization of the amino terminus of VP1 is responsible for liposome binding”. In: *Journal of virology* 64.5 (1990), pp. 1934–1945.

[47] L. Galla, D. Greif, J. Regtmeier, and D. Anselmetti. “Microfluidic carbon-blackened polydimethylsiloxane device with reduced ultra violet background fluorescence for simultaneous two-color ultra violet/visible-laser induced fluorescence detection in single cell analysis”. In: *Biomicrofluidics* 6.1 (2012), p. 014104.

[48] S. Gaseitsiwe, D. Valentini, S. Mahdavifar, I. Magalhaes, D. F. Hoft, J. Zerweck, M. Schutkowski, J. Andersson, M. Reilly, and M. J. Maeurer. “Pattern recognition in pulmonary tuberculosis defined by high content peptide microarray chip analysis representing 61 proteins from M. tuberculosis”. In: *PloS one* 3.12 (2008), e3840.

[49] G. Gauglitz. “Direct optical detection in bioanalysis: an update”. In: *Analytical and bioanalytical chemistry* 398.6 (2010), pp. 2363–2372.

[50] H. M. Geysen, S. J. Rodda, T. J. Mason, G. Tribbick, and P. G. Schoofs. “Strategies for epitope analysis using peptide synthesis”. In: *Journal of immunological methods* 102.2 (1987), pp. 259–274.

[51] R. Ghai, R. J. Falconer, and B. M. Collins. “Applications of isothermal titration calorimetry in pure and applied research—survey of the literature from 2010”. In: *Journal of Molecular Recognition* 25.1 (2012), pp. 32–52.

[52] J. Golden, L. Shriver-Lake, K. Sapsford, and F. Ligler. “A “do-it-yourself” array biosensor”. In: *Methods* 37.1 (2005), pp. 65–72.

[53] A. Gonzalez-Quintela, R. Alende, F. Gude, J. Campos, J. Rey, L. Meijide, C. Fernandez-Merino, and C. Vidal. “Serum levels of immunoglobulins (IgG, IgA, IgM) in a general adult population and their relationship with alcohol consumption, smoking and common metabolic abnormalities”. In: *Clinical & Experimental Immunology* 151.1 (2008), pp. 42–50.

[54] L. Greenfield, M. J. Bjorn, G. Horn, D. Fong, G. A. Buck, R. J. Collier, and D. A. Kaplan. “Nucleotide sequence of the structural gene for diphtheria toxin carried by corynebacteriophage beta”. In: *Proceedings of the National Academy of Sciences* 80.22 (1983), pp. 6853–6857.

[55] T. M. Gronewold. “Surface acoustic wave sensors in the bioanalytical field: Recent trends and challenges”. In: *analytica chimica acta* 603.2 (2007), pp. 119–128.

[56] M. Gude, J. Ryf, and P. D. White. “An accurate method for the quantitation of Fmoc-derivatized solid phase supports”. In: *Letters in Peptide Science* 9.4 (2002), pp. 203–206.

[57] B. Gustafsson, E. Whitmore, and M. Tiru. “Neutralization of tetanus toxin by human monoclonal antibodies directed against tetanus toxin fragment C”. In: *Hybridoma* 12.6 (1993), pp. 699–708.

[58] B. B. Haab. “Antibody arrays in cancer research”. In: *Molecular & cellular proteomics* 4.4 (2005), pp. 377–383.

[59] L. J. Harris, S. B. Larson, K. W. Hasel, and A. McPherson. “Refined structure of an intact IgG2a monoclonal antibody”. In: *Biochemistry* 36.7 (1997), pp. 1581–1597.

[60] J. Hogle, M. Chow, and D. Filman. “Three-dimensional structure of poliovirus at 2.9 A resolution”. In: *Science* 229 (1985), p. 1.358.

[61] J. J. Holland and E. D. Kiehn. “Specific cleavage of viral proteins as steps in the synthesis and maturation of enteroviruses”. In: *Proceedings of the National Academy of Sciences* 60.3 (1968), pp. 1015–1022.

[62] T. P. Hopp, K. S. Prickett, V. L. Price, R. T. Libby, C. J. March, D. P. Cerretti, D. L. Urdal, and P. J. Conlon. “A short polypeptide marker sequence useful for recombinant protein identification and purification”. In: *Nature Biotechnology* 6.10 (1988), p. 1204.

[63] B. T. Houseman, J. H. Huh, S. J. Kron, and M. Mrksich. “Peptide chips for the quantitative evaluation of protein kinase activity”. In: *Nature biotechnology* 20.3 (2002), pp. 270–274.

[64] T. Huesgen, G. Lenk, B. Albrecht, P. Vulto, T. Lemke, and P. Woias. “Optimization and characterization of wafer-level adhesive bonding with patterned dry-film photoresist for 3D MEMS integration”. In: *Sensors and Actuators A: Physical* 162.1 (2010), pp. 137–144.

[65] Intavis Bioanalytical Instruments AG. *Website*. Dec. 2018. URL: `https://intavis.com`.

[66] C. A. Janeway. “Approaching the asymptote? Evolution and revolution in immunology”. In: *Cold Spring Harbor symposia on quantitative biology*. Vol. 54. Cold Spring Harbor Laboratory Press. 1989, pp. 1–13.

[67] M. Jerabek-Willemsen, T. André, R. Wanner, H. M. Roth, S. Duhr, P. Baaske, and D. Breitsprecher. “MicroScale Thermophoresis: Interaction analysis and beyond”. In: *Journal of Molecular Structure* 1077 (2014), pp. 101–113.

[68] N. K. Jerne. “The natural-selection theory of antibody formation”. In: *Proceedings of the National Academy of Sciences of the United States of America* 41.11 (1955), p. 849.

[69] G. Jin, P. Tengvall, I. Lundström, and H. Arwin. “A biosensor concept based on imaging ellipsometry for visualization of biomolecular interactions”. In: *Analytical biochemistry* 232.1 (1995), pp. 69–72.

[70] P. Karlson and D. Doenecke. *Karlsons Biochemie und Pathobiochemie*. Stuttgart: Georg Thieme Verlag, 2005. ISBN: 9783133578158.

[71] R. Karlsson, L. Fägerstam, H. Nilshans, and B. Persson. “Analysis of active antibody concentration. Separation of affinity and concentration parameters”. In: *Journal of immunological methods* 166.1 (1993), pp. 75–84.

[72] R. Karlsson, H. Roos, L. Fägerstam, and B. Persson. “Kinetic and concentration analysis using BIA technology”. In: *Methods* 6.2 (1994), pp. 99–110.

[73] C. Katz, L. Levy-Beladev, S. Rotem-Bamberger, T. Rito, S. G. D. Rüdiger, and A. Friedler. “Studying protein–protein interactions using peptide arrays”. In: *Chemical Society Reviews* 40.5 (2011), pp. 2131–2145.

[74] T. Kawasaki and T. Kawai. “Toll-like receptor signaling pathways”. In: *Frontiers in immunology* 5 (2014), p. 461.

[75] M. Knapp, B. Segelke, and B. Rupp. “The 1.61 Angstrom structure of the tetanus toxin. Ganglioside binding region: solved by MAD and MIR phase combination”. In: *Am. Crystallogr. Assoc* 25 (1998), p. 90.

[76] M. Knip, S. M. Virtanen, and H. K. Åkerblom. “Infant feeding and the risk of type 1 diabetes”. In: *The American Journal of Clinical Nutrition* 91.5 (2010), 1506S–1513S.

[77] J. Koolman and K.-H. Röhm. *Taschenatlas der Biochemie*. Stuttgart: Georg Thieme Verlag, 2003.

[78] I. Koyuncu, J. Brant, A. Lüttge, and M. R. Wiesner. "A comparison of vertical scanning interferometry (VSI) and atomic force microscopy (AFM) for characterizing membrane surface topography". In: *Journal of Membrane Science* 278.1-2 (2006), pp. 410–417.

[79] Y. Kühne, G. Reese, B. K. Ballmer-Weber, B. Niggemann, K.-M. Hanschmann, S. Vieths, and T. Holzhauser. "A novel multipeptide microarray for the specific and sensitive mapping of linear IgE-binding epitopes of food allergens". In: *International archives of allergy and immunology* 166.3 (2015), pp. 213–224.

[80] J. Kyte and R. F. Doolittle. "A simple method for displaying the hydropathic character of a protein". In: *Journal of molecular biology* 157.1 (1982), pp. 105–132.

[81] J. N. Lambert, J. P. Mitchell, and K. D. Roberts. "The synthesis of cyclic peptides". In: *Journal of the Chemical Society, Perkin Transactions 1* 5 (2001), pp. 471–484.

[82] K. Länge, B. E. Rapp, and M. Rapp. "Surface acoustic wave biosensors: a review". In: *Analytical and bioanalytical chemistry* 391.5 (2008), pp. 1509–1519.

[83] H. Latscha, U. Kazmaier, and H. Klein. *Organische Chemie: Chemie-Basiswissen II*. Springer-Lehrbuch. Heidelberg: Springer-Verlag, 2008. ISBN: 9783540771074.

[84] J. J. Lavinder, Y. Wine, C. Giesecke, G. C. Ippolito, A. P. Horton, O. I. Lungu, K. H. Hoi, B. J. DeKosky, E. M. Murrin, and M. M. Wirth. "Identification and characterization of the constituent human serum antibodies elicited by vaccination". In: *Proceedings of the National Academy of Sciences* 111.6 (2014), pp. 2259–2264.

[85] LC Science, LLC. *Website*. Dec. 2018. URL: `https://www.lcsciences.com`.

[86] D. A. Lebman and R. L. Coffman. "Interleukin 4 causes isotype switching to IgE in T cell-stimulated clonal B cell cultures." In: *Journal of Experimental Medicine* 168.3 (1988), pp. 853–862.

[87] J. B. Legutki, Z.-G. Zhao, M. Greving, N. Woodbury, S. A. Johnston, and P. Stafford. "Scalable high-density peptide arrays for comprehensive health monitoring". In: *Nature communications* 5 (2014), p. 4785.

[88] F. S. Ligler, K. E. Sapsford, J. P. Golden, L. C. Shriver-Lake, C. R. Taitt, M. A. Dyer, S. Barone, and C. J. Myatt. "The array biosensor: portable, automated systems". In: *Analytical Sciences* 23.1 (2007), pp. 5–10.

[89] Y. Lobet, C. Feron, G. Dequesne, E. Simoen, P. Hauser, and C. Locht. "Site-specific alterations in the B oligomer that affect receptor-binding activities and mitogenicity of pertussis toxin". In: *Journal of Experimental Medicine* 177.1 (1993), pp. 79–87.

[90] F. F. Loeffler, T. C. Foertsch, R. Popov, D. S. Mattes, M. Schlageter, M. Sedlmayr, B. Ridder, F.-X. Dang, C. von Bojničić-Kninski, L. K. Weber, et al. "High-flexibility combinatorial peptide synthesis with laser-based transfer of monomers in solid matrix material". In: *Nature communications* 7 (2016), p. 11844.

[91] F. F. Loeffler, J. Pfeil, and K. Heiss. “High-Density Peptide Arrays for Malaria Vaccine Development”. In: *Vaccine Design: Methods and Protocols: Volume 1: Vaccines for Human Diseases* (2016), pp. 569–582.

[92] X. Y. Lü, Y. Huang, W. P. Qian, Z. M. Tang, and Z. H. Lu. “An effective method for quantitative evaluation of proteins adsorbed on biomaterial surfaces”. In: *Journal of Biomedical Materials Research Part A* 66.3 (2003), pp. 722–727.

[93] G. Maccari, A. Genoni, S. Sansonno, and A. Toniolo. “Properties of two enterovirus antibodies that are utilized in diabetes research”. In: *Scientific Reports* 6 (2016), p. 24757.

[94] S. Machingaidze, E. Rehfuess, R. von Kries, G. D. Hussey, and C. S. Wiysonge. “Understanding interventions for improving routine immunization coverage in children in low-and middle-income countries: a systematic review protocol”. In: *Systematic reviews* 2.1 (2013), p. 106.

[95] J. Marsian, H. Fox, M. W. Bahar, A. Kotecha, E. E. Fry, D. I. Stuart, A. J. Macadam, D. J. Rowlands, and G. P. Lomonossoff. “Plant-made polio type 3 stabilized VLPs—a candidate synthetic polio vaccine”. In: *Nature Communications* 8 (2017).

[96] M. Martin and K. Resch. *Immunologie*. UTB / UTB. Stuttgart: UTB GmbH, 2009. ISBN: 9783825231743.

[97] D. S. Mattes, S. Rentschler, T. C. Foertsch, S. W. Münch, F. F. Loeffler, A. Nesterov-Mueller, S. Bräse, and F. Breitling. “A Trifunctional Linker for Purified 3D Assembled Peptide Structure Arrays”. In: *Small Methods* 2.2 (2018), p. 1700205.

[98] R. B. Merrifield. “Solid phase peptide synthesis. I. The synthesis of a tetrapeptide”. In: *Journal of the American Chemical Society* 85.14 (1963), pp. 2149–2154.

[99] K. Metsküla, L. Salur, M. Mandel, and R. Uibo. “Demonstration of high prevalence of SS-A antibodies in a general population: association with HLA-DR and enterovirus antibodies”. In: *Immunology letters* 106.1 (2006), pp. 14–18.

[100] A. Mock and C. Herold-Mende. “Non-invasive glioblastoma immunoprofiling by printed peptide arrays”. In: *Oncoimmunology* 5.2 (2016), e1069941.

[101] C. A. G. N. Montalbetti and V. Falque. “Amide bond formation and peptide coupling”. In: *Tetrahedron* 61.46 (2005), pp. 10827–10852.

[102] A.-M. Müller, M. Bockstahler, G. Hristov, C. Weiß, A. Fischer, S. Korkmaz-Icöz, E. Giannitsis, W. Poller, H.-P. Schultheiss, H. A. Katus, et al. “Identification of novel antigens contributing to autoimmunity in cardiovascular diseases”. In: *Clinical Immunology* 173 (2016), pp. 64–75.

[103] K. Murphy, C. Weaver, and L. Seidler. *Janeway Immunologie*. Heidelberg: Springer-Verlag, 2018. ISBN: 9783662560044.

[104] K. A. Navalkar, S. A. Johnston, N. Woodbury, J. N. Galgiani, D. M. Magee, Z. Chicacz, and P. Stafford. "Application of immunosignatures for diagnosis of valley fever". In: *Clinical and Vaccine Immunology* 21.8 (2014), pp. 1169–1177.

[105] D. Nečas and P. Klapetek. "Gwyddion: an open-source software for SPM data analysis". In: *Central European Journal of Physics* 10 (1 2012), pp. 181–188.

[106] D. Nemazee. "Receptor editing in lymphocyte development and central tolerance". In: *Nature Reviews Immunology* 6.10 (2006), p. 728.

[107] A. Nicosia, M. Perugini, C. Franzini, M. C. Casagli, M. G. Borri, G. Antoni, M. Almoni, P. Neri, G. Ratti, and R. Rappuoli. "Cloning and sequencing of the pertussis toxin genes: operon structure and gene duplication". In: *Proceedings of the National Academy of Sciences* 83.13 (1986), pp. 4631–4635.

[108] K. Niespodziana, K. Napora, C. Cabauatan, M. Focke-Tejkl, W. Keller, V. Niederberger, M. Tsolia, I. Christodoulou, N. G. Papadopoulos, and R. Valenta. "Misdirected antibody responses against an N-terminal epitope on human rhinovirus VP1 as explanation for recurrent RV infections". In: *The FASEB Journal* 26.3 (2012), pp. 1001–1008.

[109] W. C. Noble, Z. Virani, and R. G. A. Cree. "Co-transfer of vancomycin and other resistance genes from Enterococcus faecalis NCTC 12201 to Staphylococcus aureus". In: *FEMS microbiology letters* 93.2 (1992), pp. 195–198.

[110] G. J. V. Nossal. "Antibody production by single cells". In: *British journal of experimental pathology* 39.5 (1958), p. 544.

[111] L. A. J. O'neill, D. Golenbock, and A. G. Bowie. "The history of Toll-like receptors—redefining innate immunity". In: *Nature Reviews Immunology* 13.6 (2013), p. 453.

[112] D. J. O'shannessy, M. Brighamburke, K. K. Soneson, P. Hensley, and I. Brooks. "Determination of rate and equilibrium binding constants for macromolecular interactions using surface plasmon resonance: use of nonlinear least squares analysis methods". In: *Analytical biochemistry* 212.2 (1993), pp. 457–468.

[113] D. J. O'Shannessy and D. J. Winzor. "Interpretation of deviations from pseudo-first-order kinetic behavior in the characterization of ligand binding by biosensor technology". In: *Analytical biochemistry* 236.2 (1996), pp. 275–283.

[114] M. S. Oberste, K. Maher, D. R. Kilpatrick, M. R. Flemister, B. A. Brown, and M. A. Pallansch. "Typing of human enteroviruses by partial sequencing of VP1". In: *Journal of clinical microbiology* 37.5 (1999), pp. 1288–1293.

[115] R. Ochs. *Biochemistry*. Burlington: Jones & Bartlett Learning, 2011. ISBN: 9780763757366.

[116] A. Palermo, R. Thelen, L. K. Weber, T. Foertsch, S. Rentschler, V. Hackert, J. Syurik, and A. Nesterov-Mueller. "Vertical Scanning Interferometry for Label-Free Detection of Peptide-Antibody Interactions". In: *High-throughput* 8.2 (2019), p. 7.

[117] A. Palermo, L. K. Weber, S. Rentschler, A. Isse, M. Sedlmayr, K. Herbster, V. List, J. Hubbuch, F. F. Löffler, A. Nesterov-Müller, et al. "Identification of a Tetanus Toxin Specific Epitope in Single Amino Acid Resolution". In: *Biotechnology Journal* 12.10 (2017).

[118] A. C. Palmenberg, D. Spiro, R. Kuzmickas, S. Wang, A. Djikeng, J. A. Rathe, C. M. Fraser-Liggett, and S. B. Liggett. "Sequencing and analyses of all known human rhinovirus genomes reveal structure and evolution". In: *Science* 324.5923 (2009), pp. 55–59.

[119] J. P. Pellois, X. Zhou, O. Srivannavit, T. Zhou, E. Gulari, and X. Gao. "Individually addressable parallel peptide synthesis on microchips". In: *Nature biotechnology* 20.9 (2002), p. 922.

[120] PEPperPRINT GmbH. *Website*. Dec. 2018. URL: `https://www.pepperprint.com`.

[121] V. Y. Perera and M. J. Corbel. "Human antibody response to fragments A and B of diphtheria toxin and a synthetic peptide of amino acid residues 141–157 of fragment A". In: *Epidemiology & Infection* 105.3 (1990), pp. 457–468.

[122] F. Perosa, E. Favoino, M. A. Caragnano, and F. Dammacco. "Generation of biologically active linear and cyclic peptides has revealed a unique fine specificity of rituximab and its possible cross-reactivity with acid sphingomyelinase-like phosphodiesterase 3b precursor". In: *Blood* 107.3 (2006), pp. 1070–1077.

[123] K. Pieper, B. Grimbacher, and H. Eibel. "B-cell biology and development". In: *Journal of Allergy and Clinical Immunology* 131.4 (2013), pp. 959–971.

[124] T. E. Plowman, J. D. Durstchi, H. K. Wang, D. A. Christensen, J. N. Herron, and W. M. Reichert. "Multiple-analyte fluoroimmunoassay using an integrated optical waveguide sensor". In: *Analytical Chemistry* 71.19 (1999), pp. 4344–4352.

[125] R. J. Pounder, M. J. Stanford, P. Brooks, S. P. Richards, and A. P. Dove. "Metal free thiol–maleimide 'Click'reaction as a mild functionalisation strategy for degradable polymers". In: *Chemical Communications* 41 (2008), pp. 5158–5160.

[126] J. V. Price, S. Tangsombatvisit, G. Xu, J. Yu, D. Levy, E. C. Baechler, O. Gozani, M. Varma, P. J. Utz, and C. L. Liu. "On silico peptide microarrays for high-resolution mapping of antibody epitopes and diverse protein-protein interactions". In: *Nature medicine* 18.9 (2012), p. 1434.

[127] R. Raju, D. Navaneetham, D. Okita, B. Diethelm-Okita, D. McCormick, and B. M. Conti-Fine. "Epitopes for human CD4+ cells on diphtheria toxin: structural features of sequence segments forming epitopes recognized by most subjects". In: *European journal of immunology* 25.12 (1995), pp. 3207–3214.

[128] S. V. Rao, N. A. Beaudry, Y. Zhao, and R. A. Chipman. "Evanescent-imaging-ellipsometry-based microarray reader". In: *Journal of Biomedical Optics* 11.1 (2006), p. 014028.

[129] R. L. Rich, M. J. Cannon, J. Jenkins, P. Pandian, S. Sundaram, R. Magyar, J. Brockman, J. Lambert, and D. G. Myszka. "Extracting kinetic rate constants from surface plasmon resonance array systems". In: *Analytical biochemistry* 373.1 (2008), pp. 112–120.

[130] W. H. Robinson, C. DiGennaro, W. Hueber, B. B. Haab, M. Kamachi, E. J. Dean, S. Fournel, D. Fong, M. C. Genovese, H. E. N. De Vegvar, et al. "Autoantigen microarrays for multiplex characterization of autoantibody responses". In: *Nature medicine* 8.3 (2002), p. 295.

[131] M. Roivainen, L. Piirainen, T. Ryä, A. Närvänen, and T. Hovi. "An immunodominant N-terminal region of VP1 protein of poliovirion that is buried in crystal structure can be exposed in solution". In: *Virology* 195.2 (1993), pp. 762–765.

[132] M. G. Rossmann, E. Arnold, J. W. Erickson, E. A. Frankenberger, J. P. Griffith, H.-J. Hecht, J. E. Johnson, G. Kamer, M. Luo, A. G. Mosser, et al. "Structure of a human common cold virus and functional relationship to other picornaviruses". In: *Nature* 317.6033 (1985), p. 145.

[133] C. A. Rowe-Taitt, J. P. Golden, M. J. Feldstein, J. J. Cras, K. E. Hoffman, and F. S. Ligler. "Array biosensor for detection of biohazards". In: *Biosensors and Bioelectronics* 14.10-11 (2000), pp. 785–794.

[134] C. A. Rowe-Taitt, J. W. Hazzard, K. E. Hoffman, J. J. Cras, J. P. Golden, and F. S. Ligler. "Simultaneous detection of six biohazardous agents using a planar waveguide array biosensor". In: *Biosensors and Bioelectronics* 15.11-12 (2000), pp. 579–589.

[135] C. A. Rowe, L. M. Tender, M. J. Feldstein, J. P. Golden, S. B. Scruggs, B. D. MacCraith, J. J. Cras, and F. S. Ligler. "Array biosensor for simultaneous identification of bacterial, viral, and protein analytes". In: *Analytical Chemistry* 71.17 (1999), pp. 3846–3852.

[136] C. M. Salisbury, D. J. Maly, and J. A. Ellman. "Peptide microarrays for the determination of protease substrate specificity". In: *Journal of the American Chemical Society* 124.50 (2002), pp. 14868–14870.

[137] M. E. Sandison and H. Morgan. "Rapid fabrication of polymer microfluidic systems for the production of artificial lipid bilayers". In: *Journal of Micromechanics and Microengineering* 15.7 (2005), S139.

[138] P. Sarkar, S. Sridharan, R. Luchowski, S. Desai, B. Dworecki, M. Nlend, Z. Gryczynski, and I. Gryczynski. "Photophysical properties of a new DyLight 594 dye". In: *Journal of Photochemistry and Photobiology B: Biology* 98.1 (2010), pp. 35–39.

[139] G. Scatchard. "The attractions of proteins for small molecules and ions". In: *Annals of the New York Academy of Sciences* 51.4 (1949), pp. 660–672.

[140] G. G. Schiavo, F. Benfenati, B. Poulain, O. Rossetto, P. P. de Laureto, B. R. DasGupta, and C. Montecucco. "Tetanus and botulinum-B neurotoxins block neurotransmitter release by proteolytic cleavage of synaptobrevin". In: *Nature* 359.6398 (1992), pp. 832–835.

[141] G. Schiavo, M. Matteoli, and C. Montecucco. “Neurotoxins affecting neuroexocytosis”. In: *Physiological reviews* 80.2 (2000), pp. 717–766.

[142] C. Schirwitz. “Purification of peptides in high-complexity arrays”. PhD thesis. Ruprecht-Karls-Universtät Heidelberg, 2012.

[143] C. Schirwitz, F. F. Loeffler, T. Felgenhauer, V. Stadler, F. Breitling, and F. R. Bischoff. “Sensing immune responses with customized peptide microarrays”. In: *Biointerphases* 7.1-4 (2012), p. 47.

[144] M. A. Schmidt, B. Raupach, M. Szulczynski, and J. Marzillier. “Identification of linear B-cell determinants of pertussis toxin associated with the receptor recognition site of the S3 subunit.” In: *Infection and immunity* 59.4 (1991), pp. 1402–1408.

[145] C. Schütt and B. Bröker. *Grundwissen Immunologie*. Heidelberg: Spektrum Akademischer Verlag, 2011. ISBN: 9783827426475.

[146] C. C. Scott, A. Luttge, and K. A. Athanasiou. “Development and validation of vertical scanning interferometry as a novel method for acquiring chondrocyte geometry”. In: *Journal of Biomedical Materials Research Part A* 72.1 (2005), pp. 83–90.

[147] D. Sesardic and M. J. Corbel. “Testing for neutralising potential of serum antibodies to tetanus and diphtheria toxin”. In: *The Lancet* 340.8821 (1992), pp. 737–738.

[148] J. N. Sheagren. “Staphylococcus aureus: the persistent pathogen”. In: *New England Journal of Medicine* 310.22 (1984), pp. 1437–1442.

[149] T. K. Shōreikai. *Peptide Chemistry*. Special publication. Washington, D. C.: Chemical Society, 1993.

[150] G. R. Siber. “Pneumococcal disease: prospects for a new generation of vaccines”. In: *Science* 265.5177 (1994), pp. 1385–1387.

[151] L. L. Simpson. “Molecular pharmacology of botulinum toxin and tetanus toxin”. In: *Annual review of pharmacology and toxicology* 26.1 (1986), pp. 427–453.

[152] S. Sjölander and C. Urbaniczky. “Integrated Fluid Handling System for Biomolecular Interaction Analysis”. In: *Analytical Chemistry* 63.20 (1991), pp. 2338–2345.

[153] P. Smejkal, M. C. Breadmore, R. M. Guijt, F. Foret, F. Bek, and M. Macka. “Analytical isotachophoresis of lactate in human serum using dry film photoresist microfluidic chips compatible with a commercially available field-deployable instrument platform”. In: *Analytica chimica acta* 803 (2013), pp. 135–142.

[154] T. J. Smith, M. J. Kremer, M. Luo, G. Vriend, E. Arnold, G. Kamer, M. G. Rossmann, M. A. McKinlay, G. D. Diana, and M. J. Otto. “The site of attachment in human rhinovirus 14 for antiviral agents that inhibit uncoating”. In: *Science* 233.4770 (1986), pp. 1286–1293.

[155] V. Souplet, R. Desmet, and O. Melnyk. “Imaging of protein layers with an optical microscope for the characterization of peptide microarrays”. In: *Journal of Peptide Science* 13.7 (2007), pp. 451–457.

[156] A. Spencer, I. Dobryden, N. Almqvist, A. Almqvist, and R. Larsson. "The influence of AFM and VSI techniques on the accurate calculation of tribological surface roughness parameters". In: *Tribology International* 57 (2013), pp. 242–250.

[157] N. Spengler, J. Höfflin, A. Moazenzadeh, D. Mager, N. MacKinnon, V. Badilita, U. Wallrabe, and J. G. Korvink. "Heteronuclear micro-Helmholtz coil facilitates μm-range spatial and sub-Hz spectral resolution NMR of nL-volume samples on customisable microfluidic chips". In: *PloS one* 11.1 (2016), e0146384.

[158] V. Stadler, T. Felgenhauer, M. Beyer, S. Fernandez, K. Leibe, S. Güttler, M. Gröning, K. König, G. Torralba, M. Hausmann, et al. "Combinatorial synthesis of peptide arrays with a laser printer". In: *Angewandte Chemie International Edition* 47.37 (2008), pp. 7132–7135.

[159] V. Stadler, R. Kirmse, M. Beyer, F. Breitling, T. Ludwig, and F. R. Bischoff. "PEGMA/MMA copolymer graftings: generation, protein resistance, and a hydrophobic domain". In: *Langmuir* 24.15 (2008), pp. 8151–8157.

[160] P. E. Stein, A. Boodhoo, G. D. Armstrong, S. A. Cockle, M. H. Klein, and R. J. Read. "The crystal structure of pertussis toxin". In: *Structure* 2.1 (1994), pp. 45–57.

[161] M. W. Steward and A. M. Lew. "The importance of antibody affinity in the performance of immunoassays for antibody". In: *Journal of immunological methods* 78.2 (1985), pp. 173–190.

[162] J. Striffler. "Replikation von µ-Peptidarrays". PhD thesis. KIT, Karlsruhe, 2014.

[163] J. Striffler, D. S. Mattes, S. Schillo, B. Muenster, A. Palermo, B. Ridder, A. Welle, V. Trouillet, V. Stadler, G. Markovic, et al. "Replication of Polymer-Based Peptide Microarrays by Multi-Step Transfer". In: *ChemNanoMat* 2.9 (2016), pp. 897–903.

[164] B. D. Systèmes. "Discovery studio modeling environment, release 4.5". In: *Dassault Systèmes, San Diego Google Scholar* (2015).

[165] L. C. Szymczak, H.-Y. Kuo, and M. Mrksich. "Peptide Arrays: Development and Application". In: *Analytical chemistry* 90.1 (2017), pp. 266–282.

[166] M. C. Timbury. *Notes on Medical Virology*. Churchill Livingstone Medical Text. London: Churchill Livingstone, 1994. ISBN: 9780443048722.

[167] F. Triebel, B. Autran, S. de Roquefeuil, P. Falmagne, and P. Debré. "Immune response to diphtheria toxin and to different CNBr fragments: evidence for different B and T cell reactivities". In: *European journal of immunology* 16.1 (1986), pp. 47–53.

[168] Y.-C. Tsai, H.-P. Jen, K.-W. Lin, and Y.-Z. Hsieh. "Fabrication of microfluidic devices using dry film photoresist for microchip capillary electrophoresis". In: *Journal of Chromatography A* 1111.2 (2006), pp. 267–271.

[169] J. Visentin, L. Couzi, C. Dromer, M. Neau-Cransac, G. Guidicelli, V. Veniard, K. N.-l. Coniat, P. Merville, C. D. Primo, and J.-L. Taupin. "Overcoming non-specific binding to measure the active concentration and kinetics of serum anti-HLA antibodies by surface plasmon resonance". In: *Biosensors and Bioelectronics* 117 (2018), pp. 191–200.

[170] W. A. Volk, B. Bizzini, R. M. Snyder, E. Bernhard, and R. R. Wagner. "Neutralization of tetanus toxin by distinct monoclonal antibodies binding to multiple epitopes on the toxin molecule". In: *Infection and immunity* 45.3 (1984), pp. 604–609.

[171] P. Vulto, N. Glade, L. Altomare, J. Bablet, L. Del Tin, G. Medoro, I. Chartier, N. Manaresi, M. Tartagni, and R. Guerrieri. "Microfluidic channel fabrication in dry film resist for production and prototyping of hybrid chips". In: *Lab on a Chip* 5.2 (2005), pp. 158–162.

[172] P. Vulto, T. Huesgen, B. Albrecht, and G. Urban. "A full-wafer fabrication process for glass microfluidic chips with integrated electroplated electrodes by direct bonding of dry film resist". In: *Journal of Micromechanics and Microengineering* 19.7 (2009), p. 077001.

[173] J. F. Watts and J. Wolstenholme. *An introduction to surface analysis by XPS and AES*. Hoboken: Wiley-VCH, 2003, p. 224. ISBN: 0-470-84713-1.

[174] L. K. Weber, A. Fischer, T. Schorb, M. Soehindrijo, T. C. Förtsch, D. Althuon, F. Löffler, F. Breitling, J. Hubbuch, and A. Nesterov-Müller. "Automated microfluidic system with optical set up for the investigation of peptide-antibody interactions in an array format". In: *Microsystems Technology in Germany 2016* 1 (2016), pp. 50–52.

[175] L. K. Weber, A. Isse, S. Rentschler, R. E. Kneusel, A. Palermo, J. Hubbuch, A. Nesterov–Mueller, F. Breitling, and F. F. Loeffler. "Antibody Fingerprints in Lyme Disease Deciphered with High Density Peptide Arrays". In: *Engineering in Life Sciences* (2017).

[176] L. K. Weber, A. Palermo, J. Kügler, O. Armant, A. Isse, S. Rentschler, T. Jaenisch, J. Hubbuch, S. Dübel, and A. Nesterov-Mueller. "Single amino acid fingerprinting of the human antibody repertoire with high density peptide arrays". In: *Journal of immunological methods* 443 (2017), pp. 45–54.

[177] D. Wild. *The Immunoassay Handbook: Theory and Applications of Ligand Binding, ELISA and Related Techniques*. Amsterdam: Elsevier Science, 2013. ISBN: 9780080970387.

[178] I. A. Wilson, H. L. Niman, R. A. Houghten, A. R. Cherenson, M. L. Connolly, and R. A. Lerner. "The structure of an antigenic determinant in a protein". In: *Cell* 37.3 (1984), pp. 767–778.

[179] World Health Organization. "Pertussis vaccines: WHO position paper—August 2015". In: *Weekly Epidemiological Record= Relevé épidémiologique hebdomadaire* 90.35 (2015), pp. 433–458.

[180] World Health Organization. *WHO Expert Committee on Biological Standardization: Sixty-sixth Report*. 999. World Health Organization, 2016.

[181] M. Yousefi, R. Khosravi-Eghbal, A. Reza Mahmoudi, M. Jeddi-Tehrani, H. Rabbani, and F. Shokri. "Comparative in vitro and in vivo assessment of toxin neutralization by anti-tetanus toxin monoclonal antibodies". In: *Human vaccines & immunotherapeutics* 10.2 (2014), pp. 344–351.

[182] R. Zhang and F. Monsma. "Fluorescence-based thermal shift assays." In: *Current opinion in drug discovery & development* 13.4 (2010), pp. 389–402.

Abbreviations

ADP adenosin diphosphate

AFM atomic force microscopy

APTES (3-aminopropyl)-triethoxysilane

BCR B cell receptor

BIBS α-bromoisobutyrylbromid

Bipy 2.2-bipyridyl

bPDMS blackened PDMS

CCD charge coupled device

CDR complementary determining region

DCM dichlormethane

DIC *N,N*-diisopropylcarbodiimide

DSC differential scanning calorimetry

DIPEA *N,N*-diisopropylethylamin

DIW deionized water

DMF *N,N*-dimethylformamide

DMSO dimethyl sulfoxide

DL DyLight

EV enterovirus

ELISA enzyme-linked immunosorbend assay

eEf-2 eucariotic elongation factor 2

FP fluorescence polarization

Fmoc 9-fluorenylmethoxycarbonyl

FOV field of view

HA hemagglutinin

HLA human leukocyte antigen

ITC isothermal titration calorimentry

IU international units

LOD limit of detection

MHC major histocompatability complex

MsT MicroScale thermophoresis

NAD nicotinamide adenine dinucleotide

NHS *N*-hydroxysuccinimide

NMI *N*-methylimidazole

OPfp pentafluorophenyl ester

PAMP pathogen-associated molecular patterns

PBB post bond bake

PBS phosphate buffered saline

PBS-T phosphate buffered saline with 0.05 % Tween 20

PC polycarbonate

PDFA piperidine dibenzofulvene adduct

PDMS polydimethylsiloxane

PEB post exposure bake

PEG polyethylene glycol

PEGMA poly(ethylene glycol)methacrylate

PMMA poly(methyl methacrylate)

PRR pattern recognition receptor

PTFE polytetrafluoroethylene

QCM quartz cristal microbalance

RB Rockland buffer

RIfS reflectometric interference spectroscopy

iRIfS reflectometric interference spectroscopy imaging

SAW surface acoustic wave

SOI spot of interest

SPPS solid phase peptide synthesis

SPR surface plasmon resonance

SPRi surface plasmon resonance imaging

SRP serum reactive peptide

TAMRA 5-(and-6)-carboxytetramethylrhodamine

TCR T cell receptor

TDP tetanus, diphtheria and pertussis

TFA trifluoroacetic acid

TIBS triisobutylsilane

TLR Toll-like receptor

TM transverse magnetic

TNT trinitrotoluene

TRIS tris(hydroxymethyl)aminomethane

ToF-SIMS time of flight secondary ion mass spectrometry

VSI vertical scanning interferometry

WHO world health organization

XPS X-ray photoelectron spectroscopy

List of Figures

List of Tables

Acknowledgments

An dieser Stelle möchte ich mich bei sehr vielen Menschen bedanken, die mich während meiner Promotion auf unterschiedliche Weise unterstützt und begleitet haben. Ohne diese Unterstützung wäre mir die Durchführung dieser Arbeit nicht möglich gewesen.

Besonderer Dank geht an Prof. A. Nesterov-Müller, der mir die Promotionsstelle mit dieser interessanten Themenstellung ermöglichte. Für die vielen Ratschläge, die Betreuung, den Ansporn und die Möglichkeit viele spannende Projekte zu bearbeiten möchte ich mich bei Prof. A. Nesterov-Müller und Prof. F. Breitling und ebenfalls bei Dr. F. Löffler und Dr. D. Mager bedanken. Ich danke allen Kollegen und Kolleginnen, die während meiner Promotion Teil der Arbeitsgruppen Molecular Search Engines und Peptide Arrays and Antibody Libraries waren, für den wissenschaftlichen Austausch, die schöne gemeinsame Zeit und die zahlreichen Partien Tischkicker: L. Hahn, B. Münster, S. Schillo, F. Märkle, J. Striffler, J. Bykovskaya, M. Sedlmayer, M. Kachinzky, K. Herbster, G. Karadka Shankara, F. Löffler, T. Förtsch, C. Bojnicic-Kninski, R. Popov, D. Mattes, B. Ridder, A. Klinkusch, F. Falk und Z. Zhou und ganz besonders L. Weber. Ohne eure Vorarbeit und Expertise wäre diese Arbeit nicht möglich gewesen. Für die Unterstützung mit dem VSI und die Durchführung der AFM Messungen geht ein besonderer Dank an R. Thelen. Ein großes Dankeschön geht auch an die IMT-Werkstatt und im Besonderen an A. Moritz und A. Wolfschläger. Für die Unterstützung im Reinraum bedanke ich mich bei H. Fornasier und Dr. U. Köhler und seinem Team. N. Spengler, M. Meissner und R. Kampmann danke ich für die Einführung und Unterstützung im Bonden mit Ordyl. Für die Möglichkeit den Spottingroboter nutzen zu können möchte ich mich bei Prof. Niemeyer und besonders bei R. Garrecht bedanken. Für die wissenschaftliche Begleitung im Rahmen von BIF IGS möchte ich meinem Thesis Advisory Committee (TAC), Prof. M. Franzreb, Dr. K. Länge und Prof. B. Rapp herzlich danken. Mein Dank gilt auch den Studenten die ich im Rahmen eines Praktikums, einer Abschlussarbeit oder als Wissenschaftliche Hilfskraft betreuen durfte, und die zum Fortschritt dieser Arbeit beigetragen haben: S. Rentschler, V. Hackert, A. Schleicher, Md. Rahim, T. Schorb und A. Offner.
Não quero esquecer a minha família de capoeira. Ela me acompanhou todos estes anos e e foram o meu equilíbrio para o trabalho. Il più grande ringraziamento va a mio marito. Per avermi sempre sostenuto e creduto in me. Mi motivava e mi spronava, anche se questo significava che avevo poco tempo per lui.